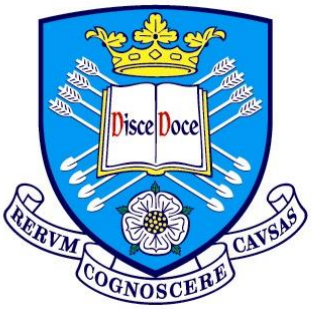

The University Of Sheffield.

Modelling and control of a novel structure two-wheeled robot with an extendable intermediate body

by

Saad A. Agouri

A thesis submitted to The University of Sheffield
for the fulfilment of the degree of

DOCTOR OF PHILOSOPHY

Department of Automatic Control and Systems Engineering
The University of Sheffield
Mappin Street
Sheffield S1 3JD
UK

May 2014

Abstract

The work presented in this thesis focuses on modelling and control of a system of two-wheeled robotic vehicle of new configuration with an additional degree of freedom by incorporating a linear actuator to the intermediate body. The main contribution of this work is in the mathematical modelling and intelligent control of the vehicle on inclined surfaces and realisation of the proposed design in real-time. Previous studies in the literature have not considered a movable payload on inverted pendulum systems while moving on inclined surfaces. The work is motivated by social need to assist physically impaired individuals towards ambient assisted living. The vehicle is to have the ability to lift up the payload to a demanded height, and manoeuvre on level or inclined surfaces. The dynamic model of the system, encompassing a highly coupled nonlinear set of relations, is developed using the Euler-Lagrange approach to characterise the system behaviour on flat and inclined surfaces. This is tested and validated through simulation exercises in the Matlab/Simulink environment. A further approach to gain confidence in the developed model has been carried out through virtual modelling of the system using MSC Visual Nastran 4D dynamic software.

Two manually tuned PID controllers are initially designed and used to control both the tilt angle and the cart displacement, and it is demonstrated that the approach works well for the robot on flat surfaces. The control approach is extended to hybrid type comprising a PD+ I fuzzy logic control (FLC) structure, with an adaptive bacterial foraging algorithm (BFA). The BFA is used for optimising the control parameters of the system. The control approach is tested in both simulations and laboratory experiments. The robustness of the control system is demonstrated with application of various disturbance forces on the

system. Moreover, the performance of the system is assessed through rigorous tests on flat and inclined surface of different frictional profiles.

By testing the design in different scenarios it is demonstrated that the proposed two-wheeled robot configuration and the proposed control approaches form a solid foundation and the framework for assisted mobility of disabled and elderly people.

Acknowledgements

Alhamdulillah. First and foremost, I would express my highest appreciation to Allah S.W.T the Almighty and Merciful for giving me strength and because of His Will; I manage to complete my PhD.

I would to like to express my deepest gratitude to my supervisor Dr Osman Tokhi for his affectionate supervision, assistance, motivation and encouragement throughout this work. His friendly approach and unbound patience have left a deep impression upon me; I will never forget your favours.

It gives me great pleasure to appreciate and thank my fellow research colleagues for their help and support in this work. Particular thanks go to Abdullah Almeshal, Omar Sayidmarie, Shawan Abdullah and Khaled Goher, their technical discussion and encouragements have been highly beneficial to my work.

I am also deeply indebted and thankful to my father and my mother who have always been good example for me, I am really proud of both of you. Many thanks to my brothers and sisters and all other family members, relatives and friends for their prayers and loving support.

I am indebted and thankful to day-to-day sacrifice, love and patients of my wife. My beloved wife; Antesar, I am rather glad that you share me the life and really appreciate your patience during my study; that was great and really supportive. My dear children I love you, and you are my future. My sweet heart; Shahaad, Ahmed, Abdelraouf, Moad and Muneera, I love you more than I can express; wishing a bright future for you.

Finally, the financial support of the Ministry of Higher Education in Libya is gratefully acknowledged.

Table of contents

List of figures

List of tables

Nomenclature

Variable	Description	Units
C	the coefficient of friction	
$e(t)$	*Error function*	
Fa	*Linear actuator force*	N
Fd	*External disturbance force*	N
Fc	*Cart drive force*	N
g	Gravitational acceleration force	$m/s2$
H	*Distance between wheels along X axis (axle length)*	m
i	*Current through armature*	A
Iw	*Moment of inertia of the wheel*	$kgm2$
Ip	*Moment of inertia of the pendulum around its centre of mass*	$kgm2$
J_L	*Inertia of the lower part of the rod*	$N.m$
J_u	*Inertia of the upper part of the rod*	$N.m$
J_M	*Inertia of the payload*	$N.m$
K_P	*Proportional gain*	
K_I	*Integral gain*	
K_D	*Derivative gain*	
K_m	*Torque constant*	Nm/A
K_e	*Back emf constant*	V_S / rad
K_f	*Frictional constant*	Nms/rad
L_M	*Position of the COM of the payload*	m
L_u	*Position of the COM of the upper part of the rod*	m
L_a	*Position of COM of the linear actuator*	m
L_l	*Position of COM of the lower part of the rod*	m
L_g	*Position of COM of the IB*	m
L	*Lagrangian function*	m

M_l	*Mass of the lower part of the rod*	*kg*
M_a	*Mass of the linear actuator*	*kg*
M_u	*Mass of the upper part of the rod*	*kg*
M	*Payload mass*	*kg*
M_w	*Wheel mass*	*kg*
M_c	*Cart mass*	*kg*
M_p	*Mass of the pendulum rod*	*kg*
n	*Number of degrees of freedom of the system*	
$OXYZ$	*Cartesian coordinate frame attached to the vehicle centre point O*	
Q	*Linear displacement of the payload along the IB*	*m*
Q_i	*Generalized force*	
$\ddot{Q}$	*Linear acceleration of the attached payload*	*m/ s2*
q_i	*Generalized coordinate*	
R	*Nominal terminal resistance*	*Ohms*
R_w	*Radius of the wheel*	*m*
$r(t)$	*Reference signal*	*N.m*
T	*Total kinetic energy of the system*	*N.m*
T_m	*Motor torque*	*N.m*
T_c	*Kinetic energy of the cart*	*N.m*
T_l	*Kinetic energy of the lower part of the rod*	*N.m*
T_a	*Kinetic energy of the linear actuator*	*N.m*
T_u	*Kinetic energy of the upper part of the rod*	*N.m*
T_v	*Kinetic energy of the vehicle*	*N.m*
T_M	*Kinetic energy of the payload*	*N.m*
$u(t)$	*Control signal*	
V	*Total potential energy of the system*	*N.m*
V_l	*Potential energy of the lower part of the rod*	*N.m*

V_a	*Potential energy of the linear actuator*	*N.m*
V_u	*Potential energy of the upper part of the rod*	*N.m*
V_m	*Potential energy of the payload*	*N.m*
V_a	*Applied terminal voltage*	*V*
V_e	*Back emf voltage*	*V*
Y	*Linear displacement of the centre point, O*	*m*
$\dot{Y}$	*Linear velocity of the centre point, O*	*m/ s*
$\ddot{Y}$	*Linear acceleration of the centre point, O*	m/s^2
θ	*Angular displacement*	*deg*
$\dot{\theta}$	*Angular velocity*	*deg/s*
$\ddot{\theta}$	*Angular acceleration*	$\deg/s^2$
θ_p	*Angular displacement of the IB*	*deg*
$\dot{\theta}_p$	*Angular velocity of the IB*	*deg/s*
$\ddot{\theta}_p$	*Angular acceleration of the IB*	$\deg/s^2$
θ_m	*Measured angular position*	*deg*
θ_d	*Desired angular position*	*deg*
τ_m	*Motor torque*	*Nm*
τ_e	*Applied torque*	*Nm*
$\Delta e(t)$	*Derivative (change) of error function*	
$\int e(t)$	*Integral (sum) of error*	
S	*Total number of the bacteria in the population. S must be even.*	
p	*The dimension of the search space*	
Nc	*Number of chemotactic steps of the bacterium lifetime between reproduction steps*	
Ns	*Number of the swims of the bacterium in the same direction*	
Nre	*Number of reproduction steps*	
Ped	*Probability of bacterium to be eliminated or dispersed*	

J	*The cost function value*
C	*Step size of the tumble of the bacterium*
Ci	*Constant values*
$k_{\max}$	*Maximum iteration number*
r	*Convergence rate of distance between a point and the origin*
N_{sw}	*Maximum number of swim*
$x_i(k)$	*Bacteria position*

Abbreviations

BFA	Bacterial Foraging Algorithm
COM	*Centre of mass*
DC	*Direct current*
DOF	*Degree of freedom*
IB	*Intermediate body*
LE	*Lagrange Euler formulation*
MSE	*Mean squared error*
NB	*Negative big*
NE	*Newton Euler formulation*
NS	*Negative small*
PB	*Positive big*
PID	*Proportional – Integra l- Derivative*
PM	*Permanent magnet*
PS	*Positive small*
QABFA	*Quadratic Adaptive Bacterial Foraging Algorithm*
TWRM	*Two-wheeled robotic machine*
TWV	*Two wheeled vehicle*
TWR	*Two-wheeled robots*
TWIP	*Two-wheeled inverted pendulum*
Z	*Zero*

Chapter 1
Introduction and literature review

1.1 Introduction

Two wheeled robots or balancing robots are one variation of robot that has become a standard topic of research and exploration for engineers and robotic enthusiasts. Such robots operate on the principle of the inverted pendulum. Inverted pendulum systems are benchmark systems in the field of automatic control. A two-wheeled robot has similar characteristics of an inverted pendulum structure, which is recognized for its nonlinear and unbalanced character. Researchers have developed mobility solutions, based on the inverted pendulum system, like robotic balancing wheelchairs, personal transporters, as well as walking gaits for humanoid robots. Balancing robots are members of a class of under actuated systems. Research on two-wheeled robots has gained the interest of researchers over the last few years in some robotics laboratories. This is because of unbalanced nature of the systems that serves as a benchmark for testing and developing control techniques. A two-wheeled vehicle system are considered to be highly nonlinear and under actuated. They present advantages over other ground vehicles for example the zero-turn radius (tight turns), simpler configuration design, smaller footprint and less friction. Applications of such systems can be developed for indoor and outdoor transportation and mobility solutions. This allows easier manoeuvrability in confined and limited travel spaces due to the ability of the vehicles to turn in sharp turns and traversing steps or curbs. All these advantages would add to the capabilities of the two-wheeled systems that could solve numerous challenges.

Modelling and control of two-wheeled robots can become very complex if it has many degrees of freedom. The work presented here develops a system of two-wheeled vehicle with a new configuration with an additional degree of freedom by incorporating a linear actuator to the intermediate body. The vehicle will have the ability to move the payload to a required height. In addition, the vehicle will have the manoeuvrability on level or inclined surfaces. These with the new control approach developed confirm that a complex, highly nonlinear system like the two-wheeled vehicle can be modelled and controlled at various conditions associated with the operation and environment of the vehicle.

1.2 Aims and objectives of the research

The aims of this research can be summarized as follows:

1- Develop mathematical model of a new configuration two-wheeled robotic vehicle with movable payload on an inclined surface, and simulate this for use as tested in the research.

2- Develop suitable robust control strategies for balancing and manoeuvring of the robot on surfaces of different inclination.

The objectives of the research are as follows:

1- Derive mathematical model for two-wheeled robotic machine moving on irregular terrains.

2- To develop mathematical model of a new two-wheeled balancing vehicle with an extendable intermediate body and moving payload moving on irregular terrains.

3- To develop control strategies on the derived models steering and manoeuvring on irregular and uneven surfaces.

4- Evaluate the robustness of the control system with dynamic movement of the payload, and with applied disturbance in terms of amplitude.

5- Evaluate the robot's ability to move on surface of different inclination angle.

6- Practical evaluation and implementation of the developed control techniques using an experimental prototype (Figure 1.3) of two-wheeled robotic vehicle for upright balance and stability while moving on flat and irregular terrains.

1.3 Motivations of the research

Currently, there are many applications of systems based balancing inverted pendulum. Advanced personal transporters, balancing wheelchairs, development of gait for humanoid robots and other applications. In the United Kingdom there are over 6.9 million disabled people of working age representing 19% of the working population. There are 1.3 million disabled people in the UK who are available for and want to work. Sales of disabled equipment in the UK have increased by 92.6% over the last 10 years and the total market size has increased by 9.2% last year. The focus in most of the aforementioned single-link inverted pendulum systems is on designing control strategies and applications. While there is a small number of research papers that have focused on movement on

irregular surfaces and inclinations, such as Lee et al. (2009). Further work is needed with more challenging movement scenarios that incorporates the surface friction and moving on different inclination angles. None of the studies have considered a movable payload on the inverted pendulum system while moving on inclined surfaces. Incorporating a movable payload would make the system more complex and increase the degrees of freedom of the structure. This would give the ability to the system to move different payload sizes to a required height and thus increase the ability of the vehicle to serve as a basis for new applications.

Based on the current literature, there is still need for a study that covers the problem of an inverted pendulum on two wheels and its application as two wheeled robotic machines moving on irregular and inclined terrains of different frictional elements This research presents the modelling and control of a new two-wheels vehicle with an extendable payload moving on irregular terrains and slopes. The vehicle will form a basis for two-wheeled mobility solutions to be developed with extended capabilities. One of the challenging points is to study the system dynamics and stabilise the vehicle while moving on an inclined surface. Another issue is to study the effect of shifting the position of the load on the system stability. This should be done in the same instance with applying disturbances to determine the robustness of the controller to keep the whole system in balance. Moreover, the study would provide analysis of the system moving on different types of, smooth, rough surfaces. The contribution of the research will be at system modelling, and control design with associated verification within simulation and experimental environments.

1.4 Thesis outlines

Chapter 1:

This chapter has introduced of concepts in the field of two-wheeled robotics control and the associated applications. The idea of balancing and controlling is presented in the context of two wheeled robots and relevant applications. The literature related to the thesis has been reviewed and discussed.

Chapter 2:

This chapter presents the derivation of mathematical model of two-wheeled robotic machine moving on inclined surfaces. The dynamic modelling includes derivation of the equations of motion using the Lagrangian method. The system motion is introduced in terms of two differential equations portraying two degree of freedom of the system; the linear movement of the vehicle and the rotational movement of the intermediate body while moving on slanted surfaces. This chapter further presents a two wheeled vehicle modelling technique using MSC Visual Nastran 4D software this software with Matlab/Simulink, for use as a platform for analysis, design and evaluation of the developed control strategies. A control strategy is developed utilizing PID conventional control and tested on both models.

Chapter 3:

In this chapter, the system comprising the vehicle with an extended rod is presented. The vehicle possesses an additional DOF along the intermediate body due to adding another actuator. A Lagrangian formulation is utilised to obtain the system dynamic equations. The effect of adding more translational degree of freedom is discussed and demonstrated via initial simulations. The proposed control scheme is presented in this chapter. The control scheme consists of three

independent hybrid control loops, comprising a fuzzy PD-like combined with conventional integrator (PD+I FLC).

Chapter 4:

This chapter shows discussion into controller tuning utilizing enhanced bacterial foraging algorithm (BFA) specifically quadratic adaptive BFA (QABFA). This is an adaptive search algorithm based on changing the chemotactic step size depending on the nutrient value. This approach is shown to speed up the search operation and find the optimal solution in less time compared to the standard BFA algorithm. QABFA is focusing on improving of BFA convergence in terms of speed and accuracy (Supriyono and Tokhi, 2012)

Chapter 5:

This chapter evaluates the performance of the vehicle in different situations. The robustness of the system is evaluated with disturbances of different amplitude applied on the vehicle. The vehicle is simulated to move on surfaces with different slopes. Moreover, tests are carried out with the robot on flat and inclined surfaces with different friction profiles, including slightly rough and very rough grounds.

Chapter 6:

This chapter presents experimental investigations testing the control approaches implemented on a two-wheeled robotic prototype. The tests include balancing the robot on inclined and flat surfaces.

Chapter 7:

This chapter summarizes the main conclusions of the work and makes recommendations for further work.

1.5 Literature review

Many applications based on mobile robots have been developed by researchers that target military, industry and mobility solutions.

In this chapter, a literature review is conducted to review the relevant work to the proposed research. A review of the various designs of two-wheeled vehicles and the methodologies used in the control systems of such vehicles is utmost important to highlight the gaps in the literature. The system considered exists in many variations such as mobile inverted pendulum on a cart, rotational inverted pendulum, linear inverted pendulum system, and the inverted pendulum system on inclined rails. Moreover, inverted pendulum systems have been extended to encompass several links, for example the double and the triple inverted pendulum systems Almeshal, et al. (2013). Thus, it has provided an ideal platform for various control techniques. Some of the researchers have developed swing up controllers for inverted pendulum systems. Others have found that designing a stabilization controller as an interesting development. Most of the controllers developed have combined both the control of the swing-up process and the stabilization of the pendulum. Various control techniques have been developed and implemented with regard to inverted pendulum systems. Such methods include but are not limited to, non-linear controllers, linear quadratic controllers, and fuzzy logic controllers, embedding neural networks with various controllers, and embedding different optimisation algorithms with various controllers Alam, et al. (2008).

1.5.1 Mobile Robots

Through different applications robot technology is ubiquitous in different fields; it brings huge profits and benefits to numerous countries. Recently, robots have been developed for use in various environments such as home or office, where they serve as security robots, care robots, service robots, and exploration robots. Mobile robots can be classified under two main categories, the environment in which they travel (land robots, aerial robots and underwater robots) and type of locomotion (legged, wheeled and crawling).

Autonomous robots operate in indoor and outdoor environments. Outdoor autonomous robot configuration is the most challenging ground vehicles, because of the terrain dimensions, the great differences in surface thickness, the climate conditions and the unsteadiness of the sensed environment.

1.5.2 Balancing Robots

The theory of balancing robot is dependent upon the inverted pendulum model. The inverted pendulum system is a classical benchmark problem in the control engineering due to the nonlinear and highly coupled nature. Balancing two-wheeled robots are designed based on the inverted pendulum system.

1.5.2.1 Inverted Pendulum

The single inverted pendulum is a conventional problem in the field of control theory, one of the greatest significant problems in dynamics and has been studied extensively in the control literature Wang & Jia-Jun, (2012). The inverted pendulum is a complex system and has been studied from laboratory

size up to the complex inverted pendulum scenarios that exist in real life. In fact, the inverted pendulum situation represents many real life situations such as balancing a broom on the palm of one's hand, having a pendulum on a cart, and people standing on movable two-wheeled vehicles such as the segway. Several control strategies based on the conventional control theory, modern control theory, and intelligent control have been used to control the inverted pendulum. Many researchers have used linear energy based controls, quadratic regulation, fuzzy logic control, neural networks, neuro-fuzzy, genetic algorithms and hybrid controller systems combining more than one control type. Other researchers have focused on the design of multi-link inverted pendulum systems. The following subsections describe various system designs that are based on the inverted pendulum concept.

1.5.2.2 Inverted pendulum system on cart

One of the major nonlinear control problems is the inverted pendulum on a cart. The development and implementation of different control strategies have been reported in the literature for inverted pendulum on a cart. Wang (2011) introduced a simple scheme to design a conventional PID controller to stabilize and track three types of inverted pendulum. Roshdy, et al. (2012), proposed a full state feedback controller using separation factor to stabilize single inverted pendulum. Ha, et al.(2010), designed and investigated the time specification performance of inverted pendulum controllers. They proposed two control strategies an innovative double, a new linear quadratic regular (LQR) control technique and proportional, integral, derivative (PID) control method. Dynamic behaviours were studied and the pendulum performed faster and smoother

during the stabilisation process and with better robustness and less oscillation with the LQR controller with than the double-PID controller. Prasad, et al. (2012) utilizing PID controller and LQR have been presented control design of inverted pendulum-cart dynamic system. Lingyan et al. (2009) demonstrated a simulation, and presented an experimental work in balancing an IP system using a LQR. The simulation shows that the pendulum angle stabilizes after 2.5 seconds, while the position of the carriage stabilizes after 3 seconds. On the other hand, the experimental work shows a slight delay in stabilizing the system because of the neglected terms in the simulation such as friction, thus idealizing the system.

Yamada et al. (2004) introduced a switching control based on energy modification, such that the potential energy is at a minimum in the upright position. The switching method used was found to be complex, where many assumptions were made during the derivation of the parameters and the equations.

Kawamoto (1996) has used fuzzy control and rigorous stability analysis for an inverted pendulum, and has shown that the fuzzy control input gives a better control response than in the linear case. Bush (2001) has discussed the application of fuzzy logic control (FLC) on the inverted pendulum problem. Three versions of FLC for the inverted pendulum problem have been discussed, including their strengths, weaknesses and performance. The three versions mainly differ in terms of the number of fuzzy sets and the number of input variables. It has been shown that the FLC, with variables membership functions and a large number of input, was the most accurate and robust model. One

drawback was the long processing time. Techniques for manually tuning complex FLCs were also implemented and addressed in the work. Xu et al. (2002) executed FLC for an inverted pendulum. They used fuzzy controller rules obtained from simplified look-up tables, designed from learning algorithms. The result obtained was good, and a stable condition was achieved with the fuzzy controller. Muskinja et al. (2006) have shown with the swing up of a pendulum, which the use of FLC theory has several advantages compared to energy-based swinging strategies. They have used adaptive state control and optimal balancing for stability balancing and cart control. The results show that fuzzy swinging algorithms swing the pendulum for any initial condition, while the cart always remains on its rail limit. Chun, et al.(2013) have made a comparison between several types of controller such as PID, FLC, and state feedback.

Miyagawa et al. (1995) have implemented a neural network based model for control, but only for stabilizing the inverted pendulum in the upright position. Mladenov (2011) has used intelligent control algorithm based on neural networks to swing up and balance an inverted pendulum on a cart system. The controller swings up the pendulum from a static downward position to an upright position. The control strategy demonstrated a successful control over the inverted pendulum on cart structure and was able to balance the system from different initial positions. Kouda et al. (2005) studied the swing-up control of an inverted pendulum using the qubit neural network, where the laws of quantum physics were employed. The result was compared with conventional neural networks, which showed that the qubit neural network was able to swing up and balancing the inverted pendulum.

Many researchers have used evolutionary algorithms in controlling an inverted pendulum. Ha et al. (1997) integrated a genetic approach with an optimal LQR. They used a genetic algorithm (GA) to choose the weighting matrices in order to obtain the optimal control gain. The result obtained by using this method was good, but not particularly reliable, since the pendulum angle was not properly stabilized at the upright position. Wang and Fan (2009) have applied an improved particle swarm optimisation (PSO) algorithm on a fuzzy-PID controller for a rotated IP system. The approach successfully balanced the pendulum within 1.5 seconds, showing its feasibility and effectiveness.

Bugeja (2003), used a nonlinear swing up controller for the nonlinear model of the inverted pendulum, and a linearized version of the model was used in the stabilization of the inverted pendulum with a linear feedback controller, using pole-placement control design. The control approach considers a linearized version of the system that will ensure the local stability within the linear operating range of the system. The nonlinear control of an inverted pendulum was introduced by Chung et al. (1995) in their research. The nonlinear control was used to regulate the swinging energy of the pendulum, while regulating the cart position for a cart-pendulum system. In this study, a numerical technique was incorporated to find certain parameters. The nonlinear approach was also used by Akesson et al. (2006) in their study. The controller has enabled the researchers to track constant pivot velocity references while stabilizing the pendulum. The results obtained were within acceptable limits.

1.5.2.3 Rotational inverted pendulum

There are a number of studies done on rotational inverted pendulums. While the system structure is different from that of the pendulum-cart system, definitive objectives are the same, i.e. to swing up the pendulum and stabilize it in an upright position. There are different methodologies of controlling this type of system.

Furuta et al. (1991) structured a rotational inverted pendulum so called Furuta pendulum. They have used two different controllers in the system in order to swing up the pendulum. These are the conventional feed forward control and the bang-bang state feedback control. It provides good performance and has shown robustness in terms of parameter uncertainties. But the bang-bang state feedback control method is only valid if the pendulum is adequately light, therefore that it can swing up with little angular velocity. The conventional optimal regulator, and consequently the observer design as proposed by Furuta, was used to stabilize the system at the upright position.

Park et al., (1999), compared three different kinds of controllers; a PID control, a fuzzy-PID control and an adaptive fuzzy control. It was confirmed both by simulation and experiments that adaptive fuzzy control gave better performance.

Self-tuning control was introduced by Ratiroch-Anant et al. (2004) for a rotational inverted pendulum. This method was found to be very useful, especially for online tuning.

Aguilar-Ibañez, et al. (2008) have stated that rotary inverted pendulum (RIP) has sufficient suitable characteristics from control point of view to be famous for one of the best systems for evaluating control strategies and controllability tests. Having multivariable nonlinear unstable non minimum phase dynamics to test the performance and efficiency of different control methods. Fuzzy logic, and LQR method were used to deal with the challenging characteristic of the system, and evaluate the used control techniques as well as new methods. The results of simulations ware also shown for comparison with a successful stabilisation of the system.

1.5.2.4 Multilink inverted pendulum

Eltohamy et al. (1999) have developed a general equation of motion for a multi-link inverted pendulum system. The mathematical modelling approach is useful for future implementation to any related system with a certain number of links. Jadlovský and Sarnovský (2013) introduced a unifying approach to the problem of mathematical model derivation for classical or rotary inverted pendulum systems with an arbitrary number of pendulum links. By means of extensive physical analysis, general algorithmic procedures were designed which determine the Euler-Lagrange equations for the base and every pendulum in a generalized system of n classical or rotary inverted pendula.

Bogdanov (2004) reported the use of an optimal control for a double inverted pendulum scheme, and investigated and analysed optimal control and LQR approaches. It has been shown that the state-dependant Riccati equation (SDRE) has several advantages over the LQR design.

Cheng-jun et al. (2009) used GA to optimize the weighting coefficients of a FLC of a double inverted pendulum system. This approach offers better stability and high velocity response than the ordinary FLC.

Ahmad et al. (2012) has designed a modular hybrid controller for a two-wheeled robotic wheelchair system. The wheelchair design is based on double inverted pendulum scheme with a variable payload. A fuzzy-PD type controller and a PID controller were combined to form a hybrid control strategy that proved to be successful in controlling the wheelchair response.

1.5.2.5 The two-wheeled inverted pendulum

Some researchers have studied the inverted pendulums on two-wheels. This type of application has emerged from work done on pendulum-carts and rotational pendulums. A model of a revolutionary two-wheeled machine was built by Grasser et al. (2002), Joe shown in Figure 1.1. Joe is A two-wheeled robot vehicle based on inverted pendulum system with added mass that mimic the human driver mass. A linear state space control strategy was implemented on the robot to stabilise its behaviour. The control strategy was proved to be successful to stabilise the system and drive it to the target paths. The control method employed comprises two decoupled state space controllers, and implemented on a DSP device. The vehicle was controlled by applying appropriate torque to the corresponding wheels obtained from using a state space control. The two decoupled state space control designs considered the stability around pitch (standard y-axis in 3D), as well as around yaw (standard z-axis in 3D). The authors assumed in the design that the moment of inertia of the chassis regarding to the z-axis is constant when the yaw angle is zero. The

cornering force was assumed to be very small and could be neglected. The motor dynamics were also neglected in the research. The performance of the system was good. The results show successful performance, while the control approach may be improved by using adaptive control or fuzzy control.

Figure 1.1: Joe robot

Akesson et al. (2006) designed and controlled an inverted pendulum on a two-wheeled robot for educational purposes. For stabilizing control, the authors used a state feedback method where the feedback vector was obtained using an LQR technique. An additional controller was introduced for controlling the robot heading. The authors also considered the friction effect in the study in order to obtain a stable mechanical system. The results show that the robot was successfully stabilized, but there was a small cycle in the wheel's velocity because of friction which was not fully compensated for.

Pathak et el. (2004, 2005) also studied the inverted pendulum on two wheels. Velocity controls as well as position control were studied in their works using partial feedback linearization. They designed two levels of control for

both position and velocity control, and the result obtained was effective. Further improvements on the robustness characteristics of the controller could be made to take into account the uncertainties of the parameters.

Salerno and Angeles (2005) presented a novel group of two-wheeled robots. They reported some results from the literature on two-wheeled mobile robots, along with a novel classification of the latter. The mathematical model of the proposed robots is formulated in the framework of the Lagrange formalism. One challenge that had been faced through this work is the control of movement of the intermediate body. Also they showed that the robot can be stabilisabled by a differentiable state feedback control system. The design of a partial-state feedback controller which is capable of stabilizing the robot while respecting specs on the static and dynamic performances of the system was outlined. Taking into account the actuator dynamics as well, a few simulations for the validation of the aforementioned design have been conducted.

A two-wheeled inverted pendulum (TWIP) robot, shown in Figure 1.2 has been developed by Nawawi et al. (2007). It consists of a power amplifier; encoders, a gyroscope, and two servo drives for actuation. A digital signal processor (DSP) board utilised to apply the controller.

Figure 1.2: Prototype of T-WIP mobile robot

Goher and Tokhi (2008,2010) introduced a new design of a two-wheeled vehicle with an extendable rod, shown in Figure 1.3 A linear actuator has been added to join two parts of the IB and give the vehicle an additional degree of freedom. An investigation has been carried out on the steering behavior of the vehicle. The system model has been derived based on Lagrangian based dynamics. The dynamic equations have been described in terms of the partial angular movements of the vehicle wheels rather than the displacement of the centre of the vehicle. This has allowed designing a control strategy based on the actual measurements of the wheels rotations where two control signals are developed to activate, independently, each driving motor. In order to check the ability of the control approaches, the system has been tested utilizing three different motion scenarios of the wheels. The control strategy showed the capability to manoeuvre the vehicle using feedback of both the angular orientations of the right and left wheels. The developed control strategy was able to track, efficiently, the desired trajectories assigned to both wheels.

Figure 1.3: Real test rig, ACSE department, University of Sheffield

Ren et al. (2008) analysed the control of a two wheeled vehicle shown in Figure 1.4. A self-tuning PID control system has been implemented on the system in order to stabilize and follow a desired motion scenario. the neural network -like PID control scheme has been improved.

Figure 1.4: Two wheeled vehicle (Ren et al., 2008)

Sun et al. (2010) analysed the issue of stability control in a two wheeled self-balancing robot. By considering the control strategy of approximate linearization of the nonlinear system and the points of interest and weaknesses of standard PID, they designed a combined controller dependent upon PID and LQR. A personal pendulum vehicle for human transportation was designed and experimented on by Fiacchini et al. (2006). They used low cost system components, which led to the use of a very simple controller. A microcontroller was used to compute the controller's action utilising the data from various sensors, which allowed online controller adjustment. The system consisted of a

platform on two wheels which are activated independently. Two controllers were used for the system; an LQR for state variable feedback and a nonlinear controller. The results obtained claimed that both LQR and nonlinear control induced approximately the same behaviour at the stability point.

Tsai et al. (2010) developed an adaptive neural network controller for a two-wheeled balancing scooter. The controller utilises a radial basis function (RBF) neural network to stabilise the scooter yaw angle. Brown, et al. (2012) aimed to designing and constructing a scaled down prototype of a personal transportation vehicle that can autonomously maintain its balance. They also aimed to minimize the cost of building the full scale personal transportation device in order to be competitive in the market while maintaining similar performance to what is already available. The robot was designed and built with lightweight materials in order to minimize the torque that the motors would need to balance the robot. A fuzzy logic program is used to balance the robot. Two different programs have been written to control the system. The first to balance the robot, and the second to allow the robot to turn. These fuzzy logic programs have been tested in MATLAB, with the aid of transfer function analysis, to properly tune their parameters for optimal performance before they are used with the prototype.

Ahmad et al. (2012) successfully implemented fuzzy logic on a two-wheeled wheelchair system where a modular fuzzy control (MFC) was developed and implemented for controlling lifting and stabilizing mechanism, linear and steering motion control. Note that since a wheelchair is a main means of transport for disabled and elderly people, this two-wheeled wheelchair

system would allow the user to achieve a higher level of height without assistance and hence independence. The wheelchair has been modeled as a double inverted pendulum. The integrated two-wheeled wheelchair with a human model has been imported as the plant into Matlab/Simulink environment for control and evaluation purposes. The presented results show an efficient and successful control of the vehicle by the MFC. The controller was able to balance the wheelchair and the strategy resulted in reducing the fuzzy rules.

Li et al. (2008) designed a portable robot with a two-coaxial wheeled structure shown in Figure 1.5. The configuration has two separate wheels connected to the rectangular frame. The robot is equipped with a gyroscope to estimate the tilt angle, two DC motors and encoders to estimate the revolution of the wheels.

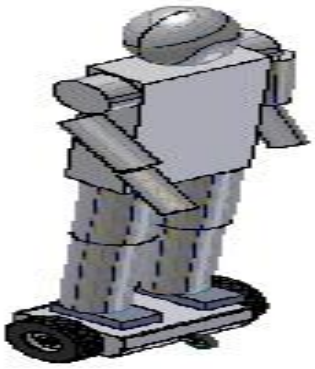

Figure 1.5: Two-wheeled inverted pendulum human-transporter
(Li et al., 2008)

1.5.3 Examples of commercial and hobby autonomous robots

A two-wheeled balancing robot, called nBot, as shown in Figure 1.6, has been developed at the Department of Geological Science's Center for Geophysics at the Southern Methodist University, Texas. Two sensors have been used; a tilt

sensor for detecting the tilt of the robot, and a wheels encoder for measuring the position of the base of the robot.

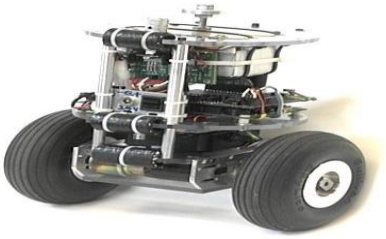

Figure 1.6: nBot Robot

Ichibot is a two wheel robot, shown in Figure 1.7, built by Roderick Lee Mann. Ichibot represents a group of feedback control systems based on inertial measurement. Other such systems include anti-skid and automobile airbag systems and aircraft navigation systems.

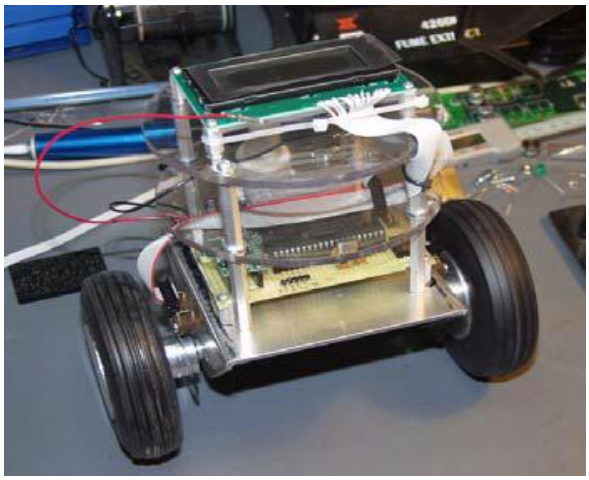

Figure 1.7: Ichibot

I-PENTAR (Inverted Pendulum Type Assistant Robot), Figure 1.8, has also been developed in this field by Jeong et al. (2008). This robot is used for applications in terms of the coexistence of safety and work. The state feedback control method was implemented on a system that mimics a single-link inverted pendulum, where the control gain was obtained using LQR.

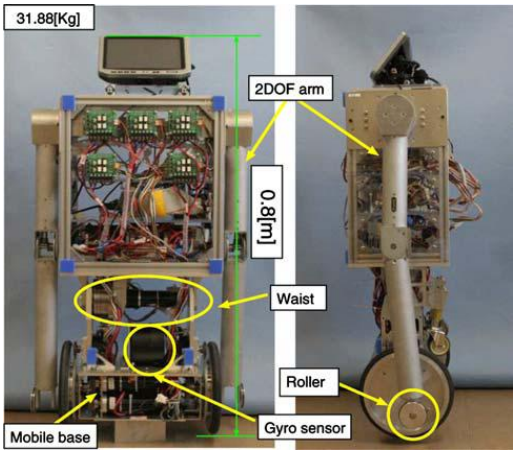

Figure 1.8: Appearance of the inverted pendulum type assistant robot I-PENTAR

There are a number of two-wheeled robots which have been commercialized for different purposes. Figure 1.9.Shows a multi-function wheelchair system known as The INDEPENDENCE® iBOT® 4000 Mobility System (Johnson & Johnson Company, 2001). It is a combination of a unique and multi-functional wheelchair that allows flexibility on the part of users. The user is able to climb curbs, have eye-to-eye conversations and is able to reach high places. The system can also easily travel over uneven terrais such as sand, gravel or grass. The operating concept is like the Segway scooter. Balance is dynamically controlled by applying torque on the two wheels. The iBOT® Mobility System represents total freedom for wheel chair users. However, the wheelchair was discontinued in 2009 due to its size and expense, such that not all disabled or aged people can afford it. The current research is aimed to develop a standard, very simple and cheap wheel chair system. The system will be suitable for various uses such as in the home, in public places or offices.

Figure 1.9: iBOT

Segway has introduced a commercial riding product using a self-balancing personal transportation device with two wheels, referred to as Segway® Personal Transporter (PT) (Segway Inc., 2001). See Figure 1.10. The PT is can move forward or backward depending on the position of the rider, and can be steered to left or right for turning.

Figure 1.10: Segway Personal Transportation (Segway, 2001)

A two-wheeled robots to be produced is the two-wheeled car by General motors -Segway, referred to as Project PUMA (Personal Urban Mobility and Accessibility) as shown in Figure 1.11. PUMA has a maximum speed of 35mph and can go as far as 35 miles on a single charge using lithium-ion batteries.

. 

Figure 1.11: GM-Segway PUMA

1.5.4 Two-wheeled robotic machine moving on irregular terrains

A few studies have been conducted in areas related to two-wheeled movement on irregular terrain. Lee et al. (2009) presented a hill climbing algorithm with regard to an inverted pendulum. Mathematical models were presented for the situations of having the inverted pendulum robot both climbing up and down a hill. The model was assumed to have no payload. The paper considered modelling the friction force, and the effect of the horizontal and vertical forces applied on the inverted pendulum cart. Experiments were carried out to provide a comparison of the controller effort for various angles. The pendulum stays in the upright position for small angles. Increasing the inclination angle increases the disturbances, and therefore decreases the controllability of the pendulum, resulting in the vehicle to collapse.

Wang et al. (2010) developed an adaptive dynamic programming method design for an angle bracket inverted pendulum which is simply an inverted pendulum system on a cart placed over an inclined surface. The pendulum experiences an inertia weight produced by the descending pull of gravity along an inclined surface. Two neural networks were utilised to accomplish the

function estimation and control action through a continuous learning process. The results proved the viability of this control technique in compensating for the inertia problem.

Kausar et al. (2010, 2012) presented a modelling and control of a two-wheeled robot on a slanted and uneven terrain. The system was modelled and simulated using a gain scheduling control strategy as well as a full state feedback control. The simulations show a successful and stable performance of the vehicle on flat as well as uneven and sloped terrains.

Kim, et al. (2005) investigated the dynamics of inverted pendulum system in order to give fundamental data for further design and construction. They investigated essential issues in the dynamics of a position with an inclined surface and likewise the impact of the turning movement on the stability of the robot

Kwon, et al. (2011) proposed an optimal posture of two wheeled inverted pendulum robot on a slanted surface. Dynamic state equation was derived from the system's structure, and an LQR regulator was designed based on the tilted angle obtained from the ultra-sonic sensor. Effectiveness of algorithms has been demonstrated and verified through simulations and real experiments.

Nasrallah, et al. (2007) discussed control design for a mobile wheeled pendulum robot moving on a slanted surface. The control law developed is worldwide, hence it is demonstrated that deep insight into the interior motion of the system in combination with suitable selection of its generalized coordinates and the system output functions are essential in the development of effective feedback controllers for nonholonomic systems with underlying unbalanced zero-dynamics. Hu et al. (2010) studied strong movement pilot control of a two-

wheeled vehicle where the response control scheme is singularly dependent upon the angle of slant. H∞ control is utilized to design a controller.

Most of the previous studies have assumed a static payload or a human payload with a defined weight and characteristics. A study of a dynamic movable payload is needed to analyse the system's behaviour with dynamic payload characteristics. A model of these capabilities will allow more space to develop more complex and useful applications. One aim of this study is to develop a system that is capable of moving on irregular and inclined slopes with a movable dynamic payload.

1.6 Contributions

The contributions of the thesis could be abridged as follows:

- Mathematical model of a novel structure of inverted pendulum-like balancing vehicle with an attached actuator to move up a payload to demanded height.
- Development of robust a control system for the vehicle to counteract the effects of the ground profiles and terrains and reject external disturbances
- Application of newly-developed optimisation technique to optimise the system controller for enhanced control execution.

1.7 Publications

Journals

1. **Agouri S A.,** Almeshal, A. M Goher, K. M., & Tokhi, M. O. (2014). Mathematical modelling and stabilization of a two-wheeled vehicle on an inclined surface using optimised hybrid fuzzy-like PD and conventional integral control. *Robotics and Autonomous Systems*. (Under revision).
2. Almeshal A M, Goher K M and Tokhi M O and **Agouri S A**, (2013), Mathematical modelling of a new configuration of a two-wheeled vehicle With an extendible intermediate body on an inclined surface, *Applied Mathematical Modeling Journal.* (Under revision).
3. **Agouri S**, Nasir A N K, Goher K M, Almeshal A M and Tokhi M O. (2013). Hybrid spiral-dynamic bacteria-chemotaxis algorithm with application to two-wheeled inverted pendulum vehicle with a new configuration, *Engineering Applications of Artificial Intelligence.* (Under revision)

Conferences

1. Corredor Rosendo A C, **Agouri S A** , Tokhi M O and Goher K M (2011) **"**Design and real-time pid control approach of a two-wheeled vehicle with an extended rod**".** *Proceedings of the 14th International Conference on Climbing and Walking Robots and the Support Technologies for Mobile Machines (CLAWAR 2011***),** Paris, France, 6-8 September, 2011. Pp 53-61
2. Almeshal,A M, Goher K M, Tokhi M O, Sayidmarie O, **Agouri S A**,(2012) Robust PD-PID Control Of A New Configuration Of Two-Wheeled Machines Under Various Operating Conditions, *Proceedings of the 15th*

International Conference on Climbing and Walking Robots and the Support Technologies for Mobile Machines (CLAWAR 2012), Baltimore, USA, 23-26 Jul. 2012. pp 673-680.

3. *Almeshal A M, Goher K M, Nasir A N K, Tokhi M O,* ***Agouri S A****, (2013). Fuzzy logic optimized control of a novel structure two-wheeled robotic vehicle using HSDBC, SDA and BFA: a comparative study, Proceedings of 18th International Conference on Methods and Models in Automation and Robotics (MMAR), Miedzyzdroje, Poland, 26-29 Aug. 2013.*

4. Almeshal,A M, Goher K M, Tokhi M O, Sayidmarie O, **Agouri S A**,(2012) Hybrid Fuzzy Logic Control Of A Two Wheeled Double Inverted Pendulum-Like Robotic Vehicle, *Proceedings of 15th International Conference on Climbing and Walking Robots and the Support Technologies for Mobile Machines (CLAWAR 2012),* Baltimore, USA, 23 - 26 July 2012.pp 681-688.

5. Short A. R. ,Sayidmarie O. K., **Agouri S. A**, Tokhi M. O, Goher K. M., and Almeshal A.M, (2012) Real time PID control of a two-wheeled robot, *Proceedings of the 15th International Conference on Climbing and Walking Robots and the Support Technologies for Mobile Machines (CLAWAR 2012),* Johns Hopkins University, USA, 23 - 26 July 2012.pp 73-80

6. Goher K M, Al-Harrasi A, Al-Abdali S, Al-Abri J, Al-Siyabi A, Tokhi M O, Almeshal A M, Sayidmarie O and **Agouri S A**,(2012). state space modelling and control of squ-two-wheeled mobility vehicle (SQU-TWMV): an Energy analysis approach, *Proceedings of* the *15th International Conference on Climbing and Walking Robots and the Support Technologies*

for Mobile Machines (CLAWAR 2012), Baltimore, USA, 23 - 26 July 2012.pp 55-62

7. Goher K M, Al-Harrasi A, Al-Abdali S, Al-Abri J, Al-Siyabi A, Tokhi M O, Almeshal A M, Sayidmarie O and **Agouri S A**,(2012). Mathematical modelling and pid control of squ-two-wheeled mobility vehicle (SQU-TWMV), *Proceedings of 15th International Conference on Climbing and Walking Robots and the Support Technologies for Mobile Machines (CLAWAR 2012)*, Baltimore, USA, 23-26 Jul. 2012. pp 137-144

8. Goher K M, Tokhi M O, Almeshal A M, Sayidmarie O and **Agouri S A**, (2012) Impact of Payload Inertia on the System Damping Characteristics of a Two-Wheeled Robotic Machine, *Proceedings of the 15th International Conference on Climbing and Walking Robots and the Support Technologies for Mobile Machines (CLAWAR 2012)*, Baltimore,, USA, 23 - 26 July 2012.pp 113-120

9. **Agouri S.**, Tokhi O, Almeshal A. M., Sayidmarie O. and Goher K M, (2012) Dynamic modelling of A new configuration of two wheeled robotic machine on an inclined surface, *Proceedings of the 17th International Conference on Methods and Models in Automation and Robotics*, 27 – 30 August 2012, Międzyzdroje, Poland. pp 315-318

10. Sayidmarie O K, Tokhi M O, Almeshal A M, **Agouri S A**, (2012)"Design and real-time implementation of a fuzzy logic control system for a two-wheeled robot", *17th International Conference on Methods and Models in Automation and Robotics (MMAR)*, Miedzyzdroje, Poland, 27-30 Aug. 2012.pp 569-572

11. Almeshal A M, Goher K M, Tokhi M O and **Agouri S A**, (2012). A new configuration of a two-wheeled double inverted pendulum-like robotic vehicle with movable payload on an inclined plane, *Proceedings of the 1st International Conference on Innovative Engineering (ICIES 2012)*, Alexandria, Egypt, 7 - 9 Dec. 2012. pp 97-102.

12. **Agouri S A**, Tokhi M O, Almeshal A, Sayidmarie O, Goher K M (2013), Modelling and control of a two-wheeled vehicle with extendable intermediate body on an inclined surface, *Proceedings of the 32nd IASTED International Conference on Modelling, Identification and Control*, Innsbruck, Austria, 11-12 February 2013.pp 388-393

13. **Agouri S A**, Tokhi M O, Almeshal A, Goher K M, (2013). Modeling and robust analysis control of a two wheeled vehicle with an extendable intermediate body on an inclined surface, *Proceaedings of the 1st International Conference on Electrical and Computer Engineering (ICECE 2013)*, Benghazi, Libya, 26th - 28th March 2013.pp161-165.

14. **Agouri S. A.,** Tokhi M O, Almeshal A M, Goher K M , (2013). Control of a two wheeled robot with extendable intermediate body on an inclined surface using bacterial foraging algorithm, *Proceedings of the 16th International Conference on Climbing and Walking Robots (CLAWAR 2013*), Sydney, Australia, 14 - 17 July 2013. pp 189-196.

15. Almeshal A M, Goher K M, Nasir A N K, Tokhi M O, **Agouri S A**, (2013). Hybrid spiral dynamic bacterial chemotaxis optimisation for hybrid fuzzy logic control of a novel two wheeled robotic vehicle, *Proceedings of 16th*

International Conference on Climbing and Walking Robots (CLAWAR 2013), Sydney, Australia, 14 - 17 July 2013. pp 179-188.

16. **Agouri S**. A, Sayidmarie O. K, Almeshal A M, Goher K M and, Tokhi M. O., (2014) "Performance evaluation of a new configuration two wheeled robot on different surfaces profiles" submitted to *the 10th International Conference on Control UKACC14,* 9th - 11th July 2014, Loughborough, UK.

17. Sayidmarie O. K., Tokhi M. O, and **Agouri S. A**., (2014) "Impact of dynamically moving payload on two wheeled robot stability*"* submitted to *the 10th International Conference on Control UKACC14*, 9th - 11th July 2014, Loughborough, UK.

18. **Agouri S. A**, Sayidmarie O. K, Almeshal A M, Goher K M and, Tokhi M. O., (2014) "Performance of a two wheeled robot with extendable intermediate body on irregular terrains" submitted to *the 17th International Conference on Climbing and Walking Robots CLAWAR 2014, 21 – 23 July 2014*, Poznan, Poznań, Poland. (Accepted)

19. Sayidmarie O. K., Tokhi M. O., and **Agouri S. A**, (2014) "Balancing and control of a two-wheeled robot on inclined surface" submitted to the *17th International Conference on Climbing and Walking Robots CLAWAR 2014*, 21 – 23 July 2014, Poznan, Poznań, Poland.(Accepted)

20. Sayidmarie O. K., M. O. Tokhi, and **Agouri S. A**., "Real-time validation of a novel two-wheeled robot with a dynamically moving payload" submitted to *the 23rd IEEE International Symposium on Robot and Human Interactive*

Communication IEEE RO-MAN`14, 25 – 29 Aug 2014, Edinburgh, Scotland, UK.

1.8 Summary

This chapter has introduced the scope of the research under taken. State of the art research and development in the area of the inverted pendulum and two-wheeled balancing robots has been presented, high lighting the main research issues of modelling and control of such systems. Aims and objectives of the research, contributions, publication arising from the research have been presented.

Chapter 2
Modelling and PID control of two-wheel robot on inclined surfaces

2.1 Introduction

Two-wheeled balancing robots have gained increasing attention in recent years as a result of their advantages over multi-wheeled robots. Two-wheeled robots are capable of manoeuvring in confined spaces and sharp turns. This encourages researchers to obtain a mathematical model and design controllers for the stability and movement of two-wheeled balancing robots on inclined surfaces.

The control theory of a two-wheeled balancing robot is relatively simple. For a two-wheeled robot that is based on inverted pendulum system on cart, the cart moves in the course of the robot falling into the opposite direction of the falling of the payload. The centre of mass of the balancing robot should always be kept vertically in order to stabilise.

When attempting to design a controller the most essential step is to obtain a mathematical model of the two-wheeled robot. Modelling the system dynamics would lead to a more precise model that allows a faster and effective control system design. There are numerous methods for deriving the mathematical equations of movement for a mechanical system. The most common methodologies utilized for deriving the equations of movement of a dynamic system are the Newtonian and Lagrangian approaches. The Newtonian methodology is a suitable dynamic definition for basic systems which do not have an extensive number of moving parts. However, utilizing this strategy for multi-figures and complex systems is highly complicated, specifically for a two-wheeled vehicle on an inclined surface, less accurate and time consuming. For

such complicated systems, the Lagrange approach provides a faster derivation, significant mathematical simplifications and a more accurate model.

A mathematical model of the proposed robot is derived in this chapter. The mathematical model describes the system dynamics performance of the two-wheeled robot. Euler-Lagrange modelling method is utilised to derive the system equations of motion. The two-wheeled robot contains of two sub-models, namely, a linear model of the permanent magnet (PM) direct current (DC) motor activating the vehicle wheels and the non-linear model of the inverted pendulum.

A visual modelling approach using MSC Visual Nastran 4D (VN) is utilised and tested in this chapter. The VN provides a visualisation of the robot model, with all of its components and masses that will be integrated into the Matlab Simulink environment to be controlled and validated.

To ensure the validity of the system model, these models should be crosschecked using the Lagrange approach and MSC Visual Nastran 4D (VN). The system parameters used in the simulation corresponds to the physical parameters of the robot prototype.

2.2 System description

In this section the mathematical model of the load-free robot on an inclined surface is derived. The model will be simulated and verified in the Matlab Simulink environment and VN. The model will be extended later to include the payload lifting ability and have a dynamic payload movement.

A robot has been built in the department, from which equations that describe the movement on an inclined surface are obtained. A schematic

diagram of the robot is presented in Figure. 2.1. The physical variables and parameters are labelled in Table 2.1 (Goher, 2008).

Table 2.1: System parameters

Description	Parameter	Unit
Nominal terminal resistance	R= 3	Ohms
Back EMF constant	K_e= 0.0061	Vs/Rad
torque constant	K_m= 0.3	Nm/A
Rotor inductance	L = 0	H
Wheel radius	R_w= 0.075	m
Wheel mass	M_w= 0.18	Kg
Pendulum mass	M_p= 3	Kg
Wheel inertia	I_w= 0.0002	Kgm^2
Length to the pendulum centre of mass	l = 0.26	m

The two-wheeled robot considered in this research is described in Figure 2.1 and Figure 2.2. The robot consists of a pendulum rod connected on an axle with two wheels. Two DC motors are used to drive the wheels of the robot. A payload is linked to the intermediate body (IB) of the robot and located at a fixed position from the centre point of the robot, O.

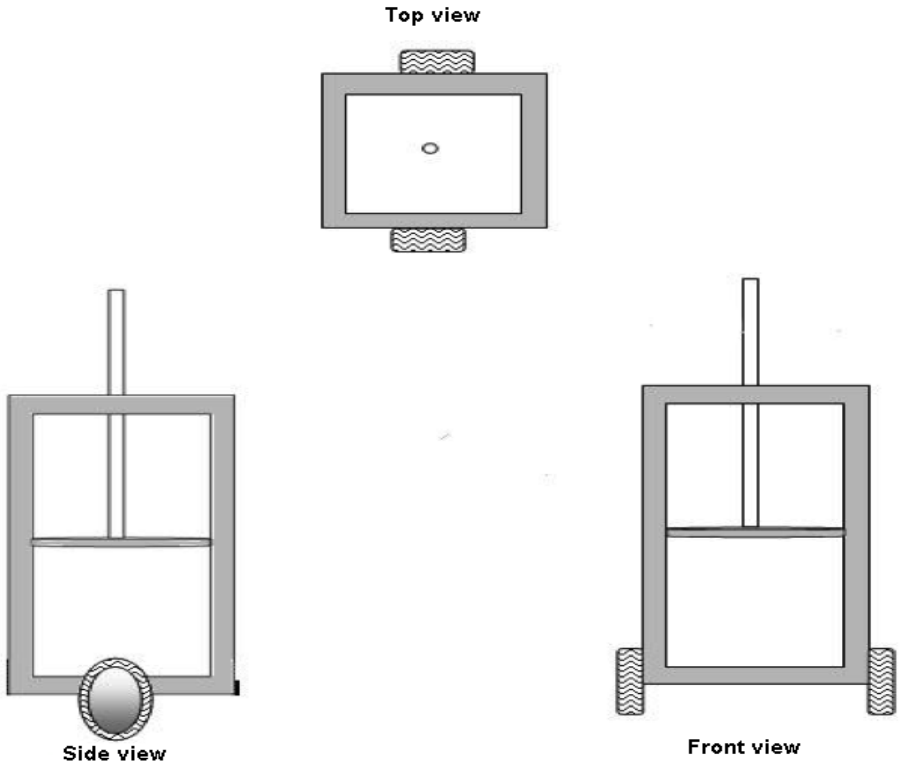

Figure 2.1: Robot structure front, side and top views

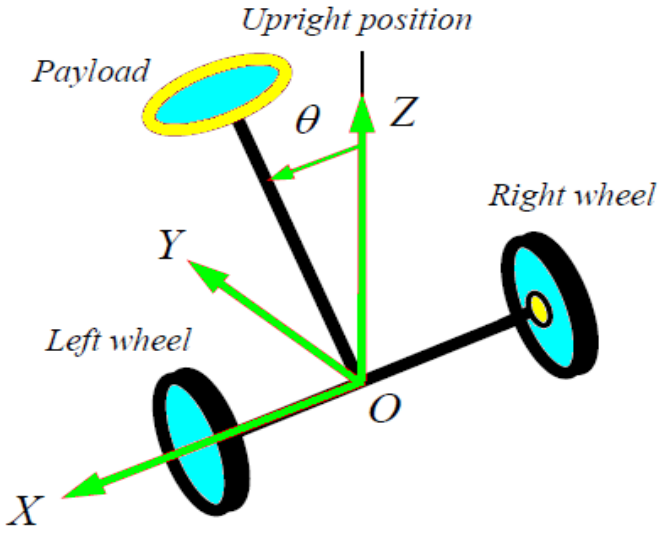

Figure 2.2: Robot schematic diagram

2.2.1 Linear model of the direct current motor

Two DC motors are attached to each wheel to control the movement of the robot. The motors mathematical model is derived and will be incorporated into the dynamic model of the vehicle to present the relevance between the control signal required to stabilise the vehicle and the input voltage. The equivalent motor circuit is presented in Figure 2.3.

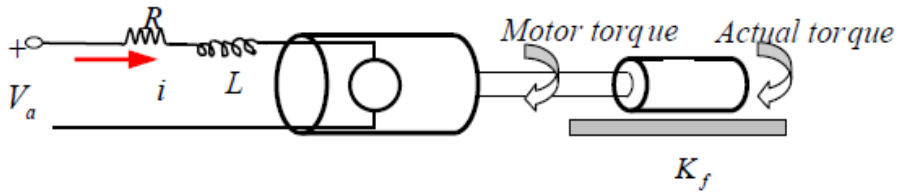

Figure 2.3: DC motor schematic diagram

The fundamental parts represented are the armature resistance, R, the armature inductance L, and the back electromagnetic force (EMF). EMF is made by the pivot of the motor's coil inside the magnetic field. It is proportional to the motor's rotational velocity. This relationship can be described as:

$$v_e = k_e w \tag{2.1}$$

Here, v_e is the EMF voltage in V, k_e is the back electromagnetic force constant in v_s / rad and w is the motor's rotational velocity in rad / s . The total torque $\tau_m (Nm)$ produced by the motor which is proportional to the current is given:

$$\tau_m = k_m i \tag{2.2}$$

where , k_m is the torque constant and i is the armature current in A. From Figure 2.3, the Kritchhoff's voltage law is used to obtain the following equation:

$$v_a = R_i + L\frac{di}{dt} + v_e \tag{2.3}$$

Where v_a the DC source voltage in V, R_i is the armature resistance in Ohms and L is the armature inductance in H. Equation (2.3) can be written as:

$$v_a = R_i + L\frac{di}{dt} + k_e w \tag{2.4}$$

Similarly, considering the mechanical properties of the DC motor when Newton's second law of motion is applied to the torque in figure (2.1), the following equation is derived:

$$\tau_m - k_f - \tau_a = I_R \frac{dw}{dt} \tag{2.5}$$

where k_f and τ_a represent a frictional constant and the motor shaft torque respectively. Substituting for *ve* from equation (2.1) into equation (2.4) and for i from equation (2.2) into equation (2.5) and rearranging leads to the following two equations:

$$\frac{di}{dt} = \frac{R}{L} i + \frac{k_e}{L} w + \frac{v_a}{L} \tag{2.6}$$

$$\frac{di}{dt} = \frac{k_m}{I_R} i - \frac{k_e}{I_R} w - \frac{\tau_a}{I_R} \tag{2.7}$$

Equations (2.6) and (2.7) are utilised to build a Simulink model in the Matlab environment. The applied torque τ_a and the applied voltage v_a are the inputs to the model. The model outputs are the motor shaft angular displacement θ and angular velocity w.

2.3 Lagrangian dynamics

The equations of motion are important in the design of system components, simulation and animation of the system, the design of the motors and drivers and the design of control algorithms. The two most common approaches used to derive the equations of motion of a dynamic system are the Newtonian and Euler-Lagrangian approaches.

The main difference between the two approaches relies in the system constraints. The Newton's method models every component of the system independently and finds the forces that are applied into each component. While Euler-Lagrange technique uses the potential and kinetic energy of the system components to find the equations of motion and thus the dynamic model of the system. For complex systems, Euler-Lagrange method provides more systematic and simply modelling approach, and thus is widely used in robotic literature. The Euler-Lagrange approach is based on the energy calculations and thus is independent of vector representation leading to generalised coordinates of the system that describes the degrees of freedom.

2.3.1 Lagrangian dynamic formulation

To utilize the Lagrangian method the following steps need to be applied:

1. Determine a set of independent coordinates that describes the motion of the system in the most convenient way; these are called generalized coordinates. The number of generalized coordinates will be equal to the degrees of freedom in the system
2. Derive expressions for the energies in the system and apply the Lagrangian function:

$$L = T - V \tag{2.8}$$

where L is the Lagrangian and T and V represent the total kinetic energy and total potential energy of the system respectively.

3. Evaluate the Lagrangian equations

$$\frac{d}{dt}\left[\frac{\partial L}{\partial q_i}\right]-\frac{\partial L}{\partial q_i}=Q_i \quad ,i=1,..,.n \tag{2.9}$$

where,

q_i is the i_{th} generalized coordinate , Q_i is the i_{th} generalized force. The generalized forces are the sum of forces projected in the direction of q_i , n presents the Number of DOF of the system.

The result of the last step is the equations of motion for the mechanical system.

For the robot in Figure 2.4, the kinetic energy of the system is given by:

$$\begin{aligned} T=&\frac{1}{2}M_C\dot{y}^2+2\frac{1}{2}M_W\dot{y}^2+\frac{1}{2}M_P\left(\dot{y}+l\cos\theta_P\dot{\theta}_P\right)^2+\frac{1}{2}M_P\left(-l\sin\theta_P\dot{\theta}_P\right)^2 \\ &+2\frac{1}{2}I_W\frac{\dot{y}^2}{R_W{}^2}+\frac{1}{2}I_M\dot{\theta}_P{}^2 \end{aligned} \tag{2.10}$$

and, the potential energy function of two wheeled robot is expressed as:

$$V=M_P gl(1-\cos\theta_P)+(M_C+M_P+2M_W)gy\sin\alpha \tag{2.11}$$

where θ_P is angular displacement of the IB, $\dot{\theta}_P$ angular velocity of the IB, $\dot{y}$ linear velocity of the centre point O, M_P mass of the pendulum rod, R_W Radius of the wheel, I_W moment of inertia of the wheel, M_C is the cart mass, and M_W is the wheels mass.

According to the Euler-Lagrangian method, the Lagrangian function is the difference between the kinetic and potential energy of the system as follows:

$$L = \frac{1}{2}M_C\dot{y}^2 + 2\frac{1}{2}M_W\dot{y}^2 + \frac{1}{2}M_P\left(\dot{y} + l\cos\theta_P\dot{\theta}_P\right)^2 + \frac{1}{2}M_P\left(-l\sin\theta_P\dot{\theta}_P\right)^2$$
$$+ 2\frac{1}{2}I_W\frac{\dot{y}^2}{R_W{}^2} + \frac{1}{2}I_M\dot{\theta}_P{}^2 - M_P gl\left(1-\cos\theta_P\right)$$
$$+ \left(M_C + M_P + 2M_W\right)gy\sin\alpha$$

$$L = \frac{1}{2}M_C\dot{y}^2 + 2\frac{1}{2}M_W\dot{y}^2 + \frac{1}{2}M_P\left(\dot{y}^2 + 2\dot{y}l\cos\theta_P\dot{\theta}_P + l^2\cos^2\theta_P\dot{\theta}_P{}^2\right)$$
$$+ \frac{1}{2}M_P l^2\sin^2\theta_P\dot{\theta}_P{}^2 + 2\frac{1}{2}I_W\frac{\dot{y}^2}{R_W{}^2} + \frac{1}{2}I_M\dot{\theta}_P{}^2 - M_P gl\left(1-\cos\theta_P\right)$$
$$+ \left(M_C + M_P + 2M_W\right)gy\sin\alpha$$

$$L = \frac{1}{2}M_C\dot{y}^2 + 2\frac{1}{2}M_W\dot{y}^2 + \frac{1}{2}M_P\dot{y}^2 + \frac{1}{2}M_P 2\dot{y}l\cos\theta_P\dot{\theta}_P +$$
$$\frac{1}{2}M_P l^2\cos^2\theta_P\dot{\theta}_P{}^2 + \frac{1}{2}M_P l^2\sin^2\theta_P\dot{\theta}_P{}^2 + 2\frac{1}{2}I_W\frac{\dot{y}^2}{R_W{}^2} + \frac{1}{2}I_M\dot{\theta}_P{}^2 -$$
$$M_P gl\left(1-\cos\theta_P\right) + \left(M_C + M_P + 2M_W\right)gy\sin\alpha$$

$$L = \frac{1}{2}M_C\dot{y}^2 + 2\frac{1}{2}M_W\dot{y}^2 + \frac{1}{2}M_P\dot{y}^2 + M_P\dot{y}l\cos\theta_P\dot{\theta}_P +$$
$$\frac{1}{2}M_P l^2\dot{\theta}_P{}^2\left[\cos^2\theta_P + \sin^2\theta_P\right] + 2\frac{1}{2}I_W\frac{\dot{y}^2}{R_W{}^2} + \frac{1}{2}I_M\dot{\theta}_P{}^2 -$$
$$M_P gl\left(1-\cos\theta_P\right) + \left(M_C + M_P + 2M_W\right)gy\sin\alpha$$

We get

$$L = \frac{1}{2}M_C\dot{y}^2 + 2\frac{1}{2}M_W\dot{y}^2 + \frac{1}{2}M_P\dot{y}^2 + M_P\dot{y}l\cos\theta_P\dot{\theta}_P +$$
$$\frac{1}{2}M_P l^2\dot{\theta}_P{}^2 + 2\frac{1}{2}I_W\frac{\dot{y}^2}{R_W{}^2} + \frac{1}{2}I_M\dot{\theta}_P{}^2 - M_P gl\left(1-\cos\theta_P\right)$$
$$+ \left(M_C + M_P + 2M_W\right)gy\sin\alpha$$

(2.12)

Using Lagrange's formulation for system dynamics, the following dynamic equation can be expressed for n (DOF) of the system:

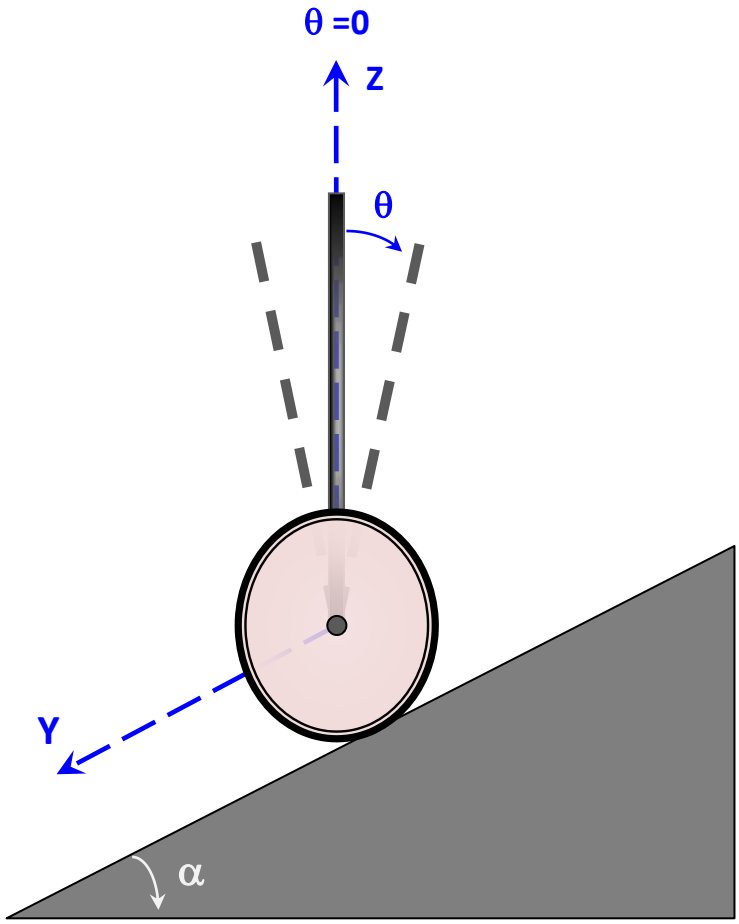

Figure 2.4: Schematic diagram of the robot on an inclined surface

The equations of motion for the robot can be derived using:

$$\frac{d}{dt}\left[\frac{\partial L}{\partial \dot{y}}\right]-\frac{\partial L}{\partial y}=\frac{1}{R_W}\left(T_L-T_R\right)-C\dot{y} \tag{2.13}$$

$$\frac{d}{dt}\left[\frac{\partial L}{\partial \dot{\theta}_P}\right]-\frac{\partial L}{\partial \theta_P}=-l\cos\theta_P \tag{2.14}$$

where T_L is torque of the left wheel, T_R torque of the right wheel and C the coefficient of friction,

$$\frac{\partial L}{\partial y} = -\left(M_C + M_P + 2M_W\right) gy \sin\alpha$$

$$\frac{\partial L}{\partial \dot{y}} = M_C \dot{y} + 2M_W \dot{y} + M_P \dot{y} + 2\frac{I_W}{R_W{}^2} \dot{y} + M_P l \cos\theta_P \dot{\theta}_P$$

$$\frac{d}{dt}\left[\frac{\partial L}{\partial \dot{y}}\right] = M_C \ddot{y} + 2M_W \ddot{y} + M_P \ddot{y} + 2\frac{I_W}{R_W{}^2} \ddot{y} + M_P l \cos\theta_P \ddot{\theta}_P - M_P l \dot{\theta}_P{}^2 \sin\theta_P$$

$$\frac{d}{dt}\left[\frac{\partial L}{\partial \dot{y}}\right] - \frac{\partial L}{\partial y} = M_C \ddot{y} + 2M_W \ddot{y} + M_P \ddot{y} + 2\frac{I_W}{R_W{}^2} \ddot{y} + M_P l \cos\theta_P \ddot{\theta}_P$$
$$- M_P l \dot{\theta}_P{}^2 \sin\theta_P + \left(M_C + M_P + 2M_W\right) g \sin\alpha = \frac{1}{R_W}\left(T_L - T_R\right) - C\dot{y}$$

Let

$$M_C + 2M_W + M_P + 2\frac{I_W}{R_W{}^2} = J\,,\left(M_C + M_P + 2M_W\right) g \sin\alpha = K\,,\frac{M_P{}^2 l^2 \cos^2\theta_P}{M_P{}^2 l^2 + I_M} = F$$

Manipulating are rearranging the following is achieved.

$$\ddot{y} = \frac{1}{J}\left[\frac{T_L}{R_W} + \frac{T_R}{R_W} - C\ddot{y} - 2M_W \ddot{y} - M_P l \cos\theta_P \ddot{\theta}_P + M_P l \dot{\theta}_P{}^2 \sin\theta_P - K\right] \quad (2.15)$$

$$\frac{\partial L}{\partial \theta_P} = -M_P l \dot{y} \dot{\theta}_P \sin\theta_P - M_P g l \sin\theta_P$$

$$\frac{\partial L}{\partial \dot{\theta}_P} = M_P \dot{y} l \cos\theta_P - M_P l^2 \dot{\theta}_P + I_M \dot{\theta}_P$$

$$\frac{d}{dt}\left[\frac{\partial L}{\partial \dot{\theta}_P}\right] = -M_P \dot{y} l \dot{\theta}_P \sin\theta_P + M_P l \ddot{y} \cos\theta_P + M_P l^2 \ddot{\theta}_P + I_M \ddot{\theta}_P$$

$$\frac{d}{dt}\left[\frac{\partial L}{\partial \dot{\theta}_P}\right] - \frac{\partial L}{\partial \theta_P} = -M_P \dot{y} l \dot{\theta}_P \sin\theta_P + M_P l \ddot{y} \cos\theta_P + M_P l^2 \ddot{\theta}_P + I_M \ddot{\theta}_P$$
$$+ M_P l \dot{y} \dot{\theta}_P \sin\theta_P + M_P g l \sin\theta_P = -l \cos\theta_P$$

Rearranging and simplifying, the equation can be written as:

$$\ddot{\theta}_P = \frac{1}{M_P l^2 + I_M}\left[M_P g l \sin\theta_P - M_P l \ddot{y} \cos\theta_P - l\cos\theta_P\right] \tag{2.16}$$

Substituting equation (2.16) into equation (2.15)

$$\ddot{y} = \left\{\begin{bmatrix}\dfrac{\left[\left[\left(\dfrac{2k_m k_e}{RR_W{}^2}\dot{y} + \dfrac{2k_m}{RR_W}v_a\right) - C\dot{y} + M_P l \dot{\theta}_P{}^2 \sin\theta_P - K\right]\right]}{J - (F)}\end{bmatrix} - \begin{bmatrix}\dfrac{\left(M_P l \cos\theta_P \left(M_P g l \sin\theta_P + l\cos\theta_P - M_P l \dot{y}\dot{\theta}_P \sin\theta_P\right)\right)}{\left[\left(M_P{}^2 l^2 + I_M\right)\left(J - (F)\right)\right]}\end{bmatrix}\right\} \tag{2.17}$$

The tilt angle dynamics equation in a two-wheeled robot is thus obtained as follows:

$$\ddot{\theta} = \left\{\begin{bmatrix}\dfrac{\left[(J)\left(M_P g l \sin\theta_P - l\cos\theta_P + M_P l \dot{y}\dot{\theta}_P \sin\theta_P\right) - \left(M_P{}^2 l^2 \cos\theta_P \sin\theta_P\right)\right]}{\left(M_P l^2 + I_M\right)(J) - \left(M_P{}^2 l^2 \cos^2\theta_p\right)}\end{bmatrix} - \begin{bmatrix}\dfrac{\left(M_P l \cos\theta_P \left(\dfrac{2k_m k_e}{RR_W{}^2}\dot{y} + \dfrac{2k_m}{RR_W}v_a\right) - C\dot{y} + K\right)}{\left(M_P l^2 + I_M\right)(J) - \left(M_P{}^2 l^2 \cos^2\theta_p\right)}\end{bmatrix}\right\} \tag{2.18}$$

With the nonlinear dynamics models in equations (2.17) and (2.18), a proper control strategy of the TWRM is designed to stabilise the vehicle on an inclined surface.

2.4 PID controller design

This section briefly introduces the PID control strategy used in this work. PID controllers are very popular and by far the most commonly used today. Most industrial controllers utilize PID control schemes since they are easily tuned to provide robust performance for most control systems. PID controllers can be adjusted by different types of tuning rules (Ogata, 2002) and automatic tuning methods (Lurie and Enright, 2000). PID control loops are becoming quite common in commercial, institutional, and industrial applications. The reason PID controllers are so popular is that using PID gives the designer a larger number of options and those options mean that there are more possibilities for changing the dynamics of the system in a way that helps the designer.

The PID controller minimises the error between a measured process variable and the desired set point. This is achieved by calculating the error and outputting a corrective signal that adjusts the process accordingly to the required amount of control signal and thus minimising the error signal.

The PID controller consists of a proportional, integral and derivative gain values. The proportional gain determines the amount of control signal to the measured error. Thus, reducing the error signal and keeping it minimum however not eliminated. The integral part determines the amount of control signal based on the sum of previous errors. The integral gain results in the reduction of the steady state error values in a system response. The derivative gain of the PID controller affects the transient period of a system response and reduces the system overshoot. The derivative gain is based on the rate of change of the error signal.

Some applications may only require one or two modes to provide the appropriate system control. The absence of the respective control actions, a PID controller will be called a PI, PD, P or I controller. In particular, PI controllers are very common since derivative action is highly sensitive to measurement noise and the absence of an integral value may prevent the system from reaching its target value due to the control action (Ogata, 2002).

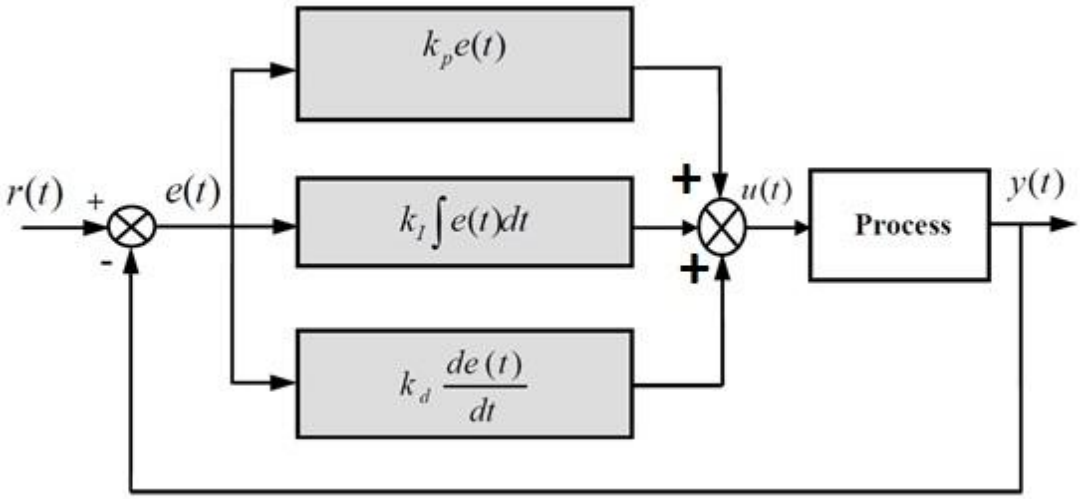

Figure 2.5: PID control diagram

The combination of proportional, integral and derivative control actions, shown in Figure 2.5, has the advantages of each of the three individual control actions. The equation of a controller with this combination can be expressed as:

$$u(t) = K_P e(t) + \frac{k_P}{T_i}\int_0^t e(t)dt + K_p T_d \frac{de(t)}{dt} \tag{2.19}$$

$$G_C(S) = \frac{US}{ES} = K_P\left(1 + \frac{1}{T_i S} + T_d S\right) \tag{2.20}$$

Although PID controllers are suitable many control problems, they can perform poorly in certain applications. When used alone, PID controllers have poor performance when the PID loop gains need to be reduced so that the

control system does not overshoot, oscillate about the control set point value (Ogata, 2002). Thus, PID controllers are used mainly in linear systems. To enhance the performance of the PID controller, a combination of PID controller and other intelligent or adaptive control methods can be used.

Anti-windup is commonly used with PID controllers. Windup is caused by the inter-action of integral action and saturations. Designing the PID controller to account for the effect of saturation will improve its performance by allowing it to operate in the linear region most of the time and recover quickly from nonlinearity. Anti-windup circuitry is one way to achieve this.

In this chapter, the PID will be used to verify the model and test the controllability of the derived model. An intelligent controller will be developed in the upcoming chapters to cope with the uncertainties of the nonlinear model, as well as the challenges of the dynamic payload lifting scenarios.

2.5 PID control system design

A PID control strategy to control the system within the linear region is adapted in this section. The main system parameters to control are the cart displacement and the tilt angle of the intermediate body. The vehicle must balance on an inclined surface and to keep the intermediate body tilt angle at the upright position. In this section, a simulation of the controlled system is presented using Matlab Simulink environment.

Figure 2.6 provides a Simulink block diagram of the control system. As there are two parameters to be controlled in the system, the system is considered a MIMO system with two inputs and two outputs.

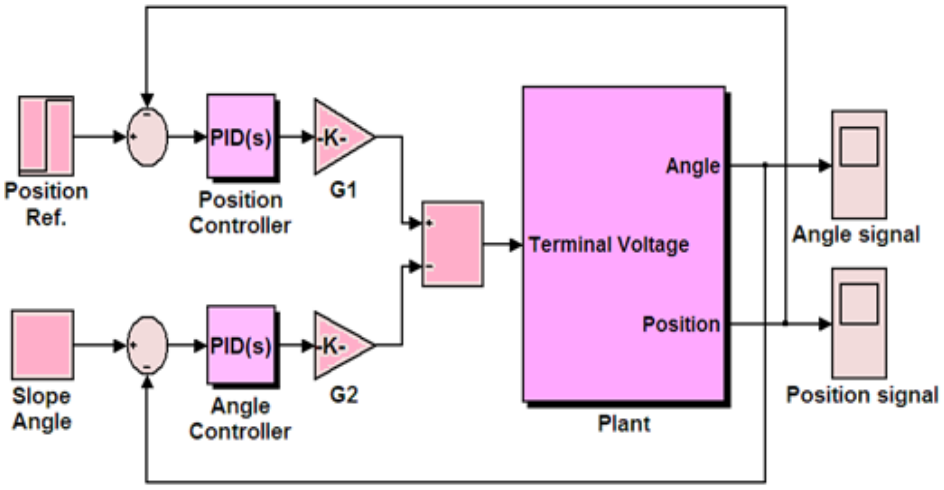

Figure 2.6: Simulink system block diagram

The control strategy is formed by first determining the measured tilt angle and calculating the error according to the desired upright position that is 0 degrees. According to the calculated error, the PID controller outputs the control signal to stabilise the tilt angle at the desired position.

In order to take control of the whole system, two PID controllers are developed as shown in Figure 2.6; one for controlling the angular position of the rod, and the other for ensuring the wheels to stay within a specified linear position from a specific reference position. The system can achieve the desired stability by tuning the PID control gains adequately. At this stage of the research, the PID control gains are tuned heuristically combined with the adjustment of the scaling factors. Table 2.2 gives the control parameters obtained through heuristic tuning.

Table 2.2: Simulation parameters and controller gains

Inclination angle	**Cart displacement controller**	**Tilt angle controller**
5 degrees	Kp= 90, Ki= 100, Kd= 80	Kp= 3 , Ki= 0.25, Kd= 5

The system was simulated initially assuming that the cart is stationary and the rod is held at the upright position. Therefore the initial conditions for the simulation are y = 0 and $\theta_P = 0$. The vehicle is commanded to move within a limited travel distance of 1 meter and to stabilise the tilt angle.

Figure 2.7 shows the cart displacement response. The cart has been successfully stabilised by the controller with the aforementioned gains within approximately 10 seconds. The tilt angle response shown in Figure 2.8 was kept at zero degrees, thus the robot at upright position and stabilised successfully. Overshoots appearing at both responses can be explained by the manual tuning of the PID control gains. The overall response is promising and further improvement and optimal tuning of the control gains may enhance the response characteristics.

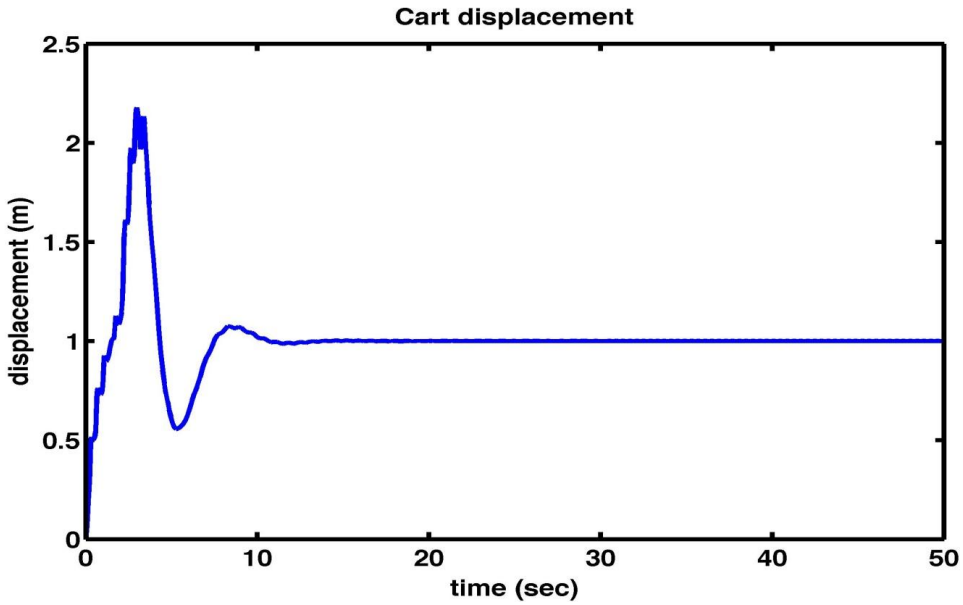

Figure 2.7: Cart displacement

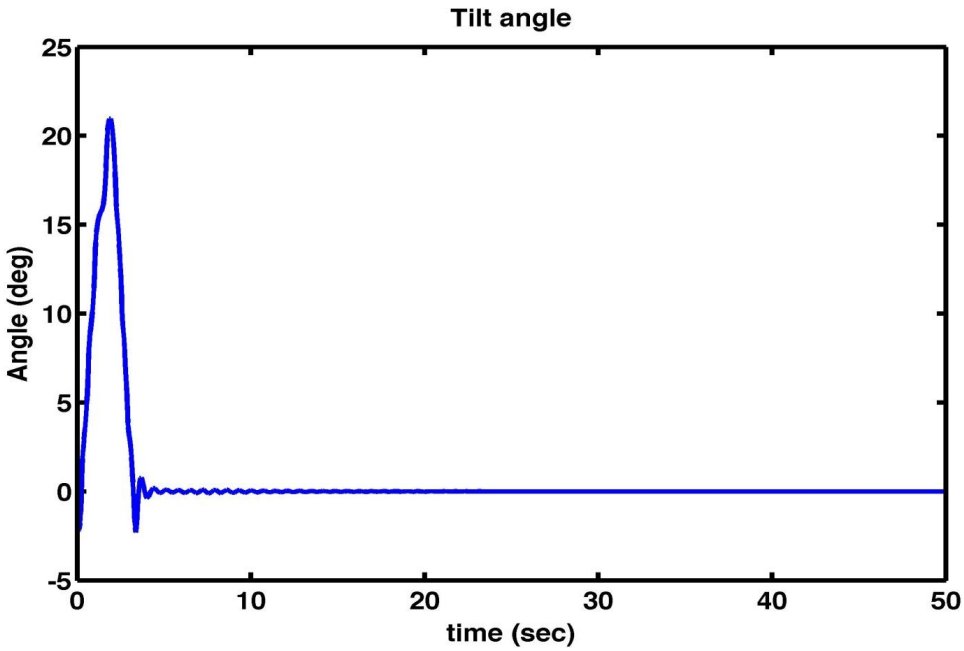

Figure 2.8: Tilt angle response

2.6 Modelling the robot using MSC Visual Nastran

The two-wheeled vehicle is an extremely complex, greatly nonlinear system and coupled nature that needs to be modelled and controlled. It is greatly important to keep up the nonlinear characteristic in the two-wheeled vehicle so that the

method may be easily applied in practice. To achieve this, the two-wheeled vehicle model is developed using a four-dimension (4D) design software named MSC Visual Nastran 4D (VN). Visual Nastran is used within industry in order to better simulate systems, rather than building costly real-world models and then performing experimental tests upon them. These tools enable rapid changes to system design, and test results that can be accurate enough to modify and improve the performance of the system when implemented on the real product. This modelling software can provide visualization of the system behaviour. It is utilised to model the two-wheeled vehicle and to integrate with Matlab/Simulink for control purposes. The two-wheeled vehicle model developed is utilised for designing and testing control systems.

In order to design model of the two-wheeled vehicle, a number of different computer-aided design packages (CAD) were used. Visual Nastran (VN) is 4-dimensional (x, y, z and time) Computer Aided Design software (CAD), which is used to build models of any kind and then simulate the model in real time. Models drawn in other specified CAD programs can be transferred to VN to be simulated. It is a very powerful tool as it gives an exact representation of reality by applying a gravitational force on all parts and then calculating all the forces in each part while showing the simulation per sampling time, which helps the viewer understand the system dynamics thoroughly and instantly. Additionally, the system offers a wide range of modelling and analysis capabilities that can handle any material type and is compatible with most drawing tools such as AutoDesk Inventor, Mechanical Desktop, Solid Edge and Solid Works. VN has various measurement capabilities including measuring forces, torques, friction, velocity and collisions using meters provided in the software environment. VN

also specialises in rendering and animation where simulation video can be captured and replayed at any time. Integration between the designed models with control strategies in Matlab/Simulink environment is also supported.

Due to the great many benefits provided by VN, the two-wheeled vehicle model is developed in this software environment and used as platform for test and verification of control designs.

2.6.1 Body specifications and modelling of the two-wheeled vehicle

To build a real two-wheeled vehicle model, the dimensions of a two-wheeled robot were obtained from a real one available in the department. These dimensions were used in VN so that the structural model will represent the real physical one. This is an important requirement so that the simulated two-wheeled vehicle behaves exactly the same as the real one. A simpler model was developed but with the same basic sizes and functions, as can be seen in Figure 2.9.

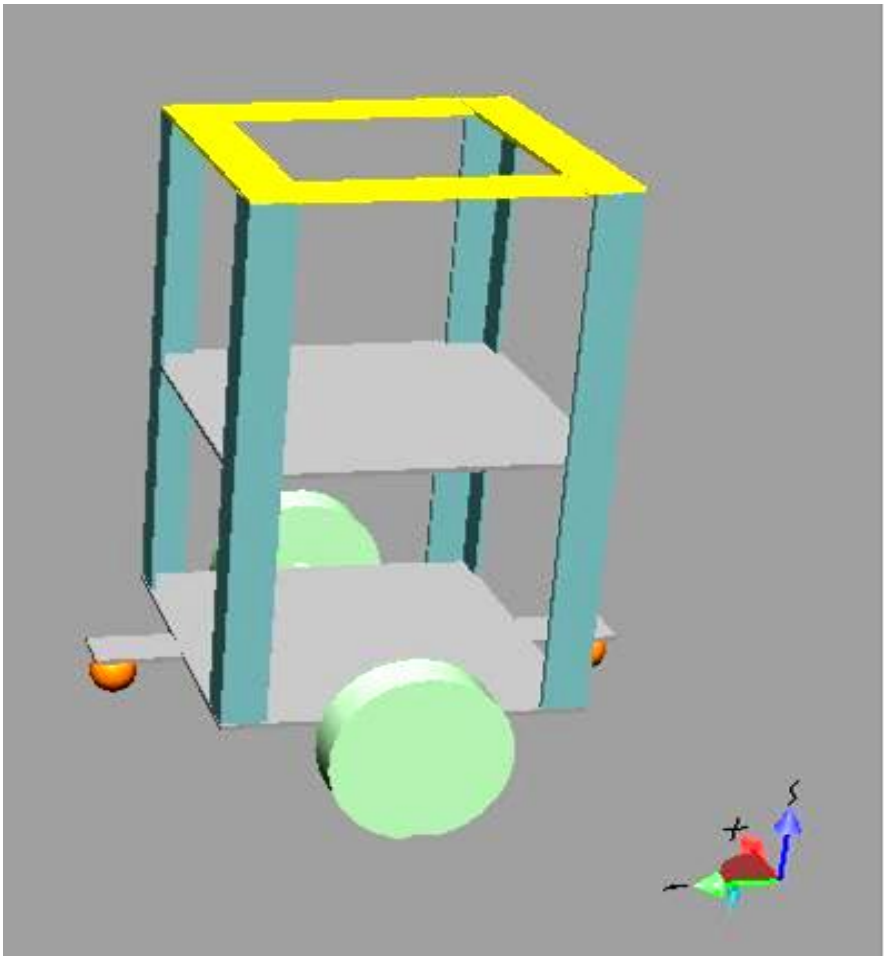

Figure 2.9: Robot 3D model in VN environment

The dimensions and specifications of two wheeled vehicle developed in VN are shown in Table 2.3.

Table 2.3: Model specifications

Part	Mass(Kg)	Radius(mm)	Height(mm)	Width(mm)	Length(mm)
Wheels	0.544	50	25	-	-
Vertical sides	0.116	-	304	25	25
Horizontal Plate (bottom)	0.332	-	3	200	200
Horizontal Plate (middle)	0.332	-	3	200	200
Upper sides (1&3)	0.0349	-	3	140	30
Upper sides (2&4)	0.0499	-	3	200	30
Auxiliary wheel holder	0.0249	-	3	30	100
Auxiliary wheel	0.0722	13	-	-	-

The two-wheeled vehicle that was built in VN has the same structure and specifications as the real one available in the department. This was an important design criterion so that it could be implemented practically in the real situation using the designed controllers.

2.6.2 Visual Nastran integrated with Matlab/Simulink

In order to control and study the behaviour of the systems developed in VN software, integration between VN and Matlab/Simulink is utilised. The VN model is linked as a Simulink block into the Simulink package and the system block diagram can be then formed. The Matlab/Simulink performs the simulation of the control system by measuring the outputs from the VN block

and feeding in the control signals accordingly. Both VN and Simulink are running simultaneously during the simulation. The user is required to specify the input and output parameters to be controlled and measured in the VN icon, as illustrated in Figure 2.10. The VN inputs are typically given in terms of control sliders, while the meters designating to respective plant output constitute the outputs. The schematic diagram of the whole system is presented in Figure 2.10.

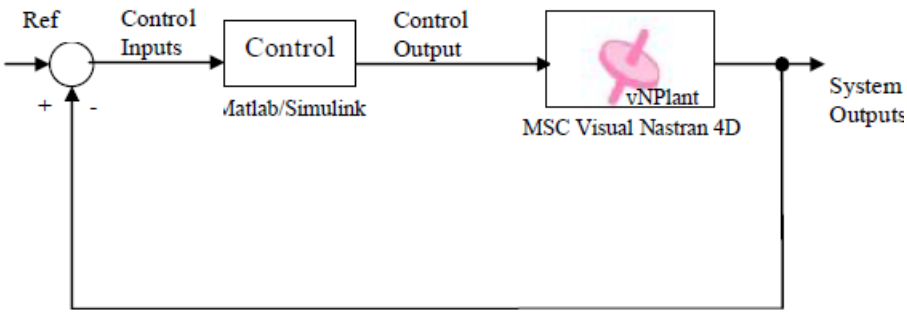

Figure 2.10: Controls and meters between VN and Matlab/Simulink

2.6.3 Control strategy

A control strategy is developed utilizing PID conventional control as the control scheme. The suggested control technique was implemented in Matlab/Simulink with VN for demonstrating the effectiveness of the control scheme for stabilizing and movement of the two wheeled robot. Both controllers (stabilizing and movement) of the two wheeled robot were incorporated into a single structure, as can be seen in Figure 2.11. Based on the tilt angle of the intermediate body and the movement of the robot described by mathematical model in this chapter, it can be seen that they are coupled to each other, thus making the system control more complex. The coupling that exists between the two links can be represented in the PID controller, as shown in Figure 2.11.

Two manually tuned PID controllers were used to control both the tilt angle and the cart displacement. The scaling factors K_1, K_2, K_3 and K_4 are adjusted to balance between the two control loops and to activate the system by generating appropriate output. Table 2.4 gives the control parameters.

To simulate the system in the VN environment, the vehicle is commanded to move on a flat surface for a distance of 0.5 metres while balancing. After 3 seconds, the vehicle is commanded to move a distance of 0.2 metres on an inclined surface of 8 degrees while balancing, therefore moving a total distance of 0.7 metres. At this stage of study and as an initial step of testing the system controllability, two sets of control parameters are used for controlling the system. The first set is suitable for controlling the system while moving on a flat surface and the second set is capable of controlling the system on an inclined surface. A switch is used to select the proper control parameters for the first and second movements in the aforementioned scenario.

Table 2.4: Simulation parameters and controller gains

Inclination angle	**Cart displacement controller**	**Tilt angle controller**
(Flat surface) Zero degrees (From 0 sec to 3sec)	Kp= 1 , Ki= 0.482 , Kd= 0.026	Kp= 50 , Ki= 18.282, Kd= 2.152
(Inclined surface) 8 degrees (From 3 sec to 10 sec)	Kp= 1.692 , Ki= 0.289 , Kd=0.687	Kp=60, Ki= 37.570, Kd = 17.539

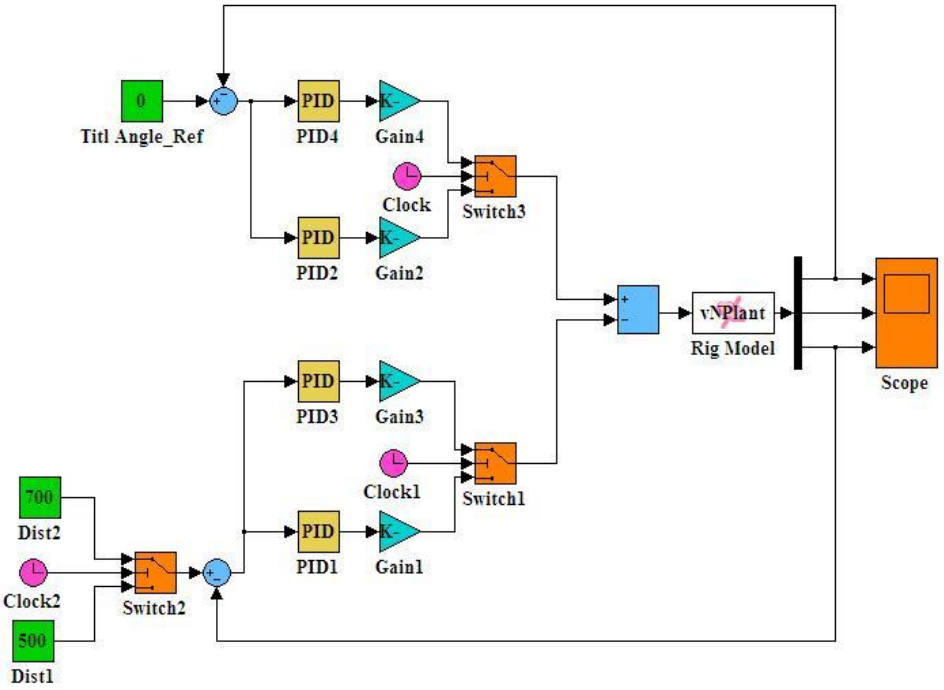

Figure 2.11: Block diagram of the control system using VN

2.6.4 Simulation Results

Figures 2.12 and 2.13 present the responses of the cart distance and the tilt angle respectively, showing a successful control and a stable response. It is noted that oscillations appeared in the tilt angle of the system, due to the manual tuning of the control parameters. Moreover, the hard switching between the two sets of control parameters has caused an overshoot in the tilt angle at approximately 3 seconds of the simulation time. Using optimal control parameters will solve this issue of overshoots.

However, the VN has some limitations regarding the use of online optimisation algorithms and does not provide smooth integration and limits the use of some control strategies. Thus, the Simulink environment will be adopted as the primary simulation package in this research.

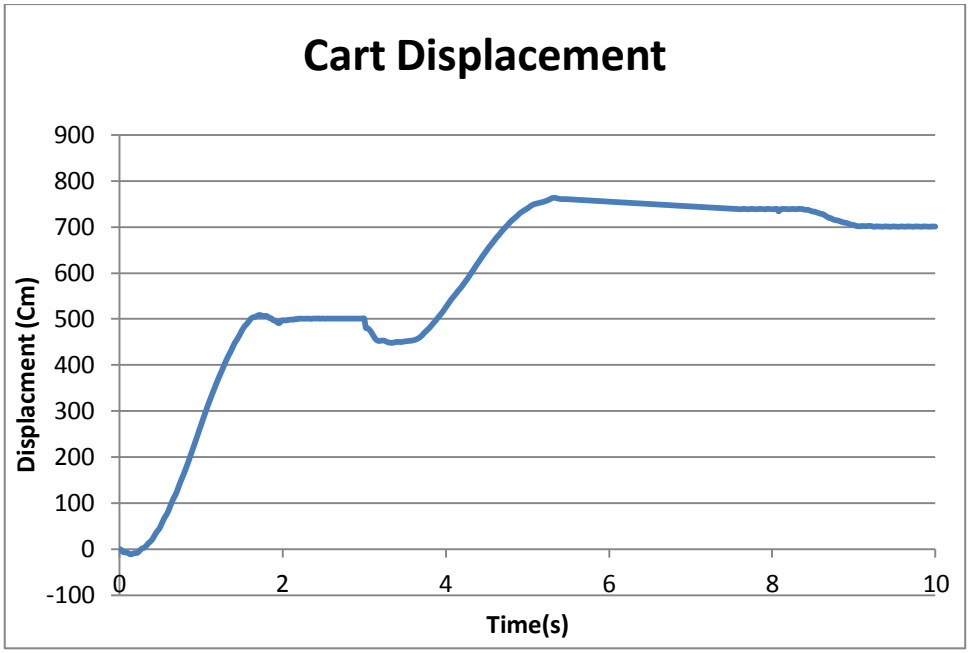

Figure 2.12: Cart distance

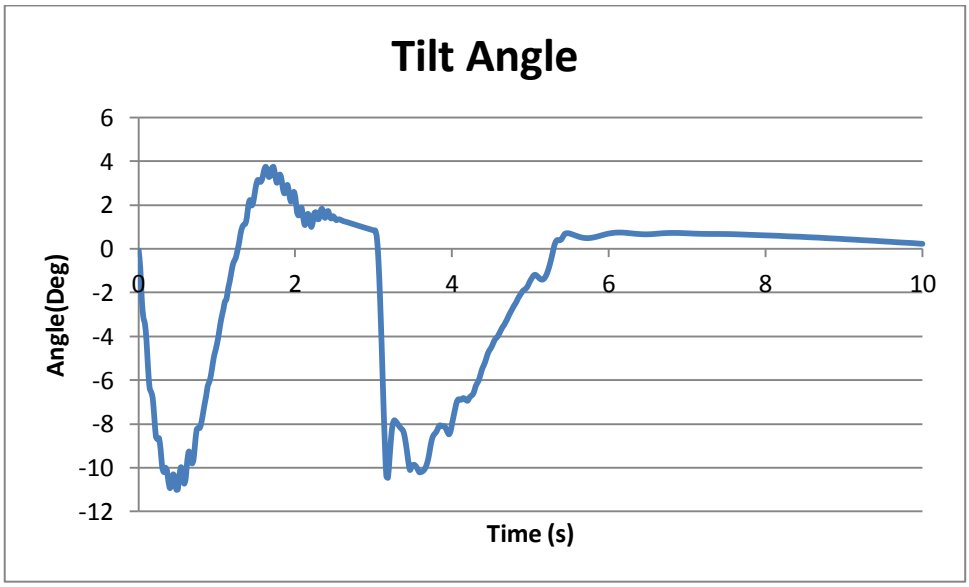

Figure 2.13: Tilt angle of the vehicle

2.7 Summary

This chapter has presented development of two different modelling approaches of two-wheeled robot. The mathematical model derivation of the proposed two wheeled robot machine has been presented in this chapter. The model has been derived using the Euler-Lagrange approach utilising the kinetic and potential energies of the system. The mathematical model has been simulated in the Simulink environment to validate and verify the model with an initial PID control strategy. The PID control has been incorporated into the vehicle model with manual tuning of the control gains. The vehicle was commanded to move within the linear region of the model so that the PID controller will be able to control the system. Promising results have been achived showing a successful stable control of the robot without the load on an inclination surface of 5 degrees. The mathematical model will be used as a basis to derive a more complex model that incorporates a dynamic payload as well as the inclination of the surface. The model will be derived in the upcoming chapter and used with an intelligent control strategy for the two wheeled robot.

To gain more confidence on modelling and visualization, as an alternative, the second approach of virtual physical modelling was made utilising MSC Visual Nastran 4D. It has been used to model two wheeled robot and to integrate with Matlab/Simulink for control purposes. The two wheeled robot model developed has been utilised for designing and testing control strategies.

Two manually tuned PID controllers were used to control both the cart displacement and the tilt angle. The PID control has been tested and has worked well in controlling the two wheeled robot system.

Chapter 3
Modelling and control of two-wheeled vehicle with an extended rod on an inclined surface

3.1 Introduction

All the previous researches have focused on investigating the dynamics and control of two-wheeled robots only on flat surfaces. In reality, mobile robots have to face the challenge of moving on irregular terrains. For humans, inclined surfaces are encountered very frequently in daily life. As mobile robots traverse uneven terrain, dynamic disturbance forces are generated at the contact point between the wheel and the terrain. These forces form the disturbances that perturb the response of the robot.

Chakraborty and Ghosal (2005) have presented dynamic analyses for statically stable wheeled robot. The authors have analysed the robot response with and without slip. Kausar at al. (2010) presented a study of the behaviour of a two-wheeled robot moving on an uneven terrain with a single bump. The authors have utilised gain scheduling control strategy to control the robot. Similarly, Jun et al. (2010) have modelled and presented the equations of motion of a two-wheeled inverted pendulum on an inclined surface. Authors have used Newton-Euler modelling approach to derive the mathematical model of the system. Lee et al. (2009) investigated the control of the inverted pendulum vehicle making an ascent while considering the gravity of the pendulum according to the inclined angle.

In chapter two, the system of the two-wheeled machine was considered to have a fixed payload position. In this chapter the behaviour of a real payload is considered by adding a linear actuator, which activates the payload to move

along the intermediate body with appropriate speeds. The intermediate body of the vehicle comprises a combination of two co-axial parts connected by the linear actuator. Adding a new actuator to the system grants an additional DOF along the intermediate body.

3.2 System description

The intermediate body comprises two coaxial parts connected by a mechanical linear actuator, as shown in Figure 3.1. The actuator is considered to activate the payload so as to move along the intermediate body with prescribed motion characteristics.

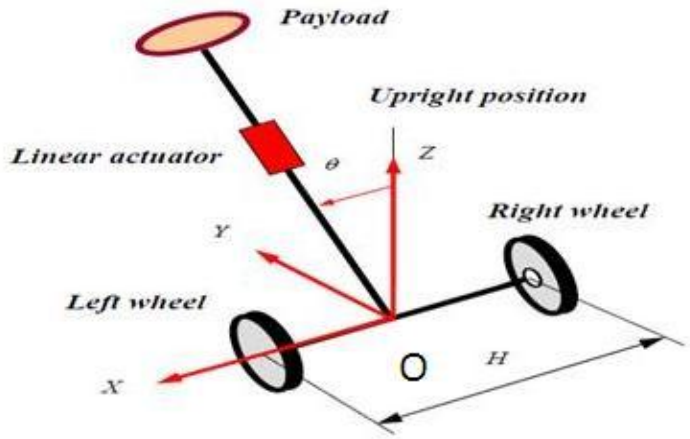

Figure 3.1: Schematic representation of the vehicle with an extended rod

3.2.1 Parts of vehicle

The vehicle with an extended rod is considered to possess the following parts: Two wheels for driving and manoeuvring connected by an axle of length H, with two DC motors driving the wheels. They produce the same torque whether a forward or backward linear motion is assigned to the vehicle. The intermediate body has two coaxial parts connected by an actuator. The lower part of mass M_1 is

connected at its lower end to the wheels axle with a rigid joint and to the linear actuator at the upper end. The upper part of the intermediate body is of mass M_u and is connected to a payload of mass M at the upper end.

During the system analysis, the following assumptions are made:

1. Homogeneous distribution of the mass of each part, and all the vehicle components are considered rigid

2. A disturbance force F_d is applied to the system as an impact force generated by means of a pulse generator in the form of finite pulses

3.2.2 Effect of adding the linear actuator

A linear actuator of mass M_a is used to activate the upper part of the intermediate body and the attached payload. The actuation causes the upper part of the IB and the attached payload to experience a linear motion along the intermediate body, with a displacement Q as shown in Figure 3.2. Due to such motion, the positions of the centres of mass L_u and Lm will depend on the variable Q and in turn the position of the entire centre of mass (COM) of the intermediate body Lg .

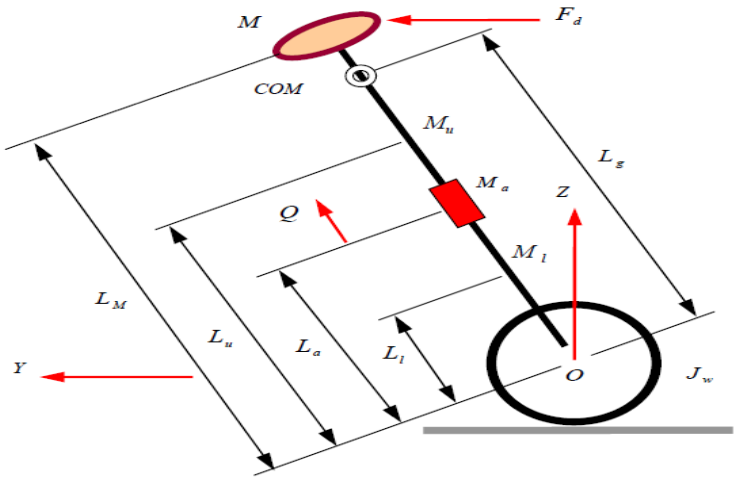

Figure 3.2: Positions of main parts of vehicle *com*

Table 3.1: Nomenclature

Variable	***Description***	***Unit***
L_M	Position of the COM of the payload	m
Lu	Position of the COM of the rod's upper part	m
La	Position of COM of the linear actuator	m
L_l	Position of COM of the lower part of the rod	m
Q	Displacement of the linear actuator	m
Y	Linear displacement of the vehicle	m
θ	The angular displacement of the IB	rad
$\dot{Y}$	Linear velocity of the IB	m/ s
$\dot{\theta}$	Angular velocity of the IB	rad/s
$\ddot{Y}$	Linear acceleration of the IB	m/s^2
$\ddot{\theta}$	Angular acceleration	rad/ s^2
$\ddot{Q}$	Linear acceleration of the attached payload	m/s^2
M_l	Mass of the lower part of the rod	kg
M_a	Mass of the linear actuator	kg
M_u	Mass of the upper part of the rod	kg
M_m	Payload mass	kg
M_w	Wheel mass	kg
M_c	Cart mass	kg
R_w	Radius of the wheel	m
g	Gravitational acceleration	m/s^2
T_C	Kinetic energy of the cart	N.m
T_l	Kinetic energy of the lower part of the rod	N.m
T_a	Kinetic energy of the linear actuator	N.m
T_l	Kinetic energy of the upper part of the rod	N.m
T_m	Kinetic energy of the payload	N.m
V_l	Potential energy of the lower part of the rod	N.m
V_a	Potential energy of the linear actuator	N.m
V_u	Potential energy of the upper part of the rod	N.m
V_m	Potential energy of the payload	N.m
V_c	Potential energy of the cart	N.m
α	Inclination angle	rad

3.3 Mathematical modelling

The system is shown in Figure 3.3 while moving along an inclined surface. Compared to the motion of a two-wheeled vehicle on flat surface, the motion on an inclined surface is considered to be more complex. The system is nonlinear with strong coupling, unstable, and multi-variable. The Lagrange-Euler (LE) modelling method is utilised to derive the equations of motion of the system so as to reduce the complexity. The Lagrange-Euler approach utilizes the use of kinetic and potential energy of the system to derive the dynamic model of the system.

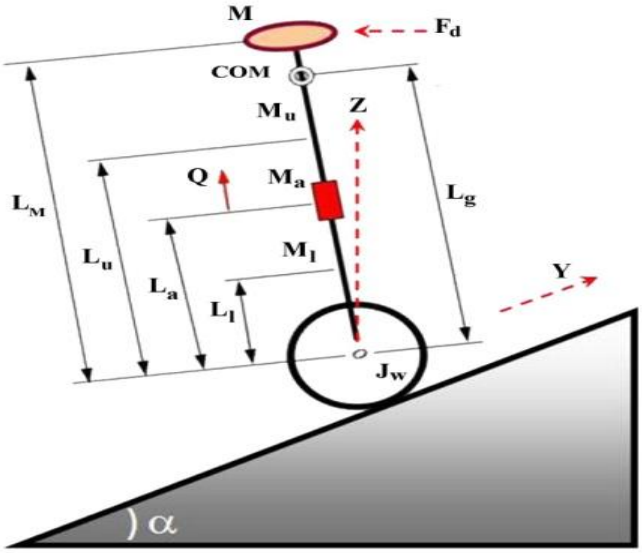

Figure 3.3: Schematic diagram of a single IP vehicle on an inclined plane

3.3.1 Vehicle Lagrangian dynamics

The dynamic equation for a system with n number of Cartesian coordinates can be expressed using the LE approach as follows:

$$\frac{d}{dt}\left(\frac{\partial L}{\partial \dot{q}_i}\right) - \frac{\partial L}{\partial q_i} = Q_i \qquad i = 1,2,..n \tag{3.1}$$

Here, L is the Lagrangian function, Q_i is generalized force vector and q_i is a generalized coordinate. The generalized forces and generalized coordinates representing the system can be formulated respectively in a matrix form as:

$$q_i = \begin{bmatrix} Y & \theta & Q \end{bmatrix}^T \tag{3.2}$$

$$Q_i = \begin{bmatrix} F_c & F_d & Fa \end{bmatrix}^T \tag{3.3}$$

where, F_a is the linear actuator force, F_d is the external disturbance force, F_c is the cart drive force.

3.3.2 System energy requirements

The total energy, the Lagrangian L of the model, can be labelled as the total of potential energy V and kinetic energy T of the system components which comprise of the cart, the lower and upper parts of IB and the attached payload as:

$$T = T_c + T_a + T_u + T_M \tag{3.4}$$

$$V = V_l + V_a + V_u + V_M \tag{3.5}$$

$$L = T - V \tag{3.6}$$

The detailed components of the system kinetic energy can be formulated as follows:

$$T_c = \frac{1}{2} M_c \{(\dot{y}\cos\alpha)^2 + (\dot{y}\sin\alpha)^2\} \tag{3.7}$$

$$T_l = \frac{1}{2} M_l \left\{\left(L_l\dot{\theta}cos\theta + \dot{y}\cos\alpha\right)^2 + \left(\dot{y}\sin\alpha - L_l\dot{\theta}sin\theta\right)^2\right\} + \frac{1}{2} J_l\dot{\theta}^2 \tag{3.8}$$

$$T_a = \frac{1}{2} M_a \left\{\left(L_a\dot{\theta}cos\theta + \dot{y}\cos\alpha\right)^2 + \left(\dot{y}\sin\alpha - L_a\dot{\theta}sin\theta\right)^2\right\} + \frac{1}{2} J_a\dot{\theta}^2 \tag{3.9}$$

$$T_u = \frac{1}{2} M_u \left\{\dot{Q}^2 + \left(L_u\dot{\theta}cos\theta + \dot{y}\cos\alpha\right)^2 + \left(\dot{y}\sin\alpha - L_u\dot{\theta}sin\theta\right)^2\right\} + \frac{1}{2} J_u\dot{\theta}^2 \tag{3.10}$$

$$T_m = \frac{1}{2} M_m \left\{\dot{Q}^2 + \left(L_m\dot{\theta}cos\theta + \dot{y}\cos\alpha\right)^2 + \left(\dot{y}\sin\alpha - L_m\dot{\theta}sin\theta\right)^2\right\} + \frac{1}{2} J_m\dot{\theta}^2 \tag{3.11}$$

where J_l, J_a, J_u, and J_m are the mass moments of inertia of the lower rod, linear actuator, upper rod and the payload respectively around the IB COM. Summing equations (3.7) – (3.11) yields the total kinetic energy of the system as:

$$T_T = \frac{1}{2} C_7 \dot{y}^2 + C_8 \dot{Q}^2 + \dot{\theta}\dot{y}\cos(\theta + \alpha)\{C_{10} + M_u(C_5 + Q) + M_m(C_6 +$$

$$Q + \theta 2\{Q2C12 + C13Q + C14\} \quad (3.12)$$

Similarly, the various components of the potential energy may be formulated as follows:

$$V_c = M_c g(R_w + y\sin\alpha) \quad (3.13)$$

$$V_l = M_l g(L_l \cos\theta + y\sin\alpha) \quad (3.14)$$

$$V_a = M_a g(L_a \cos\theta + y\sin\alpha) \quad (3.15)$$

$$V_u = M_u g\{(C_5 + Q)\cos\theta + y\sin\alpha\} \quad (3.16)$$

$$V_m = M_m g\{(C_6 + Q)\cos\theta + y\sin\alpha\} \quad (3.17)$$

The potential energy of the vehicle can be obtained by summing equations (3.13) - (3.17):

$$V_T = C_{11} y\sin\alpha + \{C_{10} g + M_m g(C_6 + Q) + M_u g(C_5 + Q)\}\cos\theta + M_c g R_w \quad (3.18)$$

Manipulating equations (3.12) and (3.18) yields the Lagrangian function of the system, which can be written as:

$$L = \frac{1}{2}C_7\dot{y}^2 + C_8\dot{Q}^2 + \dot{\theta}\,\dot{y}\cos(\theta+\alpha)\{C_{10} + M_u(C_5+Q) + M_m(C_6+Q)\}$$
$$+ \dot{\theta}^2\{Q^2C_{12} + C_{12}Q + C_{14}\} - C_{11}\,y\sin\alpha -$$
$$\{C_{10}\,g + M_m g(C_6+Q) + M_u g(C_5+Q)\}\cos\theta - M_c g R_w \qquad (3.19)$$

3.3.3 Vehicle dynamic equations

The system equations of motion of the model can be written as:

$$\frac{d}{dt}\left(\frac{\partial L}{\partial \dot{y}}\right) - \frac{\partial L}{\partial y} = F_c \qquad (3.20)$$

$$\frac{d}{dt}\left(\frac{\partial L}{\partial \dot{\theta}}\right) - \frac{\partial L}{\partial \theta} = F_d \qquad (3.21)$$

$$\frac{d}{dt}\left(\frac{\partial L}{\partial \dot{Q}}\right) - \frac{\partial L}{\partial Q} = F_a \qquad (3.22)$$

Manipulating the above equations yields three non-linear differential equations of motion of the robot as follows:

$$C_7\ddot{y} + (C_{15} + C_{16}Q)\ddot{\theta}\cos(\theta+\alpha) - (C_{15} + C_{16}Q)\dot{\theta}^2 sin(\theta +$$
$$\alpha + C16Q\,\theta\cos\theta + \alpha + C11sin\alpha = Fc \qquad (3.23)$$

$$(C_{18} + QC_{16})\ddot{y}\cos(\theta+\alpha) - (C_{18} + QC_{16})\dot{y}\,\theta\, sin(\theta +$$
$$\alpha \quad C16 \quad Q\,y\cos\theta + \alpha + 2\theta \quad (C12Q2 + C13Q + C14) + \theta$$
$$(4C_{12}Q + 2\,C_{13}\dot{Q}) + \dot{y}\dot{\theta}^2 sin(\theta+\alpha)\{C_{10} + M_u(C_5 + Q) +$$
$$MmC6 + Q - \theta\sin\theta\ C10g + MugC5 + Q + MmgC6 + Q = Fd \qquad (3.24)$$

$$2C_8\ddot{Q} - C_{16}\dot{\theta}\dot{y}\cos(\theta+\alpha) - 2C_{12}Q\,\dot{\theta}^2 - C_{13}\,\dot{\theta}^2 - C_{16}g\cos\theta = F_a \qquad (3.25)$$

Detailed explanations of the constant parameters appearing in Equations (3.12) - (3.25) are formulated in Appendix (A).

3.4 Fuzzy logic control design

The two-wheeled robot is both a very complex and extremely nonlinear system, with many complicated characteristics to be modelled requiring exceptional control methodologies. The conventional control systems are limited by the change in the plant dynamics with actuator saturation and time, increasing the nonlinearity of the system (Lin et al., 1996). When the payload rapidly varies these techniques suffer from tracking error and overshoot during transients. The use of FLC methods could be an interesting alternative to investigate (Mamdani, 1974, Mamdani and Assilian, 1975, Zadeh, 1965, 1973).

Several industrial processes are uncertainties, with un-modelled plant dynamics and extremely nonlinear. Human knowledge is therefore becoming increasingly important in the design of control systems. In many practical problems fuzzy control has been successfully utilised, especially where classical control systems do not result in acceptable performance.

In comparison to conventional controllers, fuzzy controllers have significant differences. They are dependent upon the operating experience and physical knowledge of the control process. Mathematical models of the plant are not used, as producing them can be extremely time consuming and expensive. Strategies are generated based on verbal communication. As the rules are written verbally the fuzzy sets are also defined verbally when the system demonstrates uncertainties, non-linearities and un-modelled dynamics, FLC is

very effective as it can be said to be able to produce smooth control and robust behaviour (Mahfouf, 2004).

When considering the behaviour of motor systems and muscles in humans, there is a certain degree of fuzziness present. This is due to the lack of mathematical representation of their behaviour. The underlying mechanics of fuzzy logic controllers are presented linguistically rather than mathematically and are therefore model-free. Fuzzy logic controllers are highly functional in several scenarios, including where a system is hard to model, where a system is controlled by a human worker, or where there is a high level of vagueness. A typical fuzzy system comprises of a rule-base, membership functions (MFs), and an inference procedure. A brief description of the fuzzy logic paradigm follows.

In 1965 Lotfi Zadeh first proposed the idea of fuzzy set system. The central premise was that humans do not reason in terms of separate numbers and symbols, but rather in terms of fuzzy sets. The implementation of a fuzzy logic controller to a steam engine was performed by Mamdani in 1974. Subsequently, many practical applications of fuzzy logic were developed, including the Subway Sendai Transportation control system in Japan in 1984, automated aircraft vehicle landing in 1987 and the first fuzzy TV set by Sony in 1990. Today there is an enormous amount of fuzzy logic intervention and related projects. Fuzzy logic systems are utilized as influential apparatuses in a variety of different areas for example medicine instrumentation, industry and robotics (Mahfouf, 2004).

In the areas of inverted pendulum and two-wheeled robot, fuzzy-based control has been used to an extended level. A predictive fuzzy control method

on a two wheeled machines for steering was implemented by Shi et al. (2004). Based on fuzzy logic theory Hladek (2007) applied a multi-agent fuzzy expert system for robotic soccer control. Maravall et al. (2005) built a hybrid fuzzy control system by incorporating PD control into a Takagi-Sugeno fuzzy control structure in order to stabilize an inverted pendulum. (FLC) can be considered as a method of changing expert information into an automatic control strategy where complete knowledge of the system is lacking. A hybrid fuzzy controller for robotic systems was proposed by Zadeh (1973) and Sun and Er (2004), which combined a fuzzy PID controller and a fuzzy gain scheduling technique in order to solve nonlinear control problems.

3.4.1 PD like fuzzy control scheme

Fuzzy controllers have been utilised in numerous control environments, including industrial control, quality control, elevator control and scheduling, traffic control, train control, automobile engine control, steel manufacturing, paper manufacturing, power distribution control, and various other applications. Figure 3.4 presents a general scheme of the fuzzy control system where r is a reference signal, y is the measured signal, e is the measured error and u is the control signal.

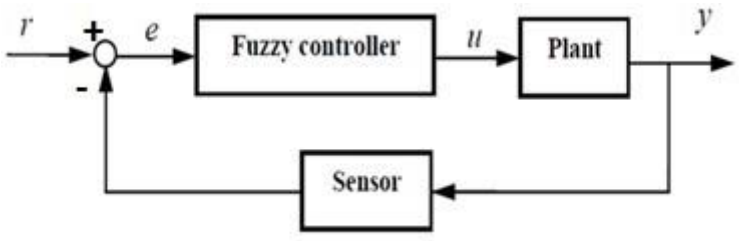

Figure 3.4: General scheme of fuzzy control system

A fuzzy controller, often (though not always) a fuzzy PD, consists of a dynamic and a fuzzy part as described in Figure 3.5, where e_p and e_D are the error and derivative of error of a signal at a time k.

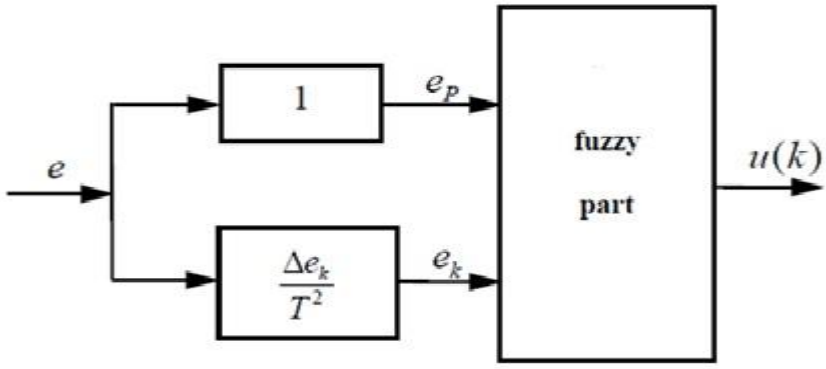

Figure 3.5: Inner structure of fuzzy PD controller

Linguistic knowledge about proper plant control is contained in the fuzzy part of the controller. There is also an inner structure as presented in Figure 3.6, where R_i is the i_{th} control rule, B_j is the J_{thi} singleton representing output fuzzy sets. The rule base of the controller is contained in the block 'inference engine'.

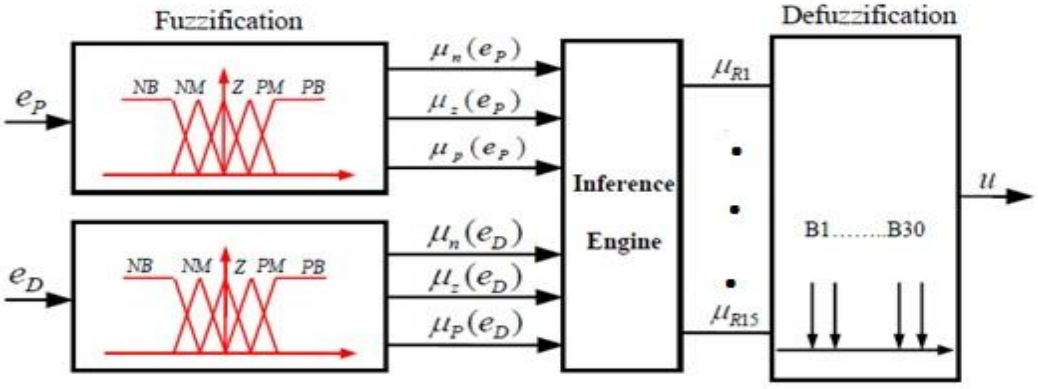

Figure 3.6 Part of the fuzzy PD controller

The mathematical model of a two-wheeled robot on an inclined surface is too complex. Attempting to describe the mathematical model of the system can seriously inhibit the development of the real system's model because of the numerous suppositions that must be made for simplification purposes in order to

derive mathematical equations of the system. Thus, various essential characteristics or considerations may be overlooked while deriving the equations.

In order to keep the features of the complex two-wheeled robot when compared to the actual structure, the basic mathematical model itself is insufficient. This is because the human level of dissatisfaction with the classical modelling method will grow as the complexity of the system increases. Thus, the use of expert human knowledge and would be a better consideration in system modelling. Implementing a computational intelligence approach may accomplish this.

3.4.2 Proportional-Derivative plus Integral fuzzy logic control

The control approach utilises the combination of PID control and FLC. The PID part of the controller would allow specific gains to be modified, based on the desired response, while FLC will add robustness to the controller to cope with disturbances and changes in the simulation scenario.

The controller consists of three control loops: a cart displacement controller, a tilt angle controller and a payload displacement controller. The system block diagram is presented in Figure 3.7. The first control loop aims to control the cart wheels to converge to the desired displacement. The second controller stabilises the pendulum tilt angle at the upright position and the third controller aims to control the lifting of the payload to the desired height. The inputs for the PD + I FLC are change of error, the error signal and the sum of previous errors (Figure 3.8). The system inputs are the driving force F_c the linear actuator force F_a and a disturbance force F_d.

The FLC inference engine is of Mamdani-type with a total of 25 fuzzy rules, as presented in Table 3.2. The generation of the fuzzy rules-base is based on the required system performance to minimize the system error between the output signal and the desired signal. Depending on the system, it may not be necessary to evaluate every possible input combination since some may rarely or never occur. Fewer rules can be evaluated, thus simplifying the processing logic and perhaps even improving the FL system performance. Increase the rule base size and complexity may also increase the quality of the control. The membership functions are of Gaussian type to allow smooth inputs and outputs, Figure 3.9.

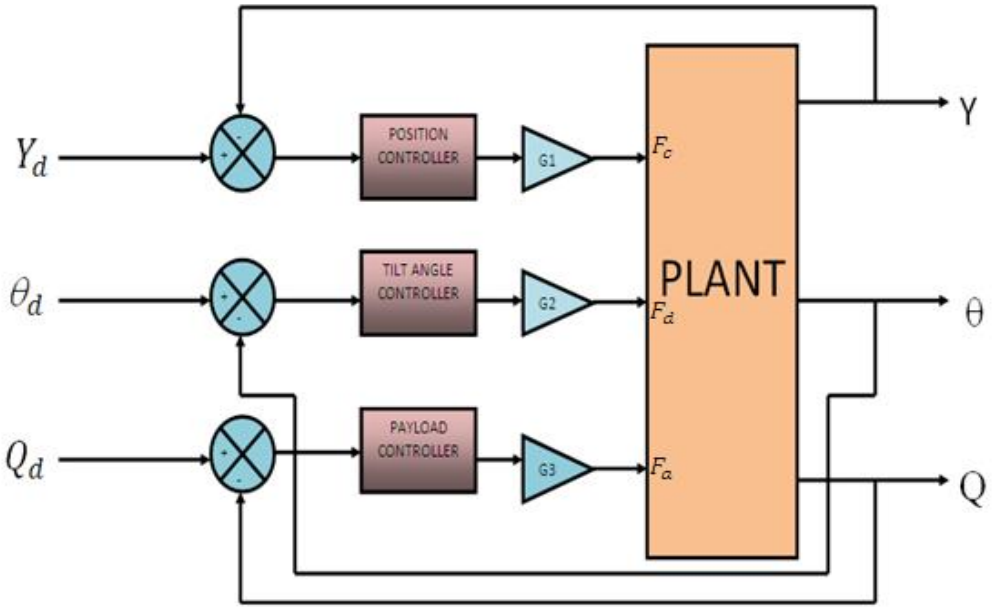

Figure 3.7: System block diagram

Table 3.2: Fuzzy rule base

e|ê	NB	NS	Z	PS	PB
NB	NB	NB	NB	NS	Z
NS	NB	NB	NS	Z	PS
Z	NB	NS	Z	PS	PB
PS	NS	Z	PS	PB	PB
PB	Z	PS	PB	PB	PB

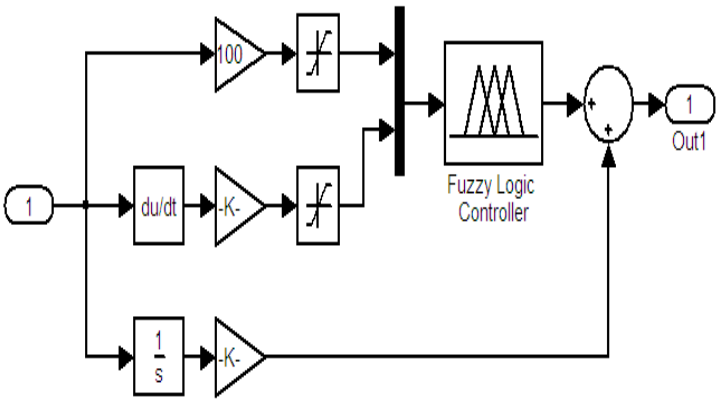

Figure 3.8: Fuzzy PD+I Controller

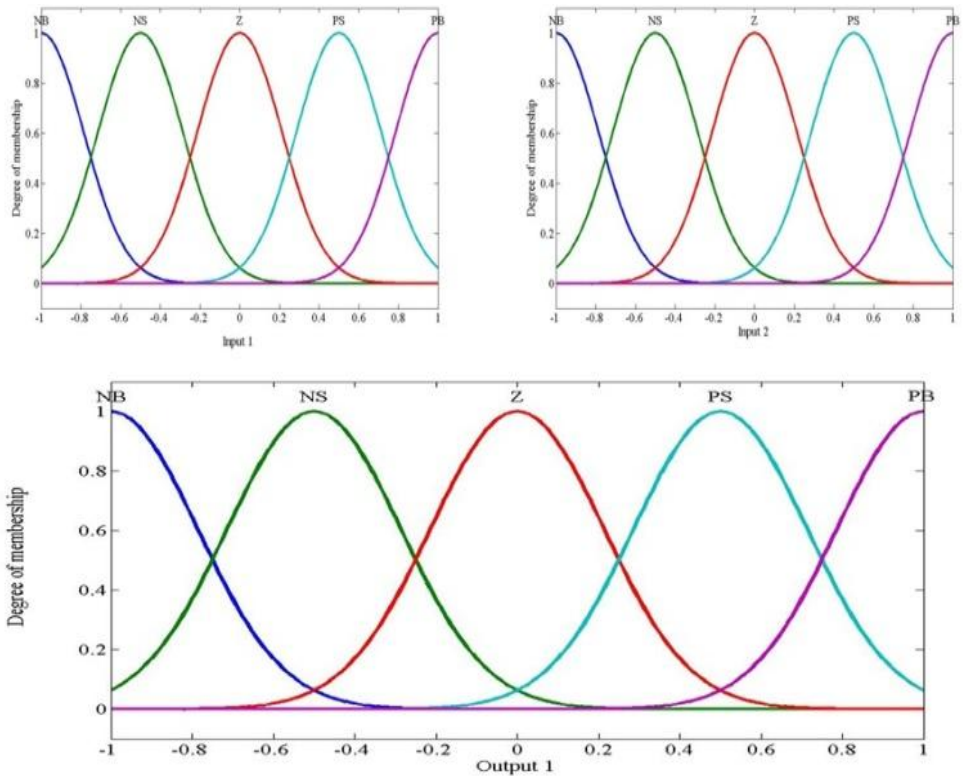

Figure 3.9: Gaussian fuzzy membership functions

3.4.3 Open loop and system loop interaction

The system was built in the Matlab Simulink environment and the open loop response obtained is shown in Figures 3.10 and Figure 3.11. The system is unstable by nature and of a highly coupled nature. This can be verified by observing the interaction among the system loops.

The loop interaction was simulated by changing the control gains of one loop of the system and observing the effect on the system response. Figure 3.12 and Figure 3.13 demonstrate the system response by detuning the parameters of the cart control gains. The tilt angle was clearly affected, thus verifying the coupling of the system parameters. The interaction of the loops is considered a barrier in tuning the control gains. Therefore, an intelligent control strategy such

as the FLC would overcome the uncertainties of the system due to the system coupling.

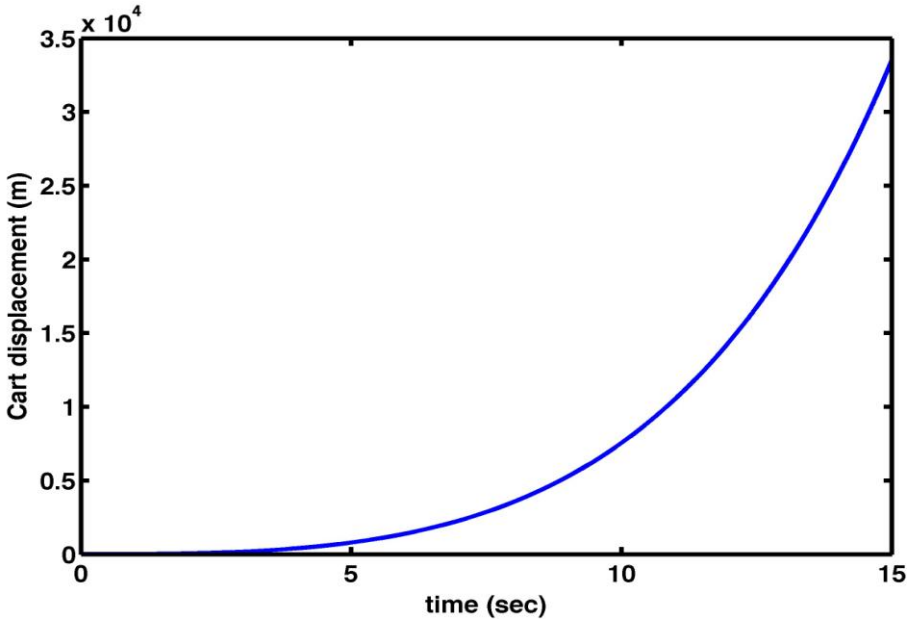

Figure 3.10: Cart displacement open loop response

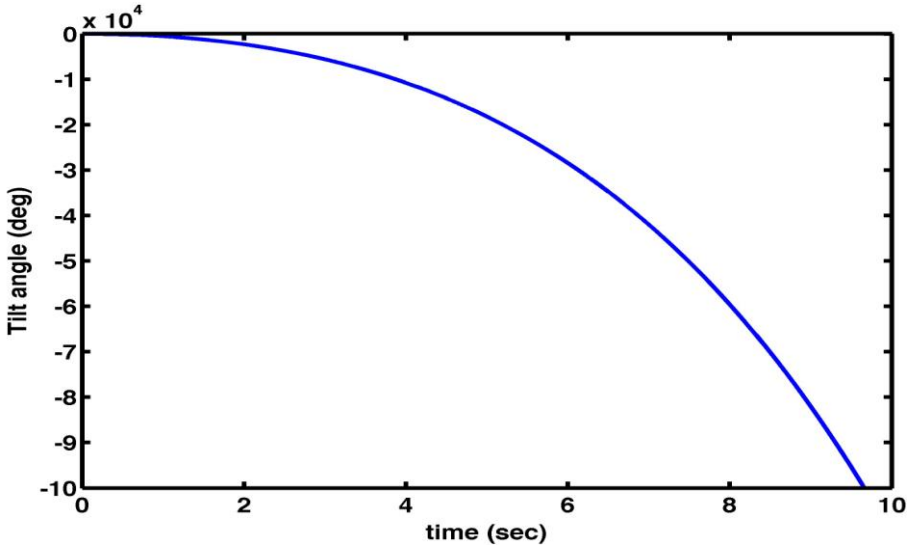

Figure 3.11: Tilt angle open loop response

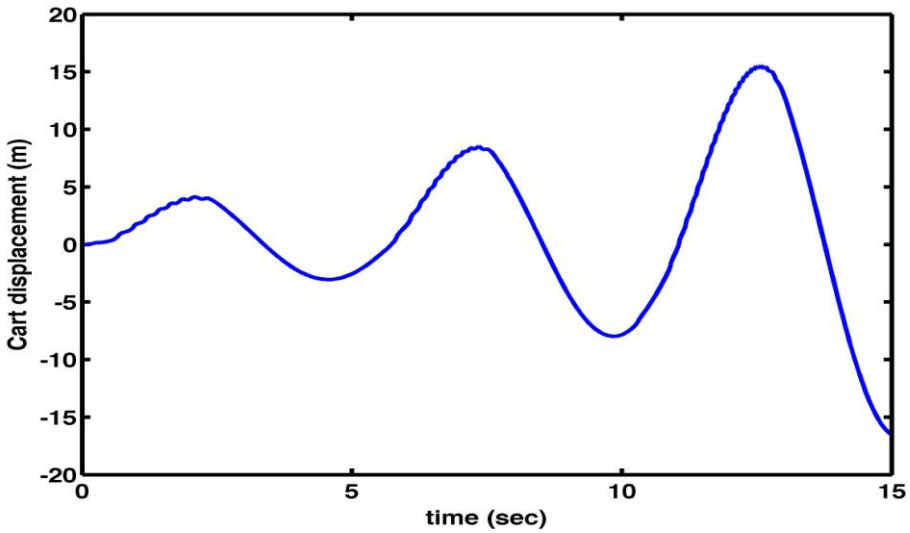

Figure 3.12: Impact of the loop interaction on the cart displacement response

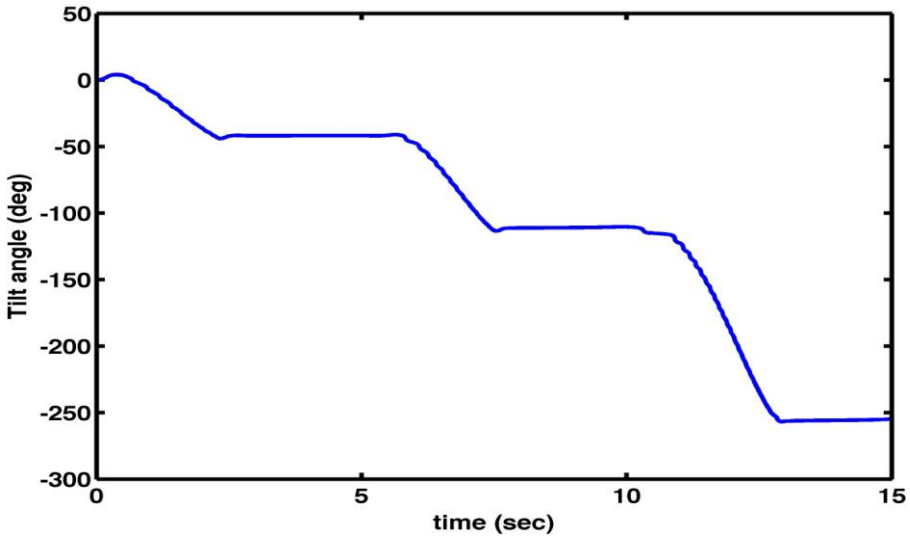

Figure 3.13: Impact of the loop interaction on the tilt angle response

3.4.4 Simulations of the system with the FLC strategy

The model was built and simulated in Matlab Simulink environment. The simulation parameters used were M=3 kg, M_m=0.3 kg, M_l=1.5 kg, M_a= 0.8 kg, M_u= 1.5 kg, M_c = 10 kg, J_a = 0.003025 kg.m^2, J_u = 0.005 kg.m^2, J_w = 0.225 kg.m^2, J_l =0.005 kg.m^2. The FLC control gains were tuned heuristically at this stage of the research and are presented in Table 3.3.

Table 3.3: FLC control gains

Loop / Parameter	***Kp***	***Ki***	***Kd***
Cart displacement	300	1	50
Tilt angle	120	0.3	10
Payload actuator	90	0.07	30

The system is commanded to move within 0.8m of cart displacement, as a tentative simulation procedure, and to lift up the payload to 0.2m while keeping the tilt angle at the upright position, i.e. zero degree angle. The simulation results are shown in Figure 3.14, it is noted that the proposed controller was capable of tracking the reference input with a satisfactory response and a reasonable overshoot. The system settled within 4 seconds. Figure. 3.15 shows the response of the tilt angle; it can be easily observed that the tilt angle was maintained at zero degree at all times with little initial oscillations before the system settled. Fig 3.16 shows that the control technique used was able to achieve the target point of the linear actuator and achieved a good result. It can be noted that the controller was able to stabilise the robot within the upright position and followed the predefined signals of both the cart displacement and the payload desired height.

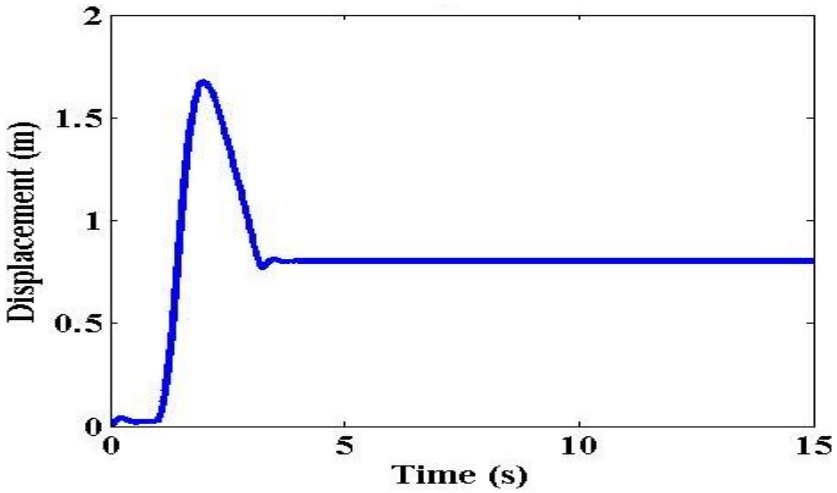

Figure 3.14: Cart displacements response

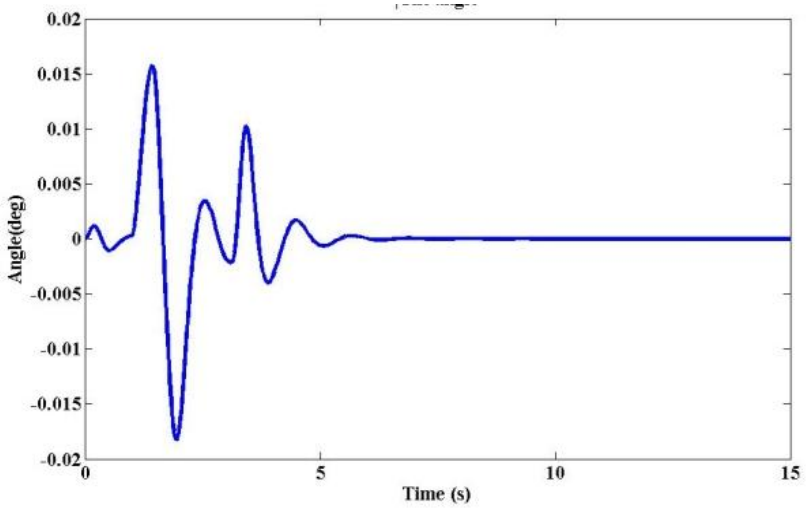

Figure 3.15: Tilt angle for different inclination angles

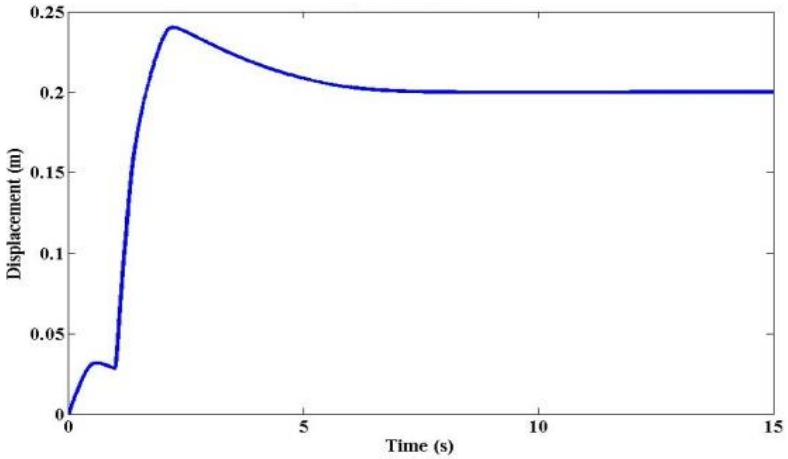

Figure 3.16: Payload displacement

Figure 3.17 - Figure 3.19 show the control efforts exerted by each controller to stabilise the vehicle. The control efforts exerted by the cart controller and payload controller were high when compared to the tilt angle controller. This is due to the heuristically-tuned control gains which are relatively large. To verify the model and the system ability to drive on an inclined surface, the vehicle was commanded to balance on an inclined surface of 10 degrees with a limited travel distance of 0.8 meters. Figure 3.20 – Figure 3.22 show the vehicle response on an inclined surface. The control strategy has successfully stabilized the vehicle on the inclined surface with an overall good response. The cart was stabilized within approximately 8 seconds while the tilt angle had a settling time within approximately 10 seconds. The payload was lifted to the demanded height of 0.2 meters and was stabilized successfully. Figures 3.23 – 3.25 present the control effort exerted to stabilize the vehicle. At this stage of the study, the gain parameters were tuned manually, thus leading to a larger amount of exerted control efforts as well as a good response of the overall system. A proper tuning of the control gains would improve the overall system response and may improve the exerted control efforts. In the next chapter, a BFA optimisation algorithm is demonstrated.

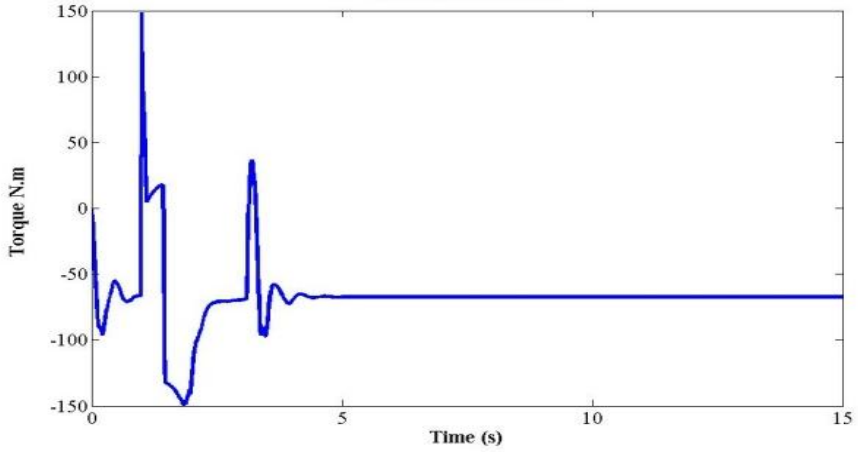

Figure 3.17: Cart displacements controller effort

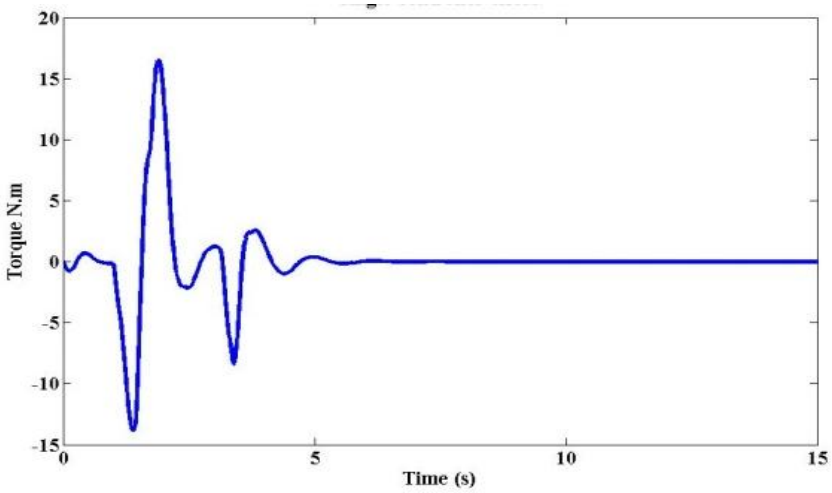

Figure 3.18: Tilt angle controller effort

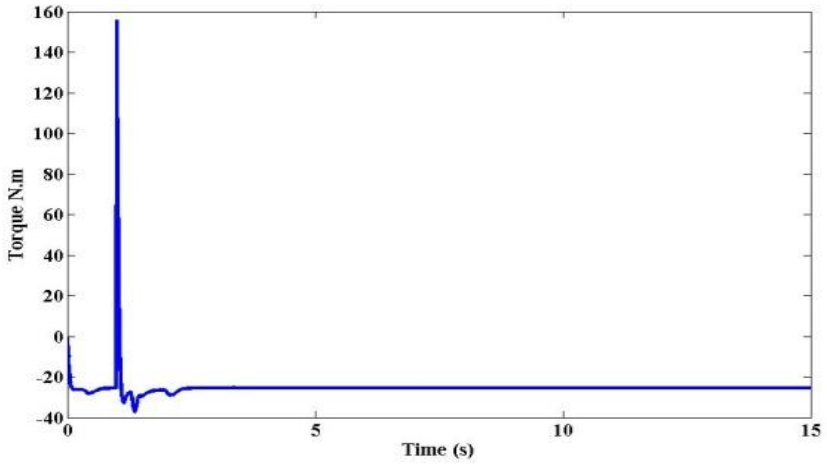

Figure 3.19: Payload controller effort

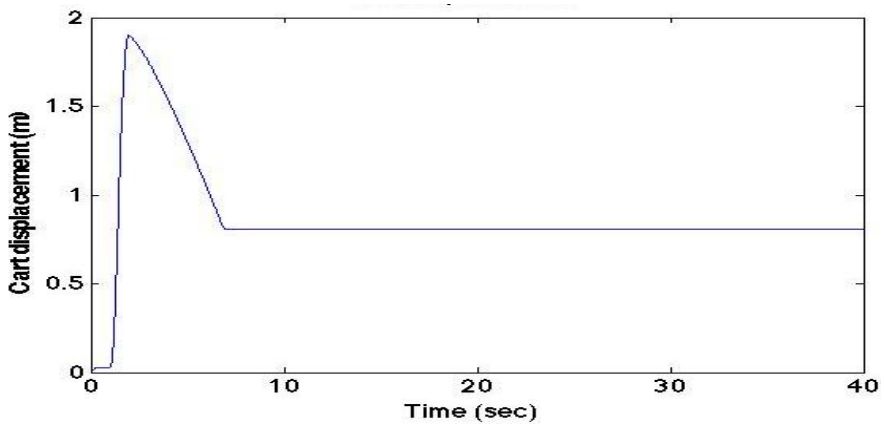

Figure 3.20: Cart displacements response on an inclined surface of 10 degrees

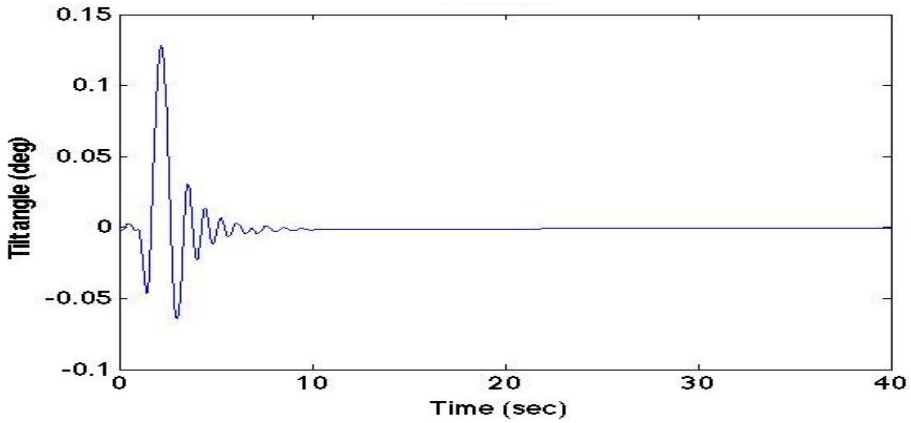

Figure 3.21: Tilt angle response on an inclined surface of 10 degrees

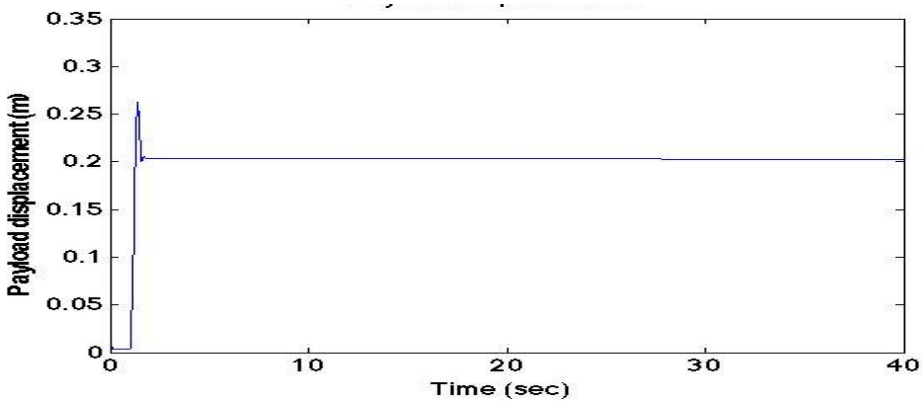

Figure 3.22: Payload displacement response on an inclined surface of 10 degrees

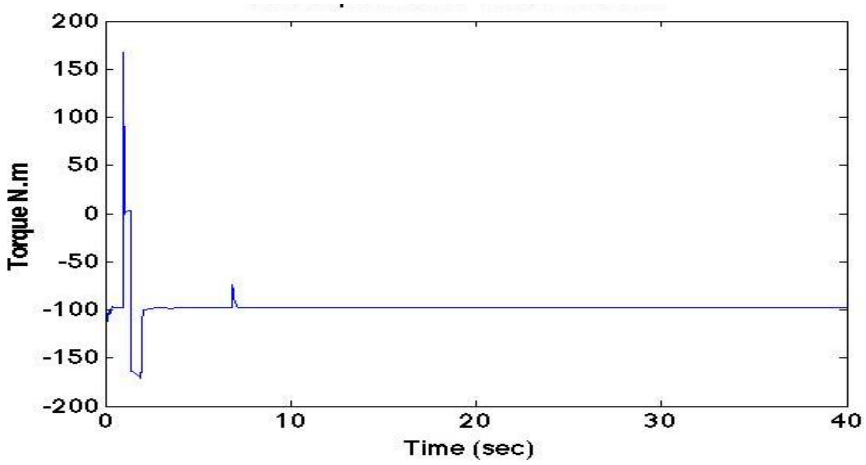

Figure 3.23: Cart displacements controller effort

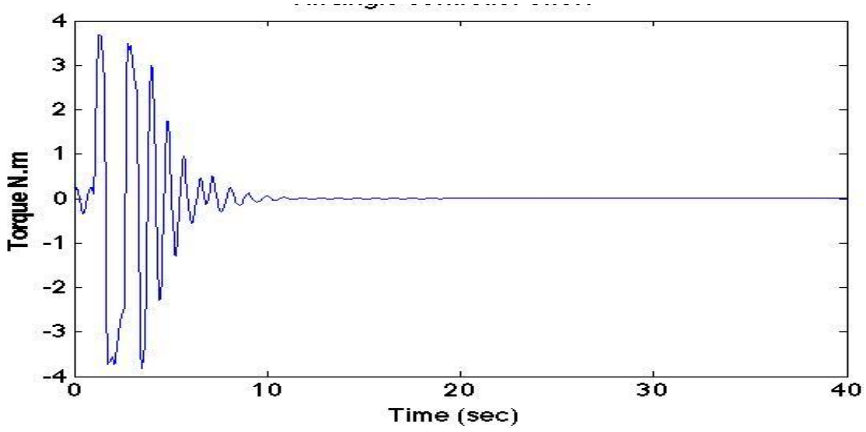

Figure 3.24: Tilt angle controller effort

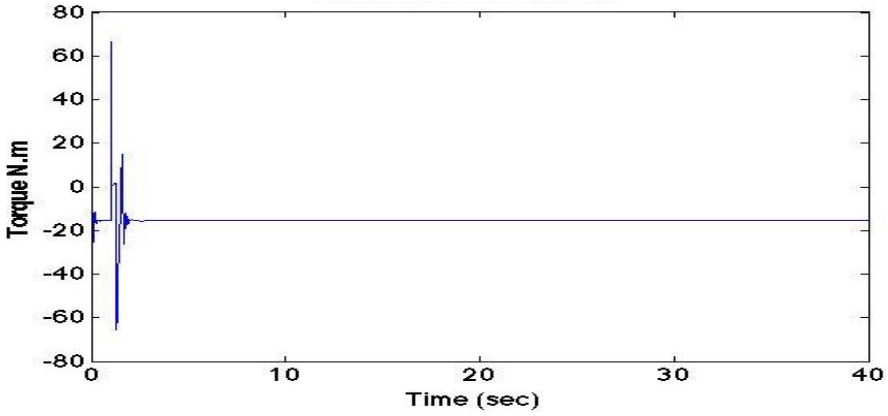

Figure 3.25: Payload displacement controller effort

3.5 Summary

Mathematical model, based on Lagrangian dynamic formulation, of a new type of two-wheeled robotic machine system with an extended rod on inclined surface has been derived and the equations of motion a presented. The presented hybrid controller consists of PD+I FLC controller to stabilise the system. The FLC is of a Mamdani-type inference engine with 25 fuzzy rules-base and Gaussian membership functions. A three-loop control scheme has been presented and applied. The model was simulated in the Matlab Simulink environment and successfully stabilized. Three control algorithms have been used; a PD plus FLC (PD+I FLC) controllers. The control system utilised was capable to reach the balance condition and payload vertical motion with limited overall system oscillations on different inclined surfaces. The results were satisfactory with the control technique used. Additional work will be executed to develop system response by optimising the FLC and applied different control approaches.

Chapter4
Optimisation of the vehicle with an extendable intermediate body

4.1 Introduction

The optimisation techniques proposed depend upon what specific objective is to be achieved. The selection of the objective may vary from one system to another. In optimizing the controllers of inverted pendulum systems, such as those found in two wheeled vehicles, evolutionary algorithms have been utilized. For example, GA optimization LQR technique was validated on an IP system by Ha et al. (1996) in this case GA was utilized in order to choose the weight matrices for the LQR controller. The technique adequately stables the pendulum system, showing acceptable results. A genetic optimization algorithm was also employed by Ahmad et al. (2009), the GA was utilized to tune the input and output scaling factors of the (FLC) for balancing a two-wheeled wheelchair. Solihin et al. (2009) used PSO to tune a state-feedback controller for swinging up an inverted pendulum.

Currently, optimization algorithms play a critical role and are acknowledged as an effective apparatus in tackling real issues in several fields Zang et al. (2010), Neri and Cotta (2012) with implementations in various problem, along with the range of options from various categories (i.e. bio-inspired, nature-inspired, etc.), means that optimization algorithms are the best approaches in solving a problem, and for this reason they have continuously received attention from researchers around the world. Bacterial foraging algorithm (BFA) (Passino, 2002) is a popular optimisation algorithm. BFA has

not been reported yet for control of two-wheeled vehicles. QABFA is focusing on improving the BFA convergence in terms of speed and accuracy (Supriyono and Tokhi, 2012)

A Lagrangian based plan was utilized in previous chapters to obtain the vehicle dynamic equations. There are three essential dynamic exercises carried out in both the modelling process and the control phase: the angular movement of the intermediate body around X hub, straight movement of the whole system in the Y course and straight movement of the payload along the vehicle intermediate body.

The control strategy applied in the previous chapters showed robustness. The control method applied indicated strength of the fuzzy PD - like combined with integrator (PD + I FLC) control scheme. In this chapter, the implementation after design of a PD + I FLC control system is done using quadratic adaptive bacterial foraging algorithm (QABFA) as an optimization scheme for the two-wheeled vehicle. Following bacterial foraging algorithm (BFA) optimization, a new approach for controlling the vehicle is introduced.

4.2 Bacterial foraging algorithm

Bacterial Foraging Algorithm is a bio-inspired algorithm developed based on the foraging strategy of Escherichia Coli bacteria population. It is possible to divide the algorithm into three distinct stages, specifically chemotaxis, reproduction and elimination and dispersal. Of these three it is the chemotaxis stage that is the most prominent, and it determines the performance of the algorithm. In this stage bacteria travel at random through tumble and swim actions. A tumbling action is where the bacteria move at random one step in the region of their initial

position in order to find a possibly better position. If such a position is discovered, then the bacteria will continuously swim a small number of steps more towards that course. This random approach is a very efficient method and may assist the algorithm in locating a global optimum solution. There is, however, an important problem in the chemotaxis stage that needs to be addressed. In the original BFA a constant step size, C, is utilized for the bacteria to travel from one position to another. This may keep the algorithm from accomplishing the required high levels of accuracy and rapid convergence speed. Additionally, it causes bacteria in the population to have an equal step size for all iterations, limiting the movement of the bacteria inside the search zone. Determining a large step size value may lead to great investigation and more rapid convergence, however it may also result in less precise solution if a global optimum point is situated at a distant area. In contrast, using a small step size value produces good exploitation and a highly precise solution but because the bacteria need more steps to arrive at a specific area it therefore results in much slower convergence. If a consistent step size is used in the chemotaxis stage then clearly there will be no balance between the exploration and exploitation.

The second stage of bacteria foraging strategy is the reproduction stage. In this stage bacteria in the population are assigned a class relating to their degree of fitness or health. The first half of the healthier bacteria is doubled in order to maintain all the existing characteristics of their antecedents.

Elimination and dispersal form the final stage of the foraging approach. Here, the lower half of the bacteria population possessing poorer health and fitness values is removed, whilst the residual bacteria are dispersed randomly inside the search zone. This ensures that just bacteria with the superior health

and fitness attributes are protected in the population, leading them to search better areas in the following life cycle. These actions performed again for a number of cycles until termination condition is achieved. Generally speaking, the foraging technique of bacteria is fairly complex and necessitates extremely lengthy computation time to complete an entire search operation.

4.2.1. Essential notion of bacteria movement

BFA Passino. (2000, 2002) is an optimisation strategy based upon the foraging strategy of Escherichia Coli (E. Coli) bacteria, that exist in the human digestive system. A foraging technique is a system used by animals for locating, handling and ingesting their food. The structure of E. Coli bacteria is such that it has a 'body' that is created from a plasma membrane, a cell wall and a capsule that contains the cytoplasm and nucleoid. In addition, E. Coli bacteria have a flagella that can move in a rotational way and is utilized for movement; assuming that the flagella moves counter clockwise it makes bacteria to shift forward with big displacement named 'swim', and if the flagella moves clockwise it makes the bacteria travel in an uncertain way with very small displacement called 'tumble'. The size of E. Coli bacterium itself is very tiny, about 1μm in diameter, 2 μm in length and 1 pictogram in weight with about 70 % of it being water. An illustration of E. Coli bacterium structure is depicted in Figure 4.1.

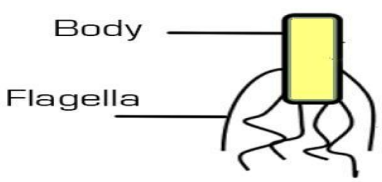

Figure 4.1: An illustration of E. Coli bacterium structure

Generally, during their lifetime in the media, E. Coli bacteria always attempt to situate where there is an elevated nutrient level and evade harmful places by utilizing a certain movement pattern named ‘taxes’. When moving in the direction of nutrient value, each bacterium discharges chemical substances as an attractant when heading to a nutritious place and repellent when they are close to a noxious place. Therefore, the movement pattern of E. Coli in finding nutrients is called “chemotaxis”. If E. Coli bacteria are moving to a higher nutrient stage than their previous position, they will move forward (swim or run) consistently. However, if the bacteria reach a place with a lesser nutrient level than the previous place, they will tumble.

Bacteria in swim and tumble are delineated in Figure 4.2. In Figure 4.2(a) the bacterium moves from its beginning position P1 to the new position P2 and then the nutrient values of P1 and P2 are compared. Because the nutrient level of P2 is higher than P1 the bacterium then moves forward in the same direction as the previous movement, i.e. swim or run, to the new position P3. Then, the same process is performed until the end of bacteria’s lifetime. The bacteria’s chemotaxis that involves both swimming and tumbling is illustrated in Figure 4.2(b). The bacterium moves from its initial position P1 to the new position P2. Because the nutrient level in P2 is lower than that in P1, the bacterium does not continue to move in the same direction as the previous movement but moves in another uncertain direction with a very small displacement, called tumbling, to new position P3. Also, because the nutrient level of P3 is lower than that in P2, the bacteria will tumble and arrive at the new position P4. Now the nutrient level in P4 is higher than that in P3, thus the bacterium is swimming in the same direction as the previous movement to the new position P5. In the

nutritious media, bacteria spend more time swimming than tumbling. On the other hand, in a media which has a low nutrient level, the bacteria will tumble more frequently than swim.

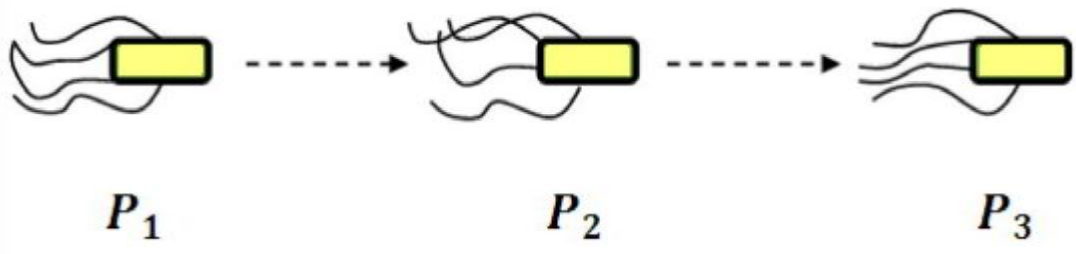

(a) Moving forward continuously (swim)

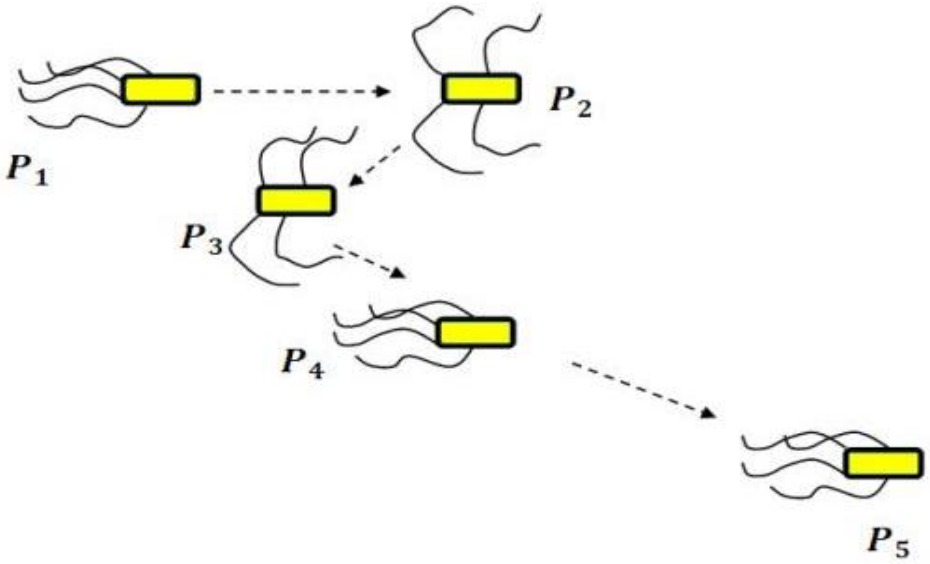

(b) Moving forward-tumbling-swim

Figure 4.2: Illustration of chemotaxis pattern of E. Coli bacterium (Passino, 2002, 2005)

The chemotaxis of bacteria in the nutrient media for their lifetime can therefore be summarised as follows (Passino, 2002, 2005):

a. In the noxious place: combination of tumble and swim to move away from the noxious place and try to find nutritious place

b. In the neutral place (where there are neither nutrients nor poison): more frequent tumble to find nutritious place (searching)

c. In the nutritious place: swim as long as possible in the direction of up the nutrient gradient

4.2.2. Optimisation technique based on bacterial foraging

The BFA is an optimisation technique developed by modelling the behaviour of E.Coli bacteria whereby they find places with a high nutrient value and avoid noxious places (Passino, 2002). If it was desired, for example, to discover the global minimum of $J(\theta)$, $\theta \in \Re p$ where θ is the location of a bacterium and $J(\theta)$ represents the nutrient media level at θ where there is no measurement or there is no analytical description of the gradient $\nabla J(\theta)$. A non-gradient optimisation method adopted from the foraging behaviour of E. Coli bacteria can be utilised to solve this minimisation problem. There are three possibilities of $J(\theta)$ value: $J(\theta) < 0$, $J(\theta) = 0$ and $J(\theta) > 0$ indicating that the bacterium at location θ is in nutrient-rich, neutral, and noxious environments, respectively. E. Coli bacteria will apply biased random walk to climb up the nutrient concentration (find lower and lower values of $J(\theta)$, avoid noxious substances (the place where $J(\theta) > 0$), and search for ways out of neutral media (location where $J(\theta) = 0$). The four optimisation steps that model how E. Coli bacteria find food; chemotaxis, swarming, reproduction and elimination and dispersal, are discussed below.

A. Chemotaxis

The position and its corresponding nutrient value (usually called as the cost function value in optimisation) of i_{th} bacterium at the j_{th} chemotactic step, k_{th} reproduction step, and l_{th} elimination and dispersal event can be denoted as θ (i, j, k,l) and J (i, j,k,l) respectively with i =1,2,...,S and θ (i, j, k, l)∈ℜp. Bacteria will walk from these initial positions toward the position that has the lower J (i, j,k,l) value. The 'speed' of the walk is governed by the value of chemotactic step size C (i) > 0,i =1,2,..., S. The bacteria's chemotaxis could be a combination of:

• Continuous swim

• Swim followed by tumble

• Tumble followed by tumble

• Tumble followed by swim

To define the direction of movement after tumble, a unit length random direction φ (j) in the range [-1,1] is generated. The movement of bacteria from one position to another position can therefore be formulated as:

$$\theta (i, j+1, k,l) = \theta (i, j, k, l) + C(i)\varphi (j) \quad (4.1)$$

If at bacteria position θ (i, j +1, k,l) the cost function value J (i, j +1, k, l) is lower than J (i, j,k,l) then the bacteria will move one step in the same direction as the previous direction with the step size C(i). Another step in the same direction

is taken if the next cost function is lower. The maximum number of continuous swim in the same direction taken is Ns. After Ns swim, bacteria have to tumble.

B. Swarming

Bacteria have the ability during the walking process to release chemical substances to attract other bacteria, allowing other bacteria to swarm together. Similarly, they are able to release chemical substances to repel other bacteria, as two bacteria cannot be in the same location at the same time and maintain a certain distance between each other. This process is referred to as 'cell-to-cell signalling via attractant and repellent', or 'swarming'. The swarming process for every bacterium is formulated as:

$$J_{cc}(\theta, P(j,k,l)) = \sum_{i=1}^{s} J_{cc}(\theta, \theta(i,j,k,l)) \tag{4.2}$$

$$J_{cc}(\theta, P(j,k,l)) = \sum_{i=1}^{s}\left[-d_{attract}\exp\left(-\omega_{attract}\sum_{m_p=1}^{p}\left(\theta_{m_p}-\theta_{m_p}(i)\right)^2\right)\right]+$$

$$\sum_{i=1}^{s}\left[-h_{repellent}\exp\left(-\omega_{repellent}\sum_{m_p=1}^{p}(\theta_{m_p}-\theta_{m_p}(i))^2\right)\right] \tag{4.3}$$

where:

- $\theta = [\theta_1, \theta_2, \dots, \theta_p]^T$ is a point on the optimisation domain
- $\theta_{mp}(i)$ is position of the $mp-th$ component of the i-th bacterium

- $d_{attract}$ is the depth of attractant released by the cell (a quantification of how much attractant is released)
- $\omega_{repellent}$ is a measure of the width of the attractant signal (a quantification of the diffusion rate of the chemical)
- $h_{repellent}$ is the height of the repellent effect (magnitude of its effect)
- $\omega_{repellent}$ is a measure of the width of the repellent.

Thus, in the optimisation, the nutrient media in which bacteria will find the optimum place is the cost function value plus cell-to-cell signalling (swarming effect) as:

$$J(i, j, k, l) + J_{cc}\big(\theta, P(j, k, l)\big) \tag{4.4}$$

To obtain the optimal nutrient media landscape the cost function value J and cell-to-cell signalling value J_{cc} have to be balanced. The cells will have a strong tendency to swarm if the attractant width is high and quite profound, even to the point where they avoid going after following nutrients and simply favour swarming. Conversely, if the attractant width is little and the profundity shallow, then there will be minimal tendency to swarm, with every cell searching on its own.

C. Reproduction

Bacteria will reproduce very fast in a rich nutrient media, resulting in the bacteria population increasing significantly. In a poor nutrient media bacteria will die and the population size will decrease significantly. In order to model the reproduction mechanism after N, chemotactic step size, the health of all bacteria is sorted in ascending order based on their accumulated cost function value;

$$J_{health} = \sum_{J=1}^{N_c+1} \mathrm{J}(i\, j, k, l) \tag{4.5}$$

In the minimisation process, the highest cost function value means the least healthy bacteria and while the lowest cost function value relates to the healthiest bacteria. Based on their health, the bacteria population is divided into two halves:

$$S_r = \frac{S}{2} \tag{4.6}$$

The S_r minimum healthy bacteria die and the S_r healthiest bacteria reproduce (each bacterium parts into two bacteria) and are located at the same place with their mother. This reproduction mechanism keeps the bacteria population constant. Following reproduction the bacteria will continue the chemotaxis process until the maximum chemotactic number Nc is achieved, after which other reproduction events will be performed.

D. Elimination and dispersal

The E. Coli bacteria populations in the nutrient media can be reduced or replaced instantly due to catastrophic events such as the nutrient media being poisoned. In the modelling, after performing N_{re} reproduction steps the elimination and dispersal events follow. Bacteria possessing probability values lower than a certain threshold value, i.e. between 0 and 1 (ped) are eliminated and dispersed to another location. Bacteria that have a probability value higher than ped will keep their current position and are not dispersed. After the elimination and dispersal event bacteria will start chemotaxis until they achieve reproduction steps N_{re}, followed by another round of elimination and dispersal events. This routine continues until maximum elimination and dispersal events *Ned* is achieved.

4.2.3. The original BFA computation

In developing the optimisation algorithm, the following parameters need to be defined:

- P as dimension of the search space (number of parameters to optimise)
- S as the number of bacteria in the population (for simplicity, S is chosen as even number)
- *Nc* as the number of chemotactic steps per bacterium lifetime between reproduction steps

- Ns as maximum number of swim of bacteria in the same direction
- N_{re} as the number of reproduction steps
- Ned as the number of elimination and dispersal events
- Ped as the probability that each bacteria will be eliminated/dispersed.
- i =1,2,3,…, S as the index for the bacterium
- $j = 1,2,3, ...,, Nc$ as the index for chemotactic step
- $k = 1,2,3, ...,, N_{re}$ as the index for reproduction step
- $l = 1,2,3, ...,, Ned$ as the index of elimination and dispersal event
- m_s as the index for number of swim

The bacteria will ceaselessly perform their random walk in their search for nutritious places until they expire. The life of bacteria can therefore be determined as a total number of steps, calculated as $Nc \times N_{re} \times Ned$. The bacterium possessing the highest nutrient level after all the steps have been performed is determined as the optimisation result. The original BFA Passino. (2002) that models chemotaxis, swarming, reproduction, elimination and dispersal in the bacterial population (initially, i=j=k=l = 0) can be formulated as follows (note that updates to θ^i automatically result in updates to P):

Elimination-dispersal loop: for $l = 1,2,3, ...,, Ned$, do $l = l + 1$

1) Reproduction loop: for $k = 1,2,3, ...,, N_{re}$, do $k = k + 1$

2) Chemotaxis loop:for $j = 1,2,3, ...,, Nc$,do $j = j + 1$

(a) For i =1,2,3,…,S, take a chemotactic step for bacterium i :

(b) Compute the nutrient media (cost function) value $J(i\,j,k,l)$. Calculate $J(i,j,k,l) = J(i,j,k,l) + J_{cc}(\theta^i(i,j,k,l), P(i,j,k,l))$ (i.e., add on the cell-to-cell attractant effect to the nutrient concentration). If there is no swarming effect then $J_{cc}\left(\theta^i(i,j,k,l), P(i\,j,k,l)\right) = 0.$

(c) Put $J_{last} = J(i,j,k,l)$ to save this value since a better cost via a run may be found.

(d) Tumble: Generate a random vector $\Delta(i) \in \Re^p$ with each element $\Delta m_p(i)$, m_p=1, 2… p, a random number on the range [-1, 1].

(e) Move: Compute $\theta^i(j+1,k,l) = \theta^i(j,k,l) + C(i)\frac{\Delta(i)}{\sqrt{\Delta^T(i)\Delta(i)}}$ this results in a step of size, C (i) in the direction of the tumble for bacterium i .

(f) Compute the nutrient media (cost function) value $J(i,j+1,k,l)$, and calculate $J(i,j+1,k,l) = J(i,j+1,k,l) + J_{cc}\left(\theta^i(j+1,k,l), P(j+1,k,l)\right)$. If there is no swarming effect then

$$J(i,j+1,k,l) + J_{cc}\left(\theta^i(j+1,k,l), P(j+1,k,l)\right) = 0.$$

Swim (note that since the swimming behaviour of each cell is decided as if the bacteria numbered {1,2, ….., i } have moved and { i + 1, i + 2,…..,S } have not, an approximation is used; this is far less complex than attempting to simulate decisions about swimming and tumbling by all the bacteria simultaneously):

Put ms = 0 (counter for swim length)

While ms < NS (if have not climbed down too long)

Count ms = ms +1

If $J(i, j+1, k, l) < J_{last}$ (if doing better), then $J_{last} = J(i, j+1, k, l)$ and

calculate $\theta^i(j+1, k, l) = \theta^i(j, k, l) + C(i) \frac{\Delta(i)}{\sqrt{\Delta^T(i)\Delta(i)}}$ this results in a step of size

C (i) in the direction of the tumble for bacteriumi. Use this $\theta^i(j+1, k, l)$ to compute the new $J(i, j+1, k, l)$ as in sub step f above.

Else, m = NS (the end of the while statement).

Go to next bacterium $(i+1)$ if $i \neq s$ (i.e.,go to sub b above) to process the next bacterium.

If j < Nc , go to step 3.

Reproduction:

For the given k and l, and for each i =1,2,3,…,S, let

$$J^i_{health} = \sum_{J=1}^{N_c+1} J(i\, j, k, l)$$

be the health of bacterium i, a measure of how many nutrients it obtained over its lifetime and how successfully it avoided noxious substances. Sort bacteria and chemotactic parameters, C (i) in order of ascending cost J_{health} (higher cost means lower health).

The S_r bacteria with the highest J_{health} values die, while the other S_r bacteria possessing the best values split. The copies that are made are located at the same position as their parent).

If k< Nre , go to step 2.

Elimination-dispersal: for i =1, 2, 3,…, S, eliminate and disperse each bacterium that has a probability value less than Ped . If one bacterium is eliminated then it

is dispersed to a random location of nutrient media. This mechanism results in simple computations and keeps a constant number of bacteria in the population.

For m =1: S

if P_{ed} < rand (Generate a random number for each bacterium and if the generated number is smaller than P_{ed} then eliminate/disperse the bacterium)

Generate new random positions for bacteria

else

Bacteria keep their current position (bacteria are not dispersed)

end

end

If l < Ned , then go to step 1; otherwise end.

The original BFA algorithm above can be presented as a flowchart as in Figure 4.3.

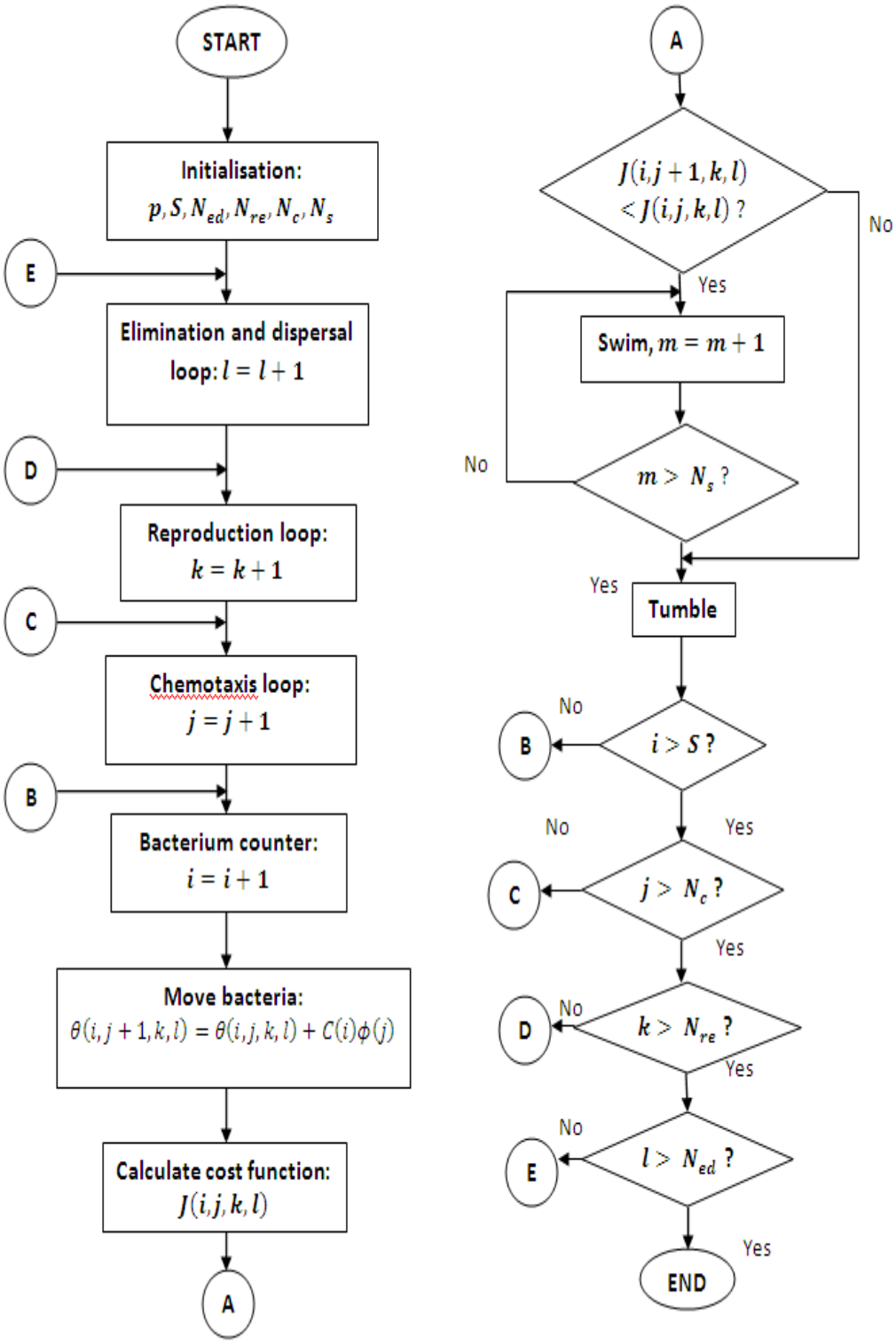

Figure 4.3: Flowchart of original BFA (Passino, 2002)

4.3 Adaptive bacterial forging algorithm

To improving BFA accuracy and convergence speed, several adaptive and hybrid approaches have been developed. A linear and nonlinear adaptive BFA was proposed by Nasir et al. (2013) here, the bacteria step size varies based on the mixture of the bacteria index and the iteration index. The step size is continuously decreased within [0, Cmax] or [0, ∞] as the iteration number of the search operation increases, where Cmax is maximum step size. The algorithms were applied to identify and optimize the parameters for auto-regression with an exogenous model for a nonlinear twin rotor system. Chen and Lin. (2009), Farhat and" (Huang and Lin, 2010) and El-Hawary (2009) used chemotaxis to change bacteria step size within a specific extent of [Cmin, Cmax], where Cmin is least step size. By using a mixture of index and sum of number of iterations Niu et al. (2010), Yan et al. (2012), Xu et al. (2012) change the step size inside a user-defined extent of [Cmin, Cmax]. These modifications result in the step size decreasing as the amount of iterations raises, Supriyono and Tokhi (2012) created a variety of adaptive versions of the BFA dependent upon linear and nonlinear mathematical formulations. There are several extra adaptive algorithms that take a very identical method to change step size based on fitness value, including the work of Majhi et al. (2006, 2009), Dasgupta et al. (2009), Sanyal et al. (2011), Sathya and Kayalvizhi (2011), Venkaiah and Kumar (2011), and (Majhi, 2009) proposed an intelligent approach towards an adaptive BFA to change bacteria run length by utilising Takagi-Sugeno type and Mamdani- type fuzzy logic systems.

Some modifications towards several aspects of the BFA have been proposed in order to further improve its performance. These include aspects such as its convergence to the optimum value, computation time, and accuracy.

4.3.1. Adaptable chemotactic step size modification

One area of improvement is how to accelerate the convergence of BFA. Within the BFA (Passino, 2002), while seeking location with a high nutrient grade, bacteria utilise random walk with a specific consistent chemotactic step size for the entire computational procedure, irrespective of the nutrient. This makes the bacteria walk with a constant speed as they move towards the optimum value. If the step size is set to a small value, bacteria need more iteration to find the optimum value. If a larger step size is used, the bacteria's walk will increase in speed and consequently reduce the iterations required.

Dasgupta et al. (2008, 2009a) proposes that chemotaxis employed by BFA typically leads to sustained oscillation when close to the global optimum. This is especially true on landscape nutrient media that is relatively flat. The chemotactic step size therefore needs to be selected as small as possible. Such conditions form a compromise between increasing the speed of the bacteria's walk and reducing the oscillation around the global optimum point. By ensuring that the chemotactic step size is adaptable, that is to say changing the value of chemotactic step size to follow up particular specific conditions will solve this problem.

An alternative chemotactic step size adaptation mechanism has been proposed by Datta et al. (2008), where step size is controlled by an adaptive delta modulation. The algorithm was used in the optimisation of an antenna array. Coelho and Silveira (2006) developed an adaptable chemotactic step size

by adopting several probability distribution functions, including uniform and Gaussian and Cauchy distribution, and have utilised the algorithm to tune the PID controller of robotic manipulator systems. A modified BFA was also proposed by Chen et al. (2009), which was called cooperative bacterial foraging optimization (CBFO). There is two stages in this algorithm; the first stage begins with a large chemotactic step size and then continues to the second stage which has a smaller step size. The initial big step size phase has been used to narrow down possible region of the optimum solution without getting trapped into the local optima, while the smaller step size in the second phase is used to locate the optimum point. The algorithm has been validated by finding the optimum value of several benchmark functions.

Some efforts have been made via researchers to propose an adaptable chemotactic step size for BFA. Dasgupta et al. (2008; 2009a), Dasgupta et al. (2009) proposed simple linear functions of the nutrient value of every bacterium. They tested this on several well recognized benchmark functions and similarly applied it to a parameter estimation problem. The algorithm has been used in practical applications such as forecasting stock market indices (Majhi et al., 2009), detecting a circle in a digital image (Dasgupta et al., 2010) designing an optimal three-phase energy efficient induction motor (Sakthivel et al., 2010).

Farhat and El-Hawary (2010) proposed modified BFA to introduce nonlinear decreasing chemotactic step size and stopping criteria. This means that after the cost function has achieved a pre-specified value the optimisation process is stopped. However, while the stopping criteria regarding a pre-specified value are able to save computation time, it could not show that the predetermined value is the real global optimum point.

4.3.2. Quadratic Adaptive Bacterial Foraging Algorithm

Developed by Supriyono et al. (2010) and based on the original BFA Passino. (2002) the QABFA introduces adaptation of the chemotactic step size by using a quadratic function. The adaptation scheme is formed from changing the chemotactic step size based on the nutrient value. To achieve this, a quadratic function is utilised in order to find the next chemotactic step size. As a result the approach has a faster search operation in finding the optimal solution when compared to the original BFA algorithm. The QABFA step size is calculated using

$$a_q^i = \frac{C_{\max}}{1 + \frac{b}{d\left(\left|J^i\right|^2 + \left|J^i\right|\right)}} \tag{4.7}$$

where $C_{\max}$ = maximum step size, b = tuneable positive scaling factor, d = scaling factor, J^i = nutrient value for every bacterium. Thus, the new adaptive chemotactic step size can be expressed as

$$C_{GABFA}(i) = C(i) \times a_q^i \tag{4.8}$$

4.4 Optimisation parameters

Table 4.1 shows the simulation parameters which were obtained heuristically and used with the QABFA optimisation.

Table 4.1: Simulation parameters

Parameter	Description	Value
P	Dimension of the search space	9
S	Number of bacteria population	40
Nc	Number of chemotactic steps per bacteria	9
Ns	Number of swim per bacteria in a constant direction	6
Nre	Production steps	4
Ned	Elimination and dispersal events	2
ped	Probability elimination and dispersal per bacteria	0.25
cmax	Maximum step size	0.1
b	Tuneable positive scaling factor	1
d	Scaling factor	0.045

4.5 Constrained optimisation

The optimisation process will be constrained within the stability region of the system. Each parameter will have a feasible interval that guarantees the stability of the system within the defined controller gain limits, as shown in Table 4.2. The selection of the parameters was based on the results reported by Supriyono et al. (2010). The authors have studied the impact of changing each BFA algorithm parameter and its impact on the convergence time and the cost function. The have recommended the optimal selection of the BFA parameters that help in achieving faster convergence while minimising the error.

Table 4. 2: Boundary limits of the controller gain parameters

Gain parameter	Minimum value	Maximum value
Kp_1	4	5
Kd_1	3	4
Ki_1	0.4	0.8
Kp_2	4	5
Kd_2	3	4
Ki_2	1	1.3
Kp_3	10	13
Kd_3	15	20
Ki_3	2	3

4.6 Objective function

The performance index of the system is chosen as the minimum mean square error of each loop. The MSE is calculated for each control loop of the vehicle system as follows:

$$\text{Objective \_Function 1= min } \left[\frac{1}{N}\sum_{i=1}^{N}(\mathrm{Y_d}-\mathrm{Y_m})^2\right] \quad (4.9)$$

$$\text{Objective \_Function 2= min } \left[\frac{1}{N}\sum_{i=1}^{N}(\theta_\mathrm{d}-\theta_\mathrm{m})^2\right] \quad (4.10)$$

$$\text{Objective \_Function 3= min } \left[\frac{1}{N}\sum_{i=1}^{N}(\mathrm{Q_d}-\mathrm{Q_m})^2\right] \quad (4.11)$$

The first objective function represents minimisation of the error in the cart position. The second objective function represents minimisation of the error in the tilt angle and similarly the third objective function represents minimisation of the error in the payload position. The main objective function will be considered as the sum these three objective functions with equal weights to minimise the mean square error for the total system and thus achieve an overall stable system with all the vehicle components;

$$J = \min[\sum_{i=1}^{3} Objective\_function(i)] \quad (4.12)$$

4.7 Simulation results

Figures 4.5 - 4.10 compare the results obtained by simulating the manual tuned controller gains with the optimised QABFA controller gains. It is noted that the optimisation algorithm has led to the optimal gain values that successfully stabilised the system with minimum cost function value. The convergence curve of the cost function is presented in Figure 4.4. The minimum value of the cost function achieved was 0.9. The optimised gain values are shown in Table 4.3.

Table 4.3: Optimised gain values

Gain parameter	**Optimal value**
Kp1	4.23
Kd1	3.01
Ki1	0.47
Kp2	4.56
Kd2	3.26
Ki2	1.03
Kp3	11.45
Kd3	19.34
Ki3	2.65

The cost function presented in Figure 4.4 shows that the algorithm has converged to the optimal minimum value within 24 iterations. Figure 4.5 shows that the optimised gain values resulted in better system response with a faster settling time and lower percentage overshoot value. The tilt angle response in Figure 4.6 is noted to have less oscillation and a faster settling time

with the optimised gain values. It can be noted that the oscillation in the tilt angle is very small. Due to the selection of the loop scaling factors and due to the fact that the initial position of the tilt angle equals zero and the controllers were effective in supressing the oscillation in the angle and keeping the vehicle stable within very short time. On the other hand, the payload displacement shown in Figure 4.7 is noted to have zero steady state errors and lower overshoot but with a longer settling time. The QABFA has achieved either comparable or better performance when compared to manual tuning.

Energy consumption has been given consideration in this investigation; the control effort components have been obtained as shown in Figure 4.8. The QABFA was more robust as it resulted in less oscillation of the control effort components that could be seen in Figures 4.8, 4.9 and 4.10. A significant amount of energy saving has been achieved specifically in the cart and tilt angle control efforts as noted in Figures 4.8 and 4.9. Furthermore, the QABFA resulted in significant improvement in the control effort for the payload, as shown in Figure 4.10 in terms of reduced oscillations and the short time taken by the control signal to stabilize.

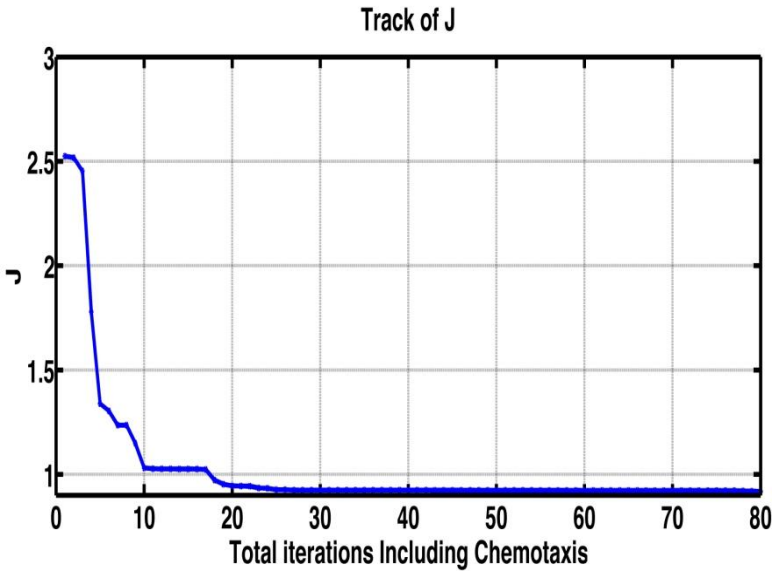

Figure 4.4: Track of the cost function convergence curve

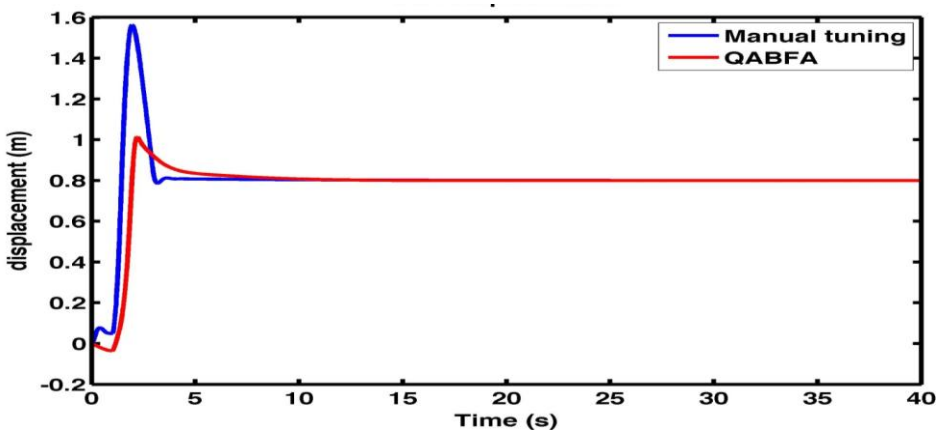

Figure 4.5: Cart displacement optimised performance compared to manual tuned values

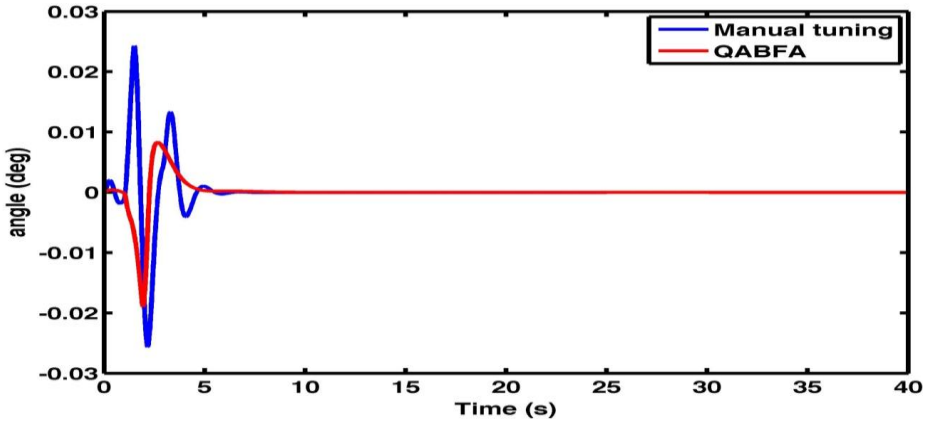

Figure 4.6: Tilt angle optimised performance compared to manual tuned values

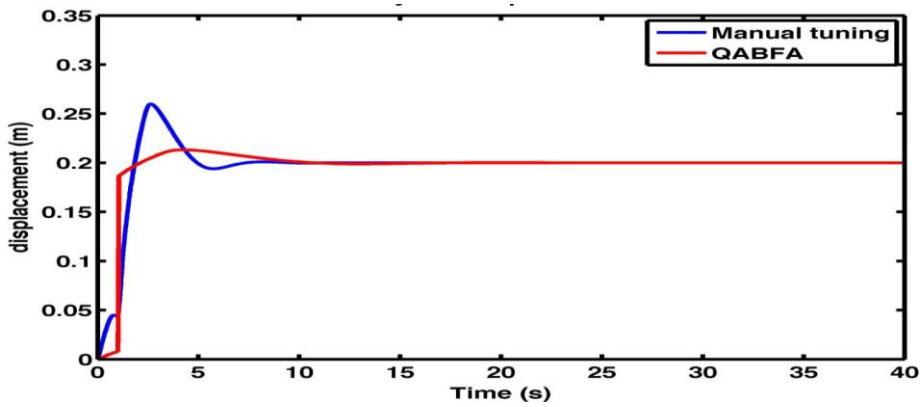

Figure 4.7: Payload displacement optimised performance compared to manual tuned value

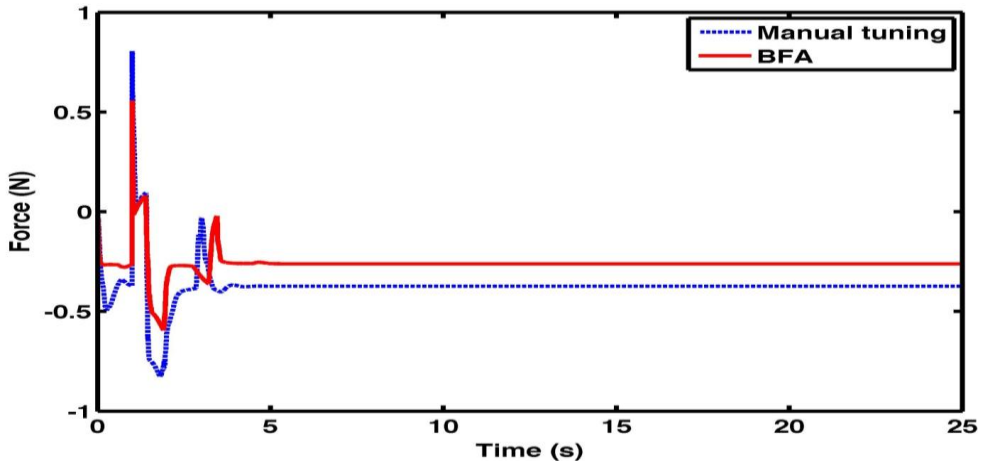

Figure 4.8 Cart displacement controller effort optimised performance compared to manual tuned values

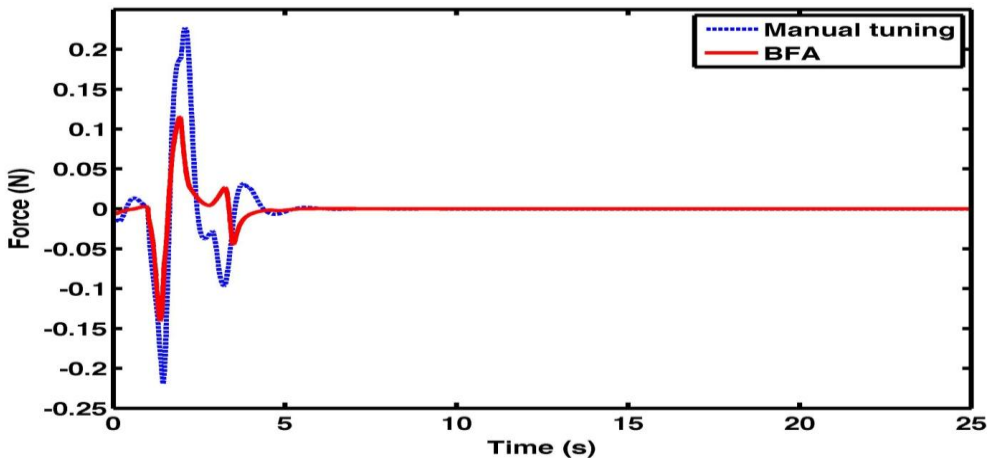

Figure 4.9: Tilt angle controller effort optimised performance compared to manual tuned values

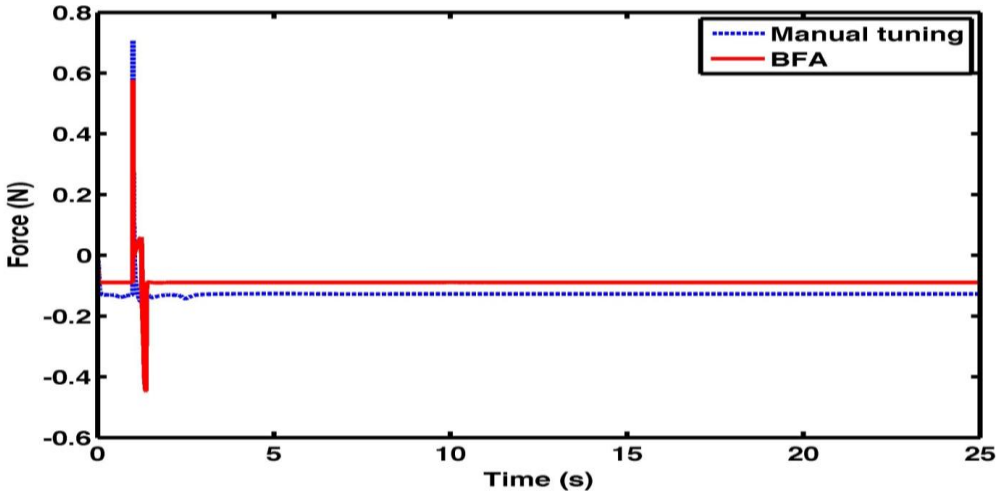

Figure 4.10: Payload controller effort optimised performance compared to manual tuned values

4.8 Summary

In this chapter PD +I FLC control algorithm with QABFA has been implemented on a two-wheeled robot with an extendable intermediate body. This novel two-wheeled robot design offers an extra DOF in the vertical direction which allows the robot to be used for applications such as managing things at different heights in industrial applications. The QABFA optimisation to the control system of the vehicle has resulted in an important reduction in the control efforts, with a superior overall system performance than the manually tuned control system. Simulations have been presented to show the superior performance of the optimised controller. The optimised control system will be adapted and more simulation scenarios that test the robustness of the controller are presented in the next chapter.

Chapter 5
Vehicle performance on irregular terrains and dynamic inclinations

5.1 Introduction

To develop a robust vehicle that is able to drive and manoeuvre on irregular terrains is a significant part of this research. The capability of the vehicle to adapt to different terrains allows a variety of mobility solutions to be developed using the vehicle as a basis. Furthermore, the simulations would give a measure of how robust is the vehicle to work in different environments in the real life. In this chapter, various simulation scenarios are presented that incorporate the variation of the surface characteristics in terms of the slope, friction and payload movement behaviour.

5.2 Smooth inclined surfaces

Firstly, the vehicle is simulated to move on surfaces with different slopes. Slopes of 20 degrees and 45 degrees are simulated. In Figure 5.1, the system responses are presented. As noted the vehicle was able to move on the selected slopes without losing the postural balance. The larger the slope of the surface, the larger overshoot appeared in the system response. Moreover, increase in the surface slope increased the settling time of the system response in each of the vehicle components. However, this increase is insignificant and had a maximum value of approximately 5 seconds in the payload displacement. In Figure 5.2, control efforts are presented. The larger the slope of the surface the larger the torque was required to drive the cart. A maximum value of approximately 1 Nm is required to control the cart displacement on the 45 degrees slope. A maximum control effort of 1 Nm can be noted at the tilt angle control effort.

While on the payload actuator, a constant value of approximately 0.25N.m is noted to control the payload displacement. A conclusion can be stated that on inclined slopes the cart will be the most affected part and needs to exert more efforts in order to overcome the inclination and the gravity force. With the coupling effect among the vehicle components, the tilt angle and the payload actuator will depend mainly on the cart stability in order to be stabilised and controlled.

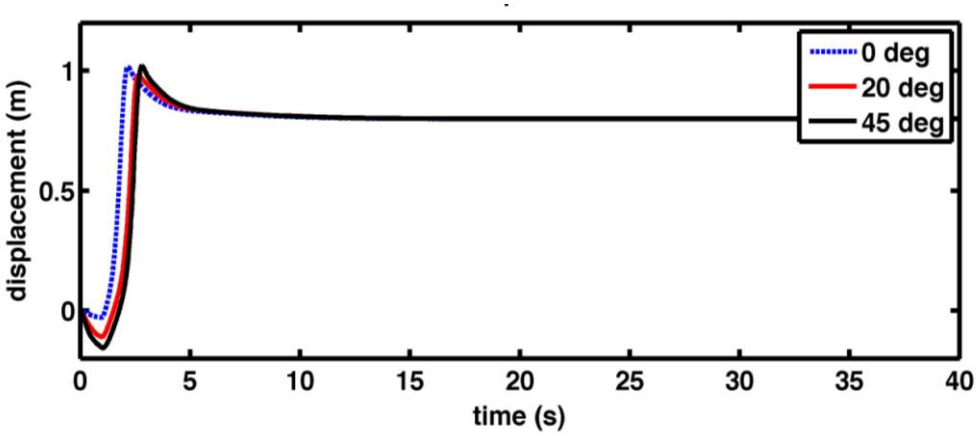

(a) Cart displacement

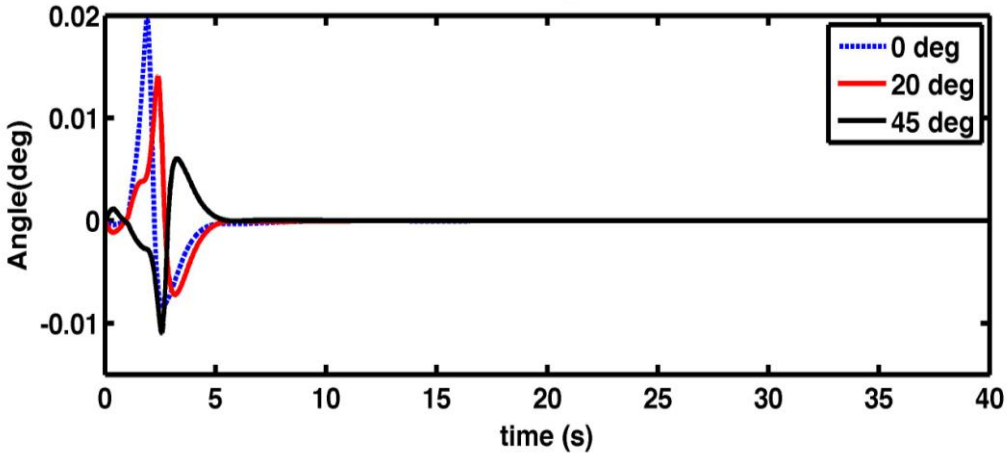

(b) Tilt angle

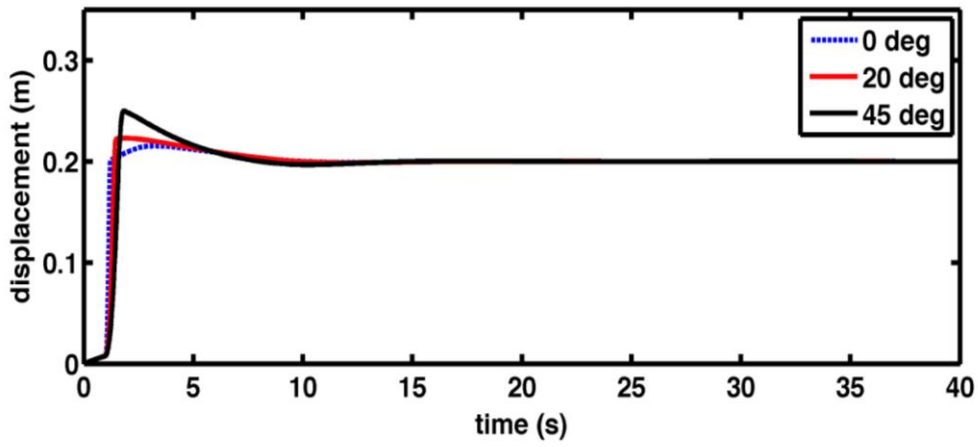

(c) Payload displacement

Figure 5.1: System response on different inclined surfaces

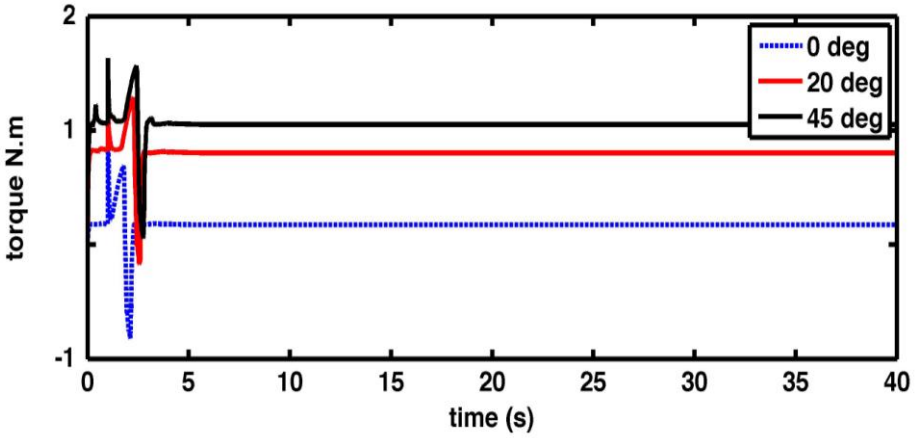

(a) Cart controller effort

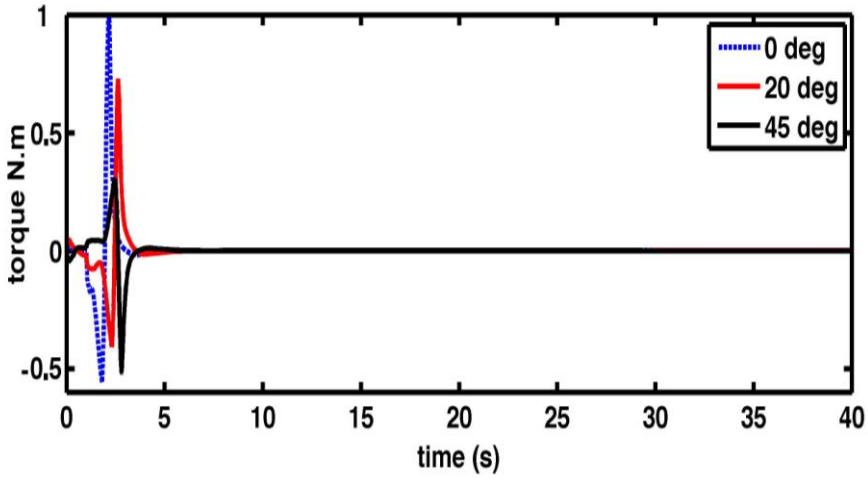

(b) Angle controller effort

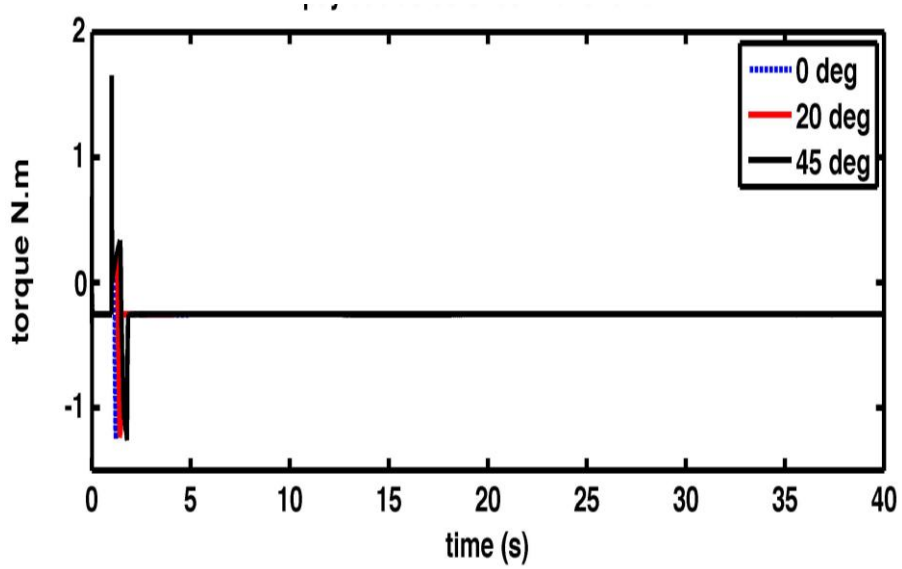

(c) Payload actuator effort

Figure 5.2: Control efforts of the system controller on inclined surfaces

5.3 Maximum inclination angle

Every system has its limitations and operation boundaries. It is important to investigate the vehicle limitation on inclined angles by finding the maximum surface inclination angle. To find the maximum inclination angle beyond with the vehicle will collapse, the system is simulated with ascending values of inclination angle until the vehicle is no longer able to stabilise. This simulation was implemented and the maximum inclination angle was found to be 50 degrees. Simulating the system with an inclination angle larger than 50 degrees would lead to the vehicle to collapse. To demonstrate that, the system was simulated with inclination angle of 55 degrees and yielded the unstable response illustrated in Figure 5.3.

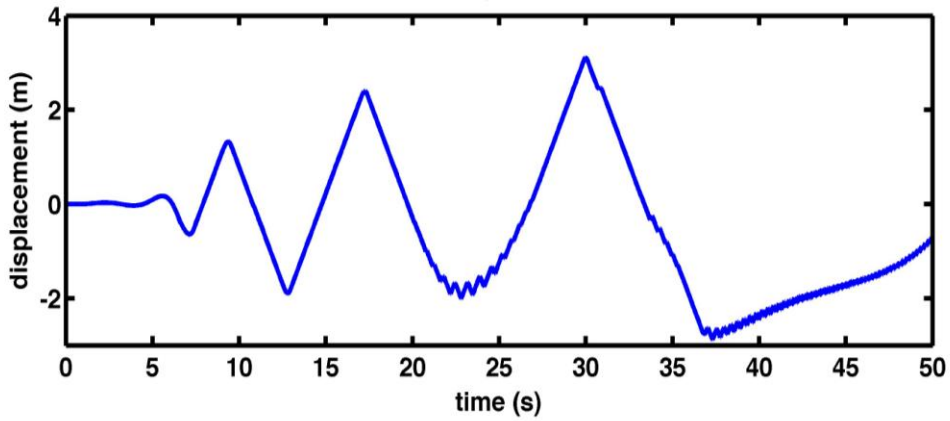

(a) Cart displacement

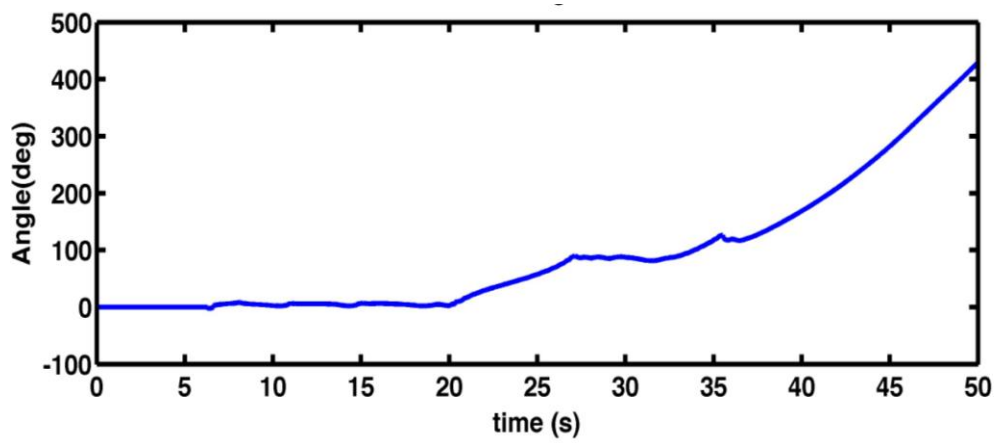

(b) Tilt angle

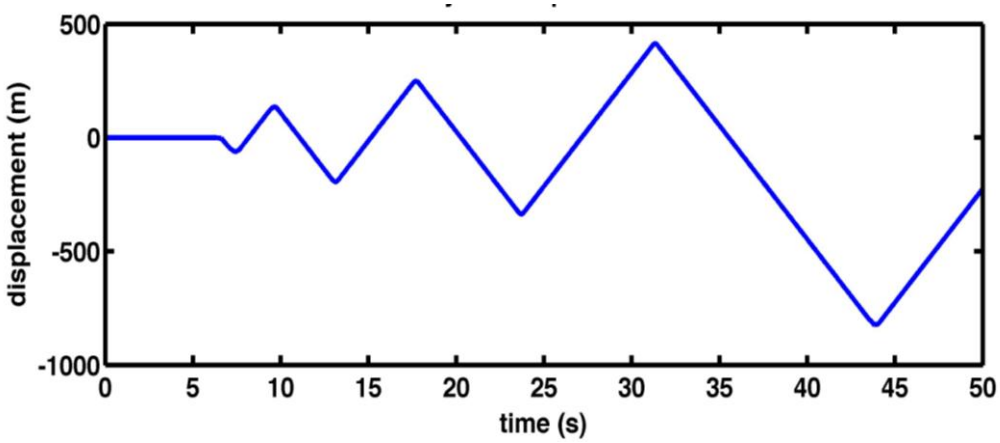

(c) Payload displacement

Figure 5.3: System response with inclination angle of 55 degrees

5.4 Performance of the vehicle subjected to disturbances

In order to test the controller's ability to cope with external disturbances, the vehicle it was simulated to work in a perturbed environment. Disturbance forces of varying amplitudes were applied to the vehicle to analyse the performance in such perturbed environments. Force magnitudes of 50N, 100N and 150N were applied at the centre of the intermediate body of the vehicle. The vehicle response with disturbances thus achieved is presented in Figure 5.4 with the associated control efforts presented in Figure 5.5. It could be noted that the vehicle successfully rejected the effect of the disturbance and converged back to the desired set points. Overshoots were noted at the time of application of the disturbance force, the higher the disturbance magnitude the higher the overshoots. However, these overshoots were negligible and the controller was able to cope with such disturbance amplitudes. Figure 5.5 shows the control efforts exerted to overcome the effect of the disturbances. The payload displacement was not affected by the disturbances. This can be explained by the fact that the payload actuator operates when lifting the payload to the desired extent and locks the position of the payload. Thus, the displacement is not affected.

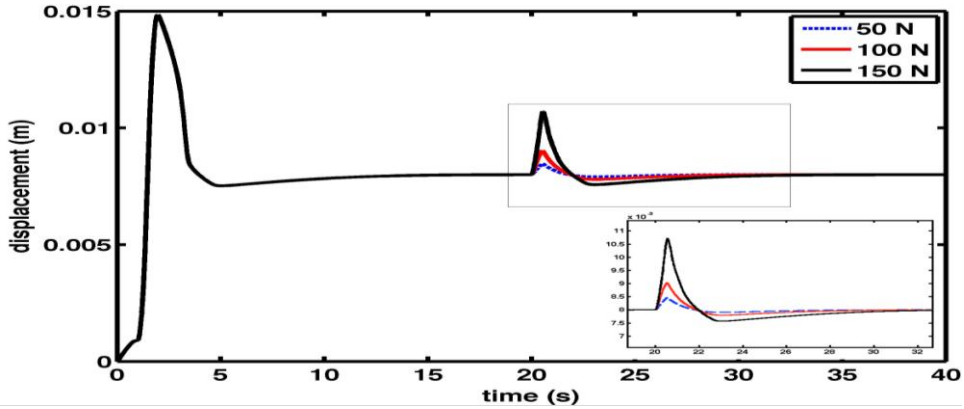

(a) Cart displacement response with disturbances of varying amplitudes

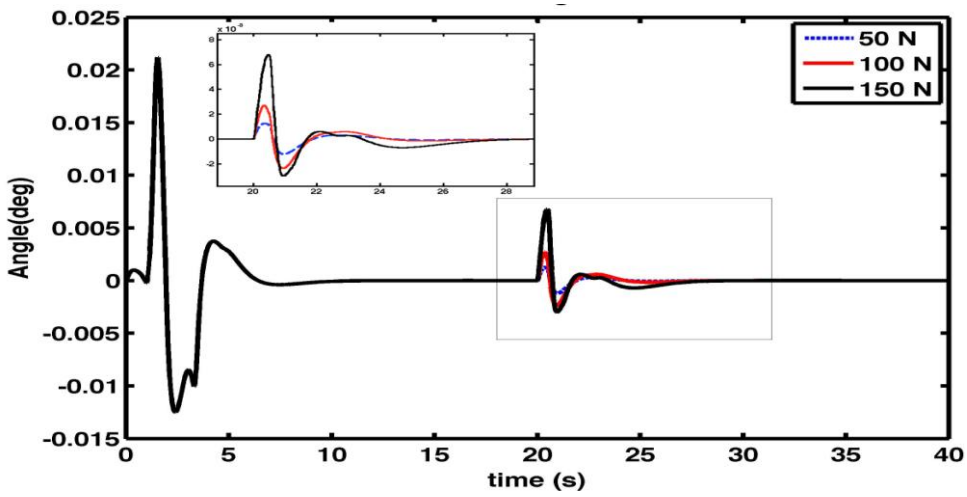

(b) Tilt angle response with disturbances of varying amplitudes

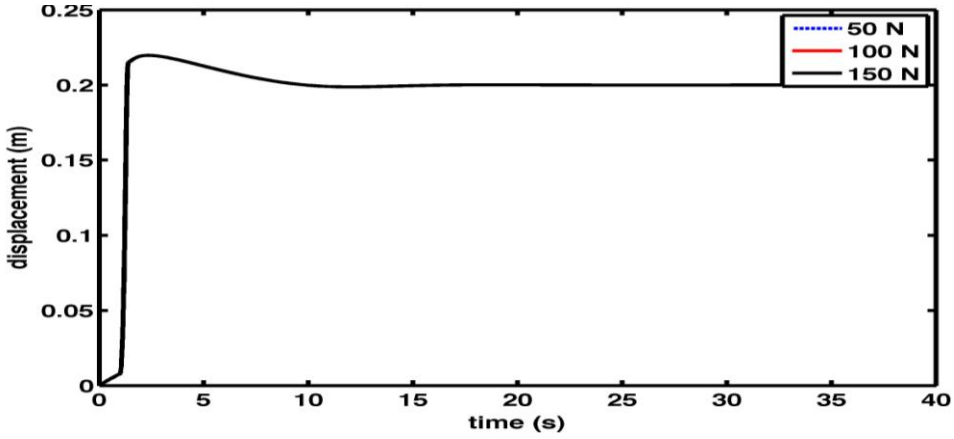

(c) Payload actuator displacement response with disturbances of varying amplitudes

Figure 5.4: Vehicle response with external disturbances of varying amplitudes

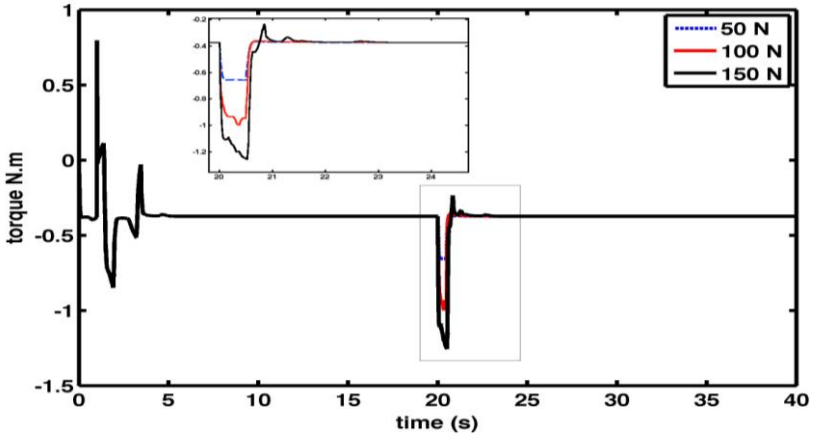

(a) Cart displacement controller effort with disturbances of varying amplitudes

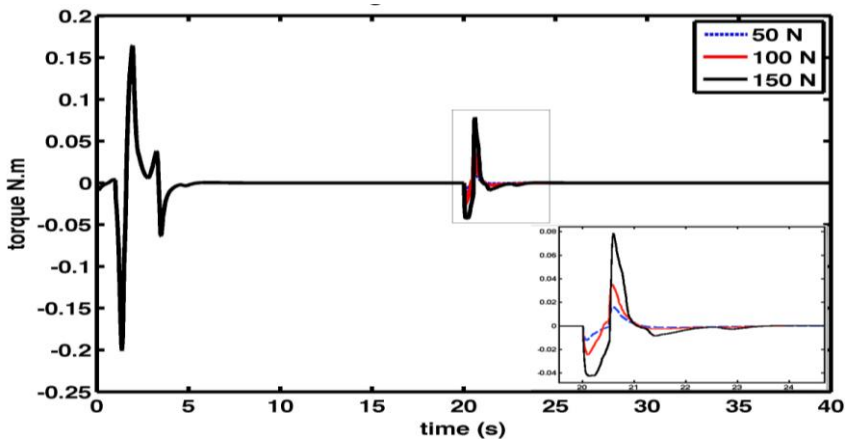

(b) Tilt angle controller effort with disturbances of varying amplitudes

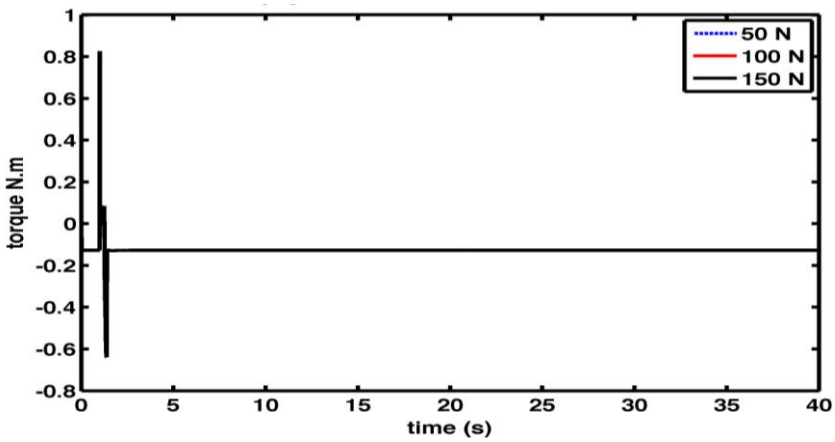

(c) Payload actuator displacement controller effort with disturbances of varying amplitudes

Figure 5.5 Control efforts with external disturbances of varying amplitudes

With the encouraging results of the system performance with disturbances, more realistic simulation scenarios were carried out to demonstrate the vehicle's ability working on frictional flat and inclined surfaces. This will be presented in the next part.

5.5 Manoeuvres on flat and inclined terrains of various frictional grounds

In order to test the versatility of the vehicle in moving on both smooth and frictional surfaces, the vehicle is simulated to drive on surfaces with various frictional degrees.

In this section, the vehicle is commanded to move on flat surfaces with different friction profiles to simulate slightly rough, rough and very rough grounds. The grounds are simply modelled by white noise signals of different noise power spectral density and sampling time that depend on the required roughness of the ground. The selection of white noise signal to model the ground is to ensure that the surface has a randomly distributed friction forces each time the model is simulated. Thus, rigorous investigations can be carried out and proving the vehicle ability to work on terrains with uncertain friction profiles. The ground profiles describing the ground friction are shown in Figure 5.6 and Figure 5.7.

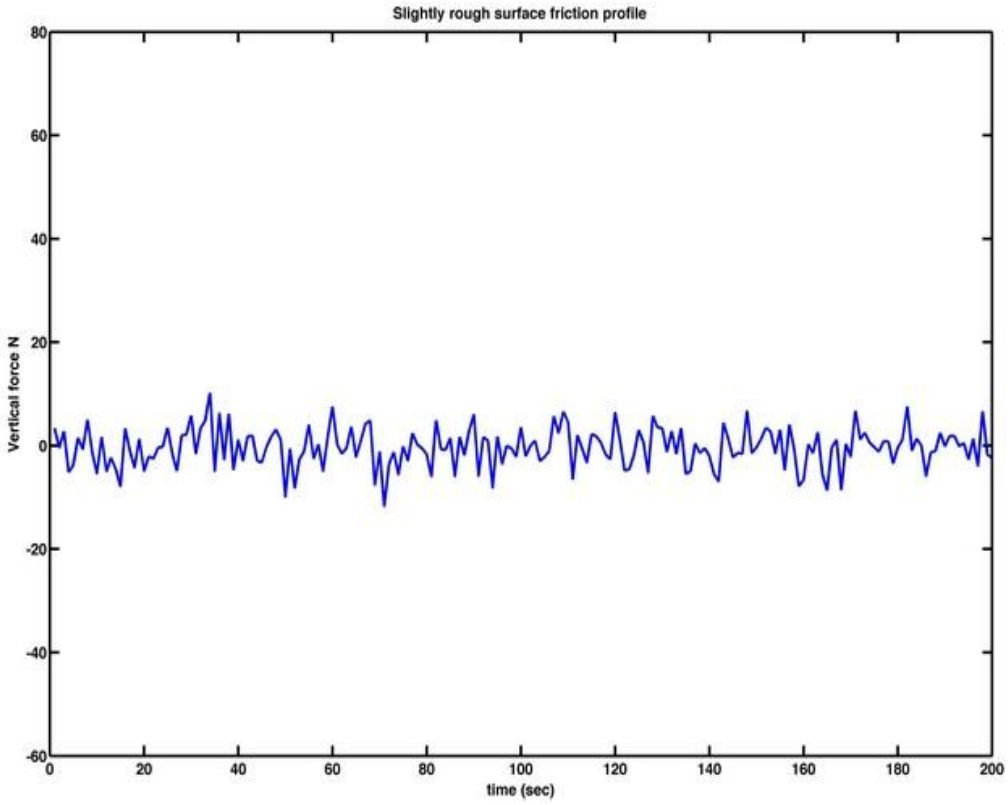

Figure 5.6: Slightly rough ground friction profile

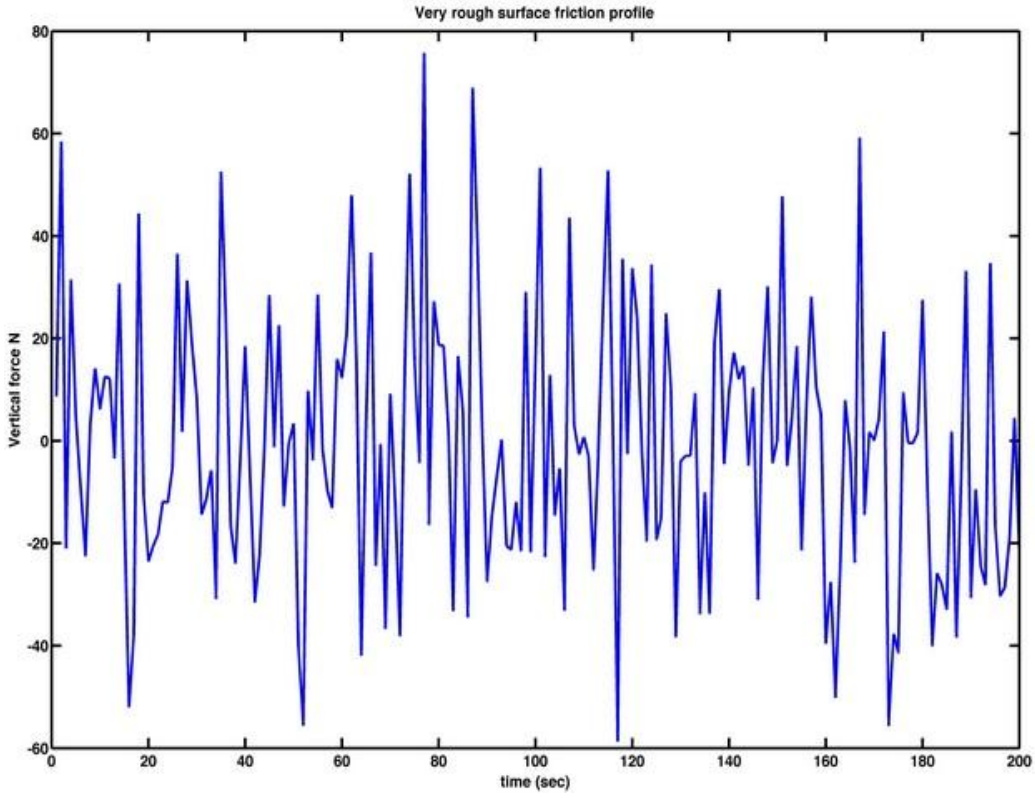

Figure 5.7: Very rough ground friction profile

5.5.1 Flat surfaces with different frictions and dynamic payload movement

In this section, the vehicle is simulated to drive on flat terrains of different friction profiles with dynamic payload lifting scenario. This approach shows the ability of the control system in adapting with the changes of the payload position while driving on frictional grounds. The vehicle is simulated to move on the described grounds of slightly rough and very rough friction profiles. The system is assumed to be initially stable and at the upright position. The vehicle will move on a straight line for a distance of 8 metres. The payload is then lifted to 0.2 meters and then descends back to zero position. The lifting scenario is repeated over the simulation time to mimic a continuous ascending and descending movement of the payload toward the demanded height and then back to the initial position.

5.5.1.1 Slightly rough surface with dynamic payload movement

Figure 5.8 – Figure 5.10 represent the vehicle response while driving on a slightly rough surface with a dynamic payload movement. It is noted that the system had a stable response with some negligible oscillations at the tilt angle and the payload. These oscillations are due to the friction of the surface and are of a small scale. Figure 5.11 – Figure 5.13 represent the control effort exerted to stabilise the vehicle on the surface. The cart displacement controller has exerted a maximum of 1 Nm of torque to drive the vehicle to track the reference trajectory. The control efforts of the tilt angle controller and the payload actuator controller were minimal. The slight increase in the amount of control effort at certain times is linked to the movement of the payload. This is due to the fact that the controller must exert a slightly larger amount of torque to lift up and stabilise the payload.

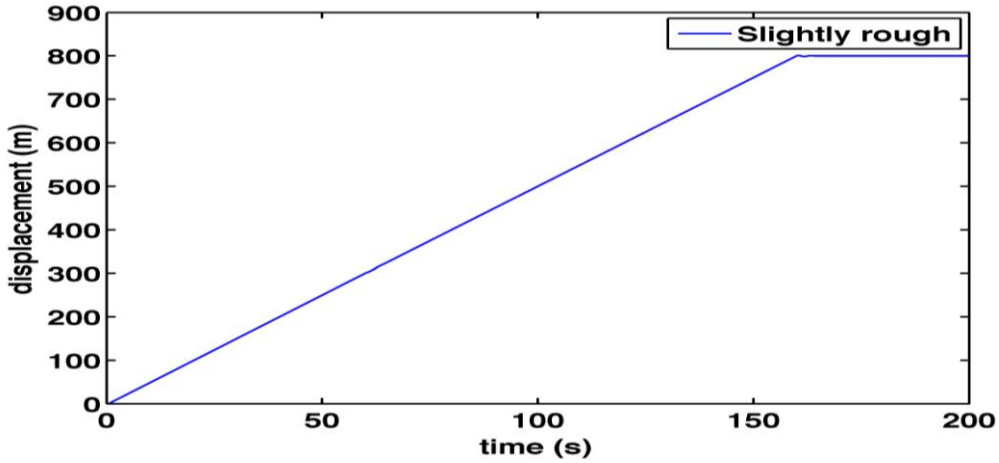

Figure 5.8 Cart displacement response over a slightly rough frictional surface with dynamic payload

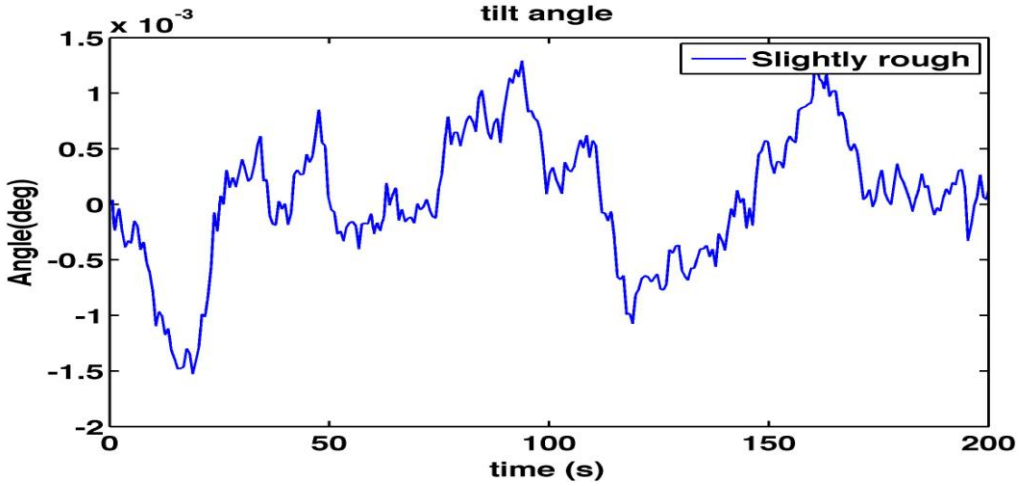

Figure 5.9 tilt angle response over a slightly rough frictional surface with dynamic payload

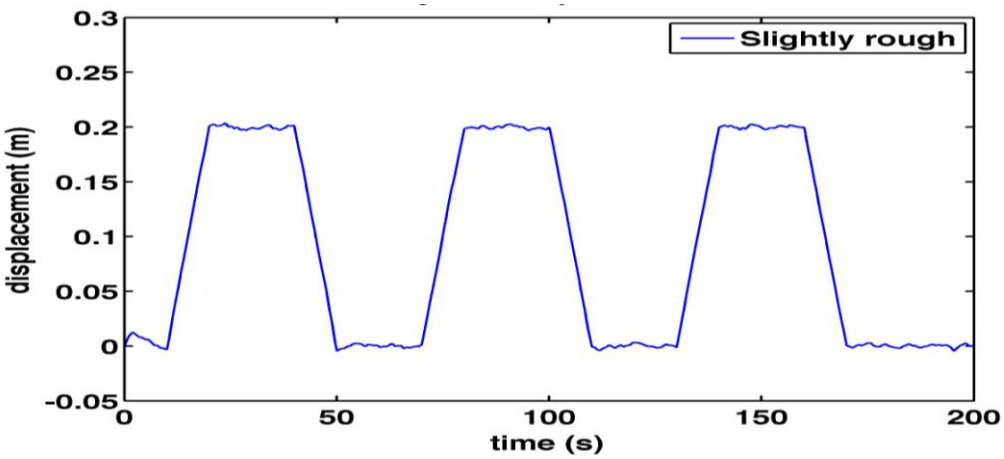

Figure 5.10 payload response over a slightly rough frictional surface with dynamic payload

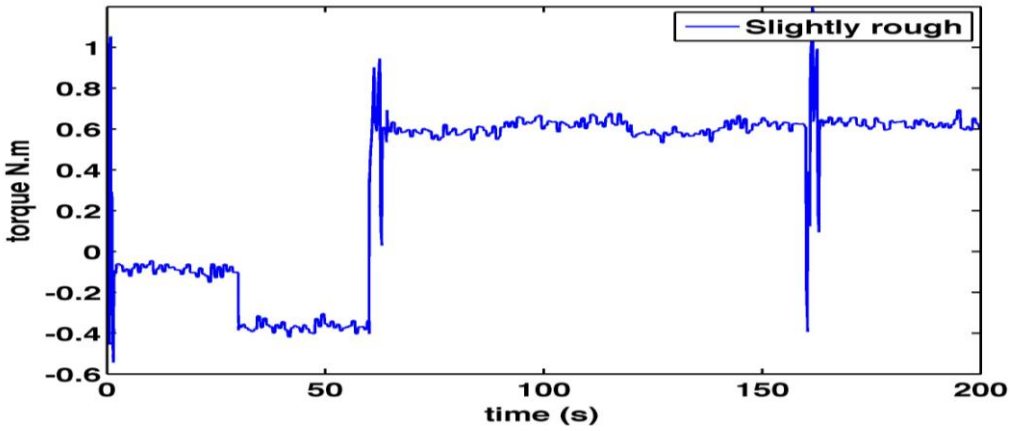

Figure 5.11 Cart displacement control effort over a slightly rough frictional surface with dynamic payload

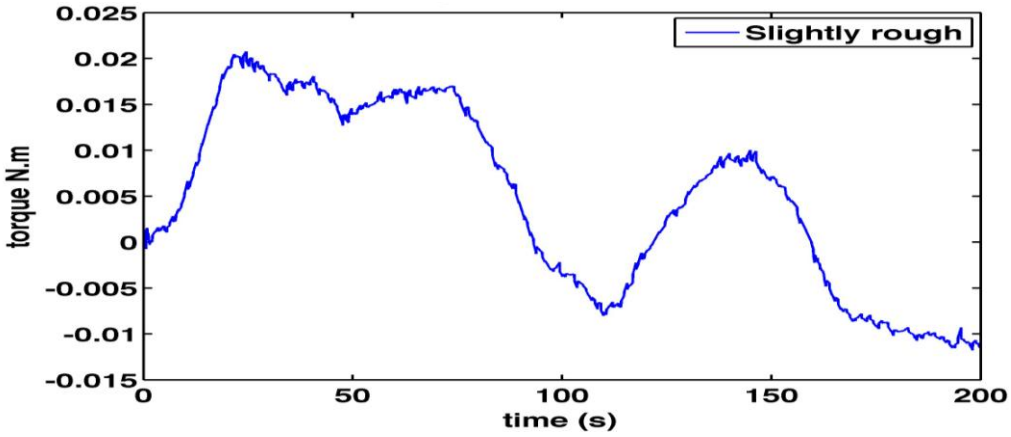

Figure 5.12 Tilt angle control effort over a slightly rough frictional surface with dynamic payload

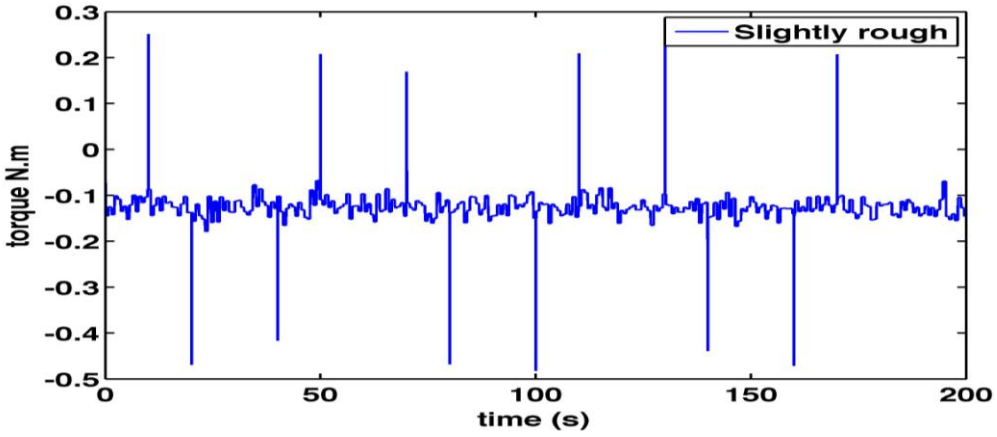

Figure 5.13 Payload control effort over a slightly rough frictional surface with dynamic payload

5.5.1.2 Very rough surface with dynamic payload movement

Figure 5.14 – Figure 5.16 show the response of the vehicle moving on a very rough frictional surface with a dynamic payload movement. It is noted that the vehicle was able to drive on the surface with a high degree of robustness and stability. Slightly larger oscillations are noted in the tilt angle compared to the tilt angle response on the slightly rough surface but still within a very small scale that do not affect the overall stability of the vehicle. The payload actuator has achieved a successful payload lifting mechanism and a stable response in tracking the predefined signals for lifting the payload with negligible oscillations that are due to the friction of the surface. The control efforts exerted to drive the vehicle are presented in Figure 5.17 – Figure 5.19. When compared to the control efforts in case of slightly rough surface, a slight increase in the tilt angle control effort is noticed. The cart displacement control effort shows a significant increase in the frequency but with a negligible increase in the amount of effort. A similar observation can be noted in the payload control effort. The increase in frequency of the control effort may be referred to the continuous counteraction of the vehicle to adapt to the surface friction and maintain stability.

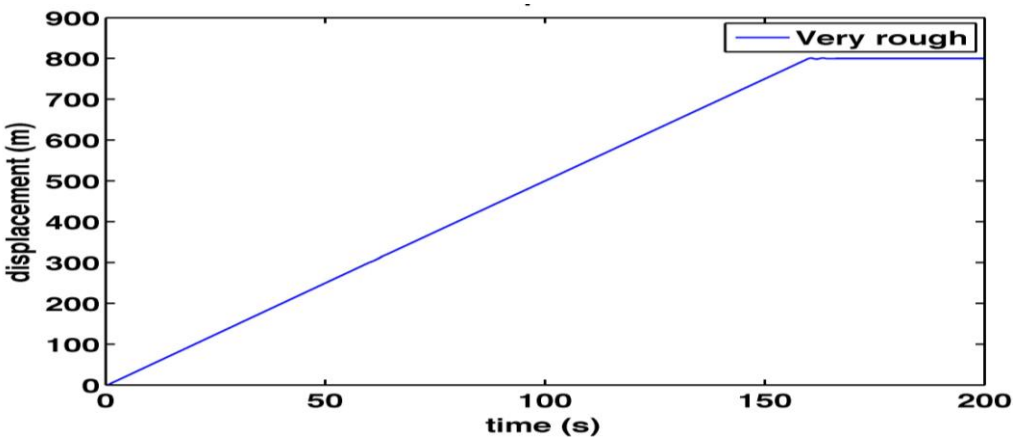

Figure 5.14 Cart displacement response over a very rough frictional surface with dynamic payload

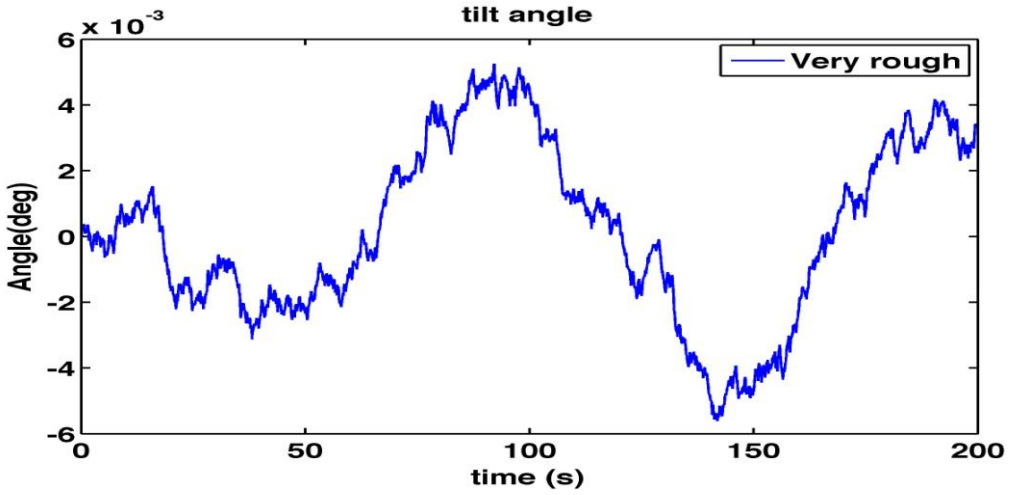

Figure 5.15 Tilt angle response over a very rough frictional surface with dynamic payload

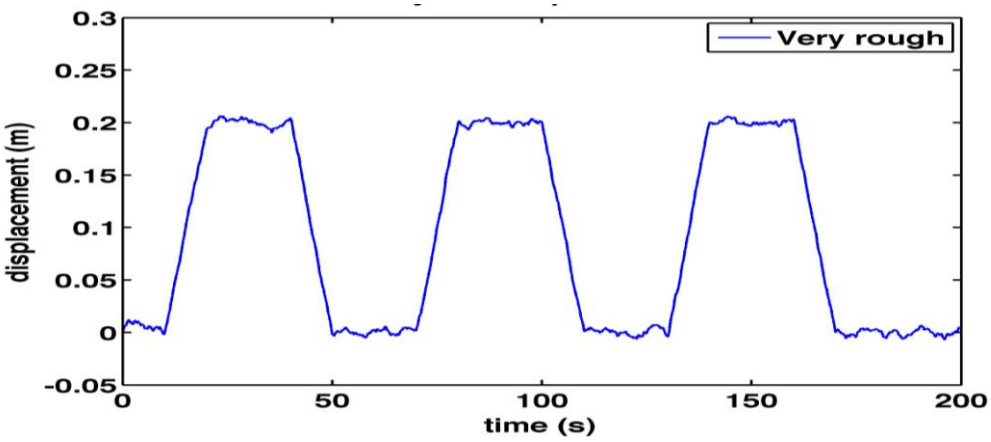

Figure 5.16 Payload response over a very rough frictional surface with dynamic payload

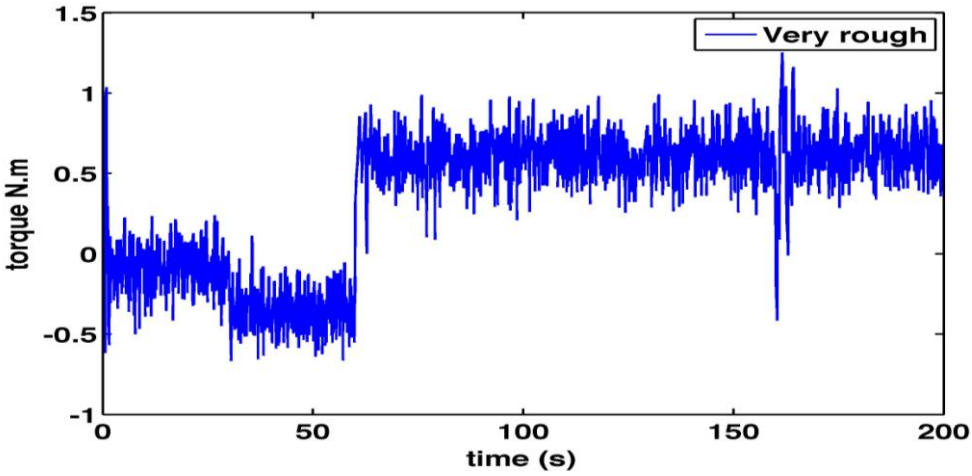

Figure 5.17 Cart displacement control effort over a very rough frictional surface with dynamic payload

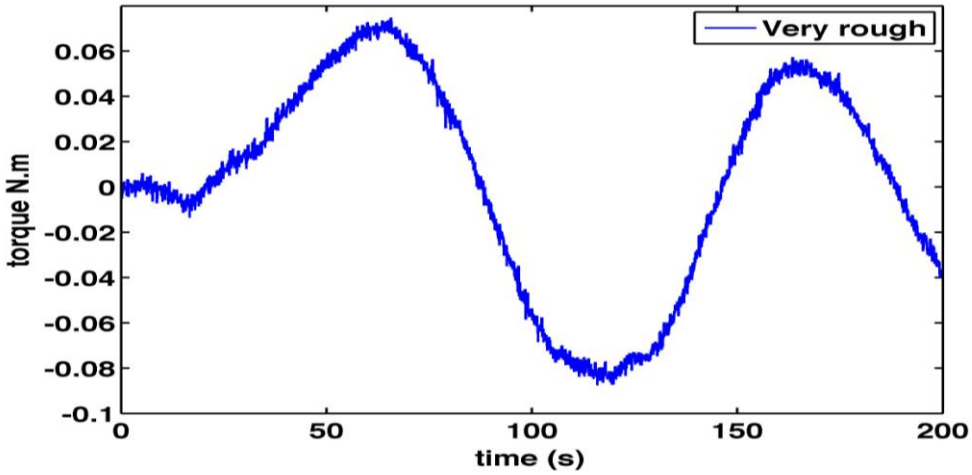

Figure 5.18 Tilt angle control effort over a very rough frictional surface with dynamic payload

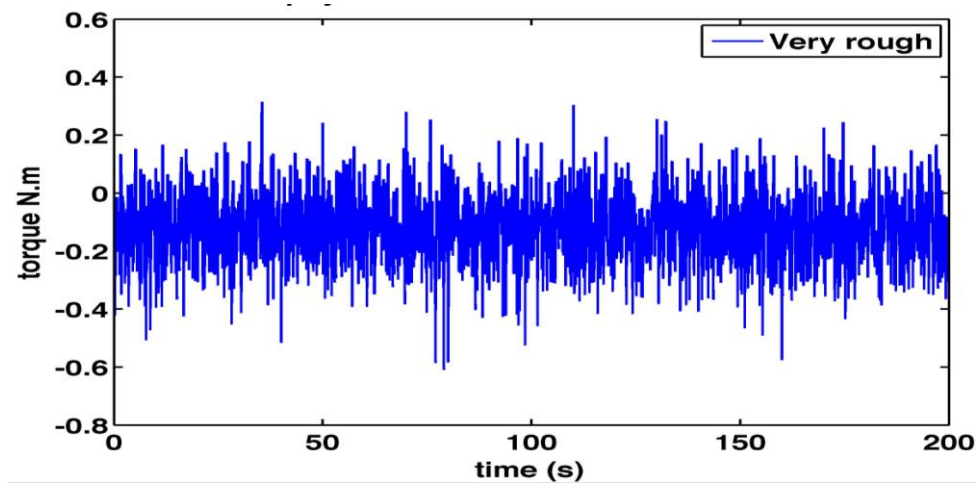

Figure 5.19 Payload control effort over a very rough frictional surface with dynamic payload

5.5.2 Inclined terrains with dynamic payload movement

In a similar approach to the previous section, the vehicle was simulated on inclined surfaces of 10 degrees and 30 degrees with contrastive frictional profiles. The payload was to follow a predefined signal to lift it up to a demanded height and then to descend it down to the initial position to mimic a dynamic payload movement.

5.5.2.1 Inclined terrains of 10 degrees with dynamic payload

Slightly rough and very rough frictions were incorporated into an inclined surface of 10 degrees. Figure 5.20 shows the vehicle response after completing a distance of 8 meters on the surface. It is noted that the system was stable and the vehicle successfully followed the reference signal. There was some oscillations the tilt angle that increase with increase of the surface frictional force however within a controllable range. The payload response was stable with minor oscillations that did not affect the tracking of the predefined signal. The larger the friction the larger the oscillations appeared in the response.

Figure 5.21 shows the corresponding control efforts of the vehicle controllers to complete the simulation scenario. It can be noted that the system exerted larger control efforts while on very rough surface profile to overcome the roughness of the surface and counteract the gravitational effect. However, the control efforts were still within feasible range.

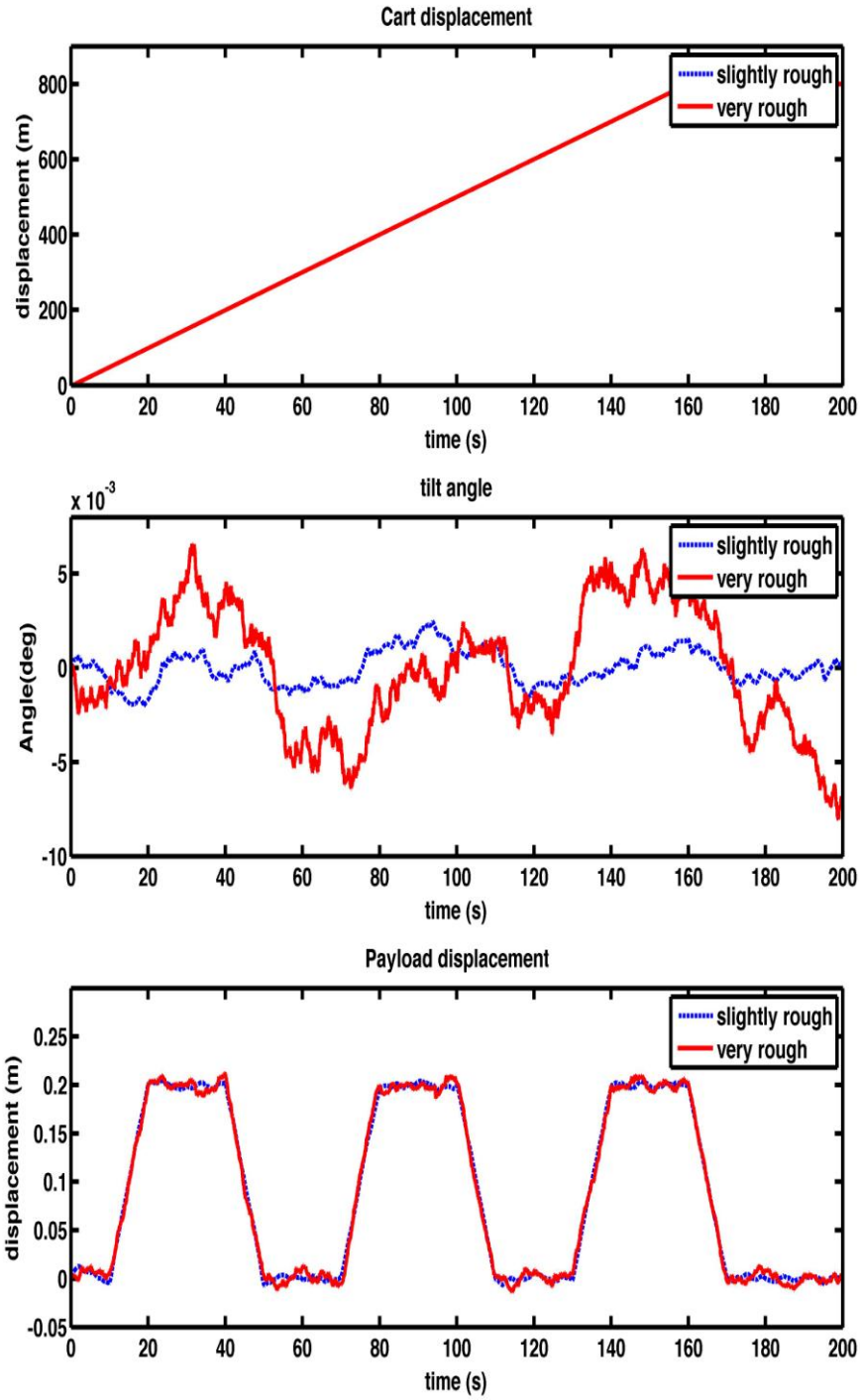

Figure 5.20: Vehicle response on inclined terrains of 10 degrees with dynamic payload

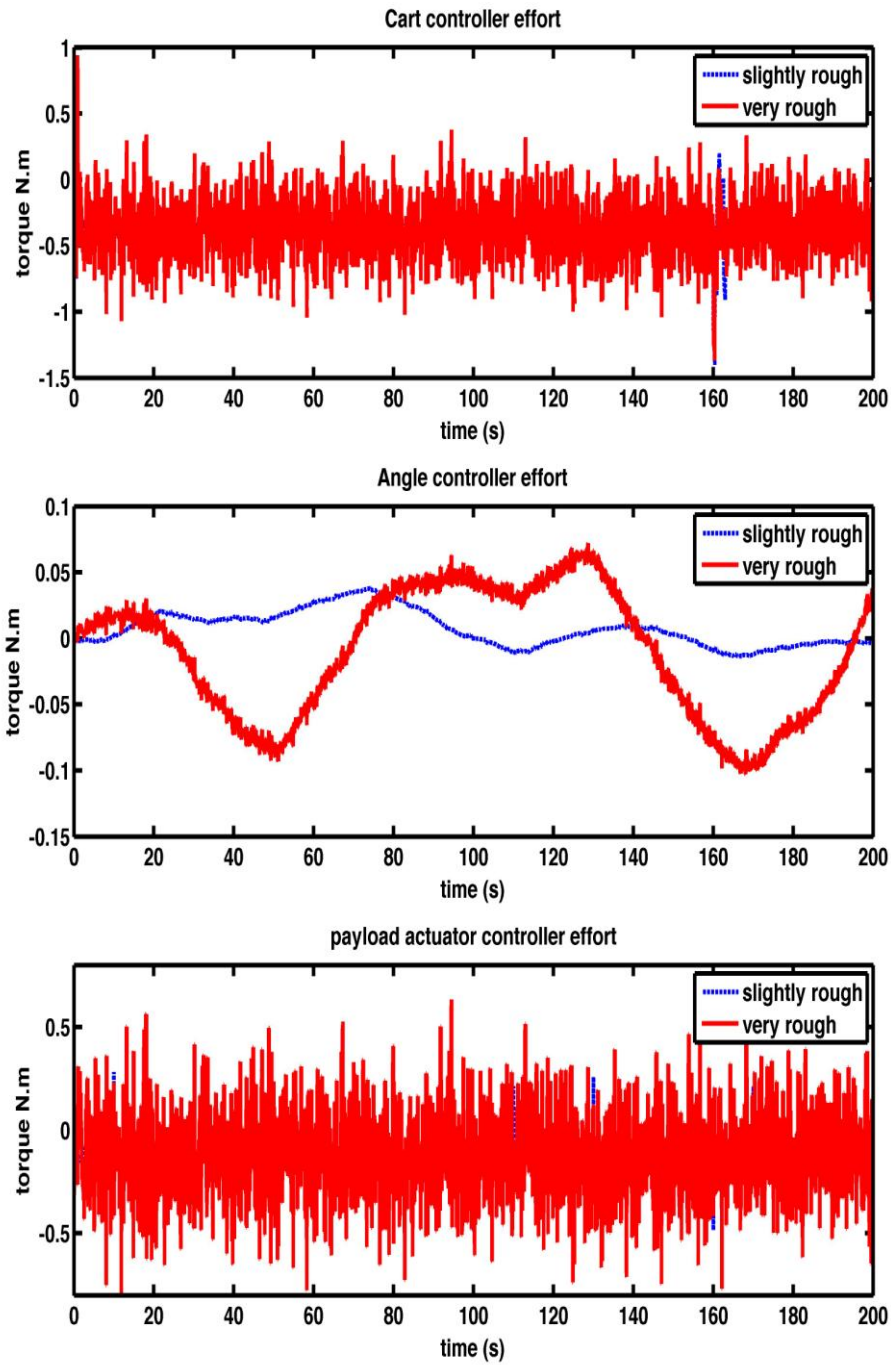

Figure 5.21 Control efforts on inclined terrains of 10 degrees with dynamic payload

5.5.2.2 Inclined terrains of 30 degrees with dynamic payload

Figures 5.22 and 5.23 show the vehicle response and the corresponding control efforts while moving on inclined terrains of 30 degrees with dynamic payload movement. It is noted that the vehicle was able to complete the movement with a high degree of robustness without losing the postural balance of the payload. The system was stable with some minor oscillations appearing at the tilt angle due to the friction of the surface. Oscillations appeared at the payload actuator response, and were still within controllable region, but this indicates that rougher grounds may affect the balance of the payload and as a result may affect the postural balance of the whole structure of the vehicle. More challenging simulation scenarios may be needed for further analysis.

The control efforts, shown in Figure 5.23, of the cart displacement and the tilt angle are almost similar to the case of moving on surface of 10 degrees inclination. However, a slight increase in the control effort can be noted in the payload actuator controller. The increase is obviously due to the need for higher efforts to balance the vehicle on the very rough surface profile and to counteract the disturbances.

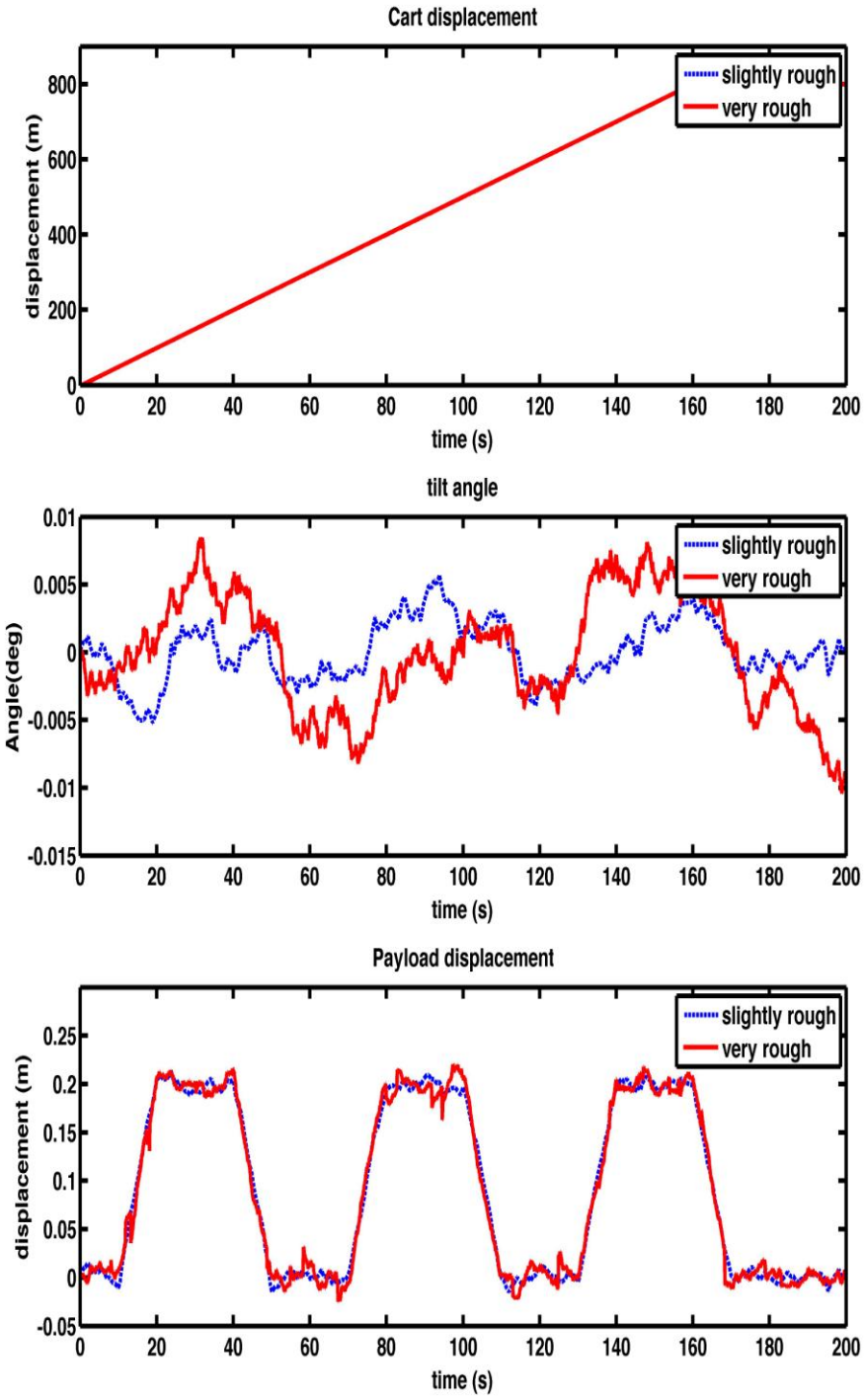

Figure 5.22: Vehicle response on inclined terrains of 30 degrees with dynamic payload

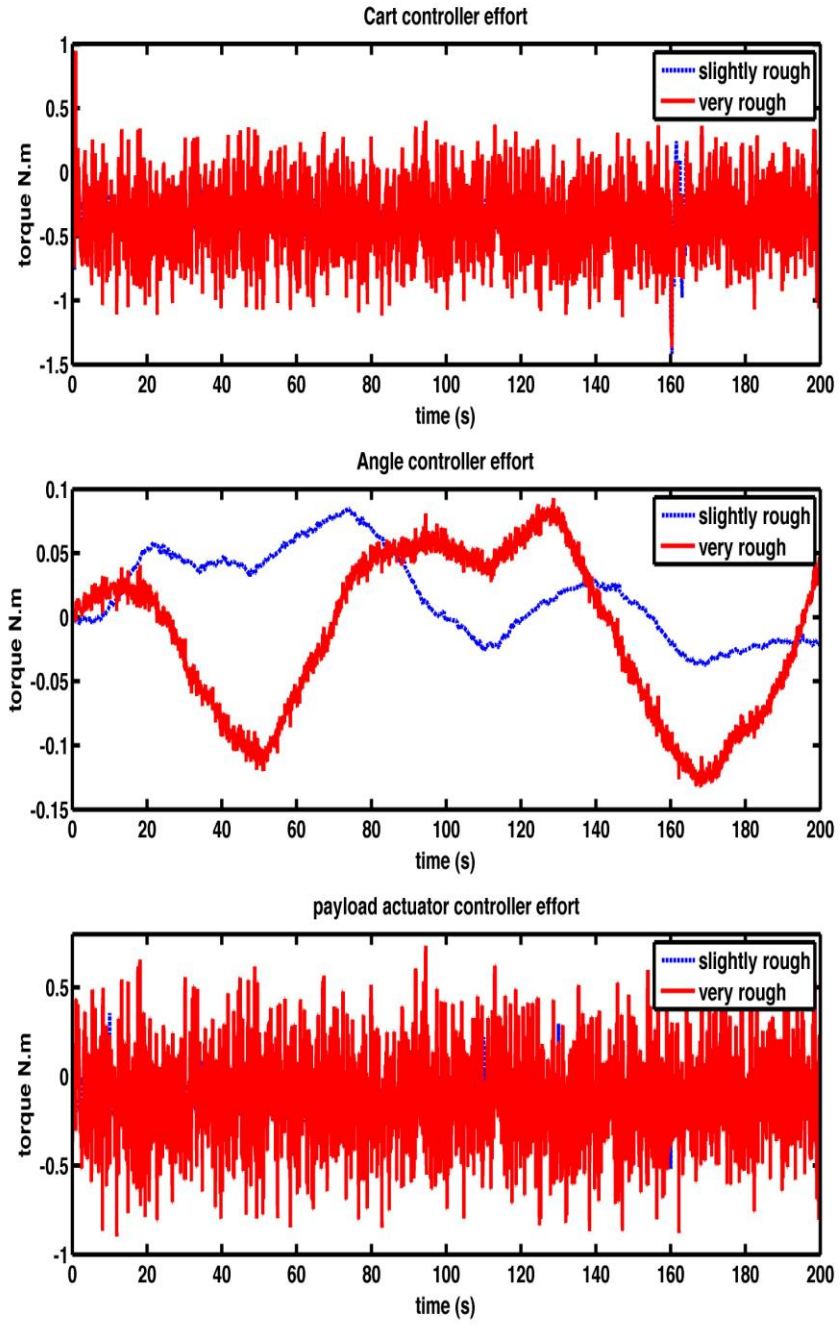

Figure 5.23: Control efforts on inclined terrains of 30 degrees with dynamic payload

5.5.3 Dynamic inclined terrain with variable friction profiles and dynamic payload movement

To test the vehicle in a more challenging simulation scenario, a highly irregular terrain is considered in this section. The irregular terrain is a dynamic terrain with variable inclination angles and frictional profiles. The surface inclination angle has a variable value in this simulation and is shown in Figure 5.24. The ground friction profile in this scenario consists of a random white noise with variable noise power to simulate the roughness of the surface and mimic the irregularity of such terrains in real life.

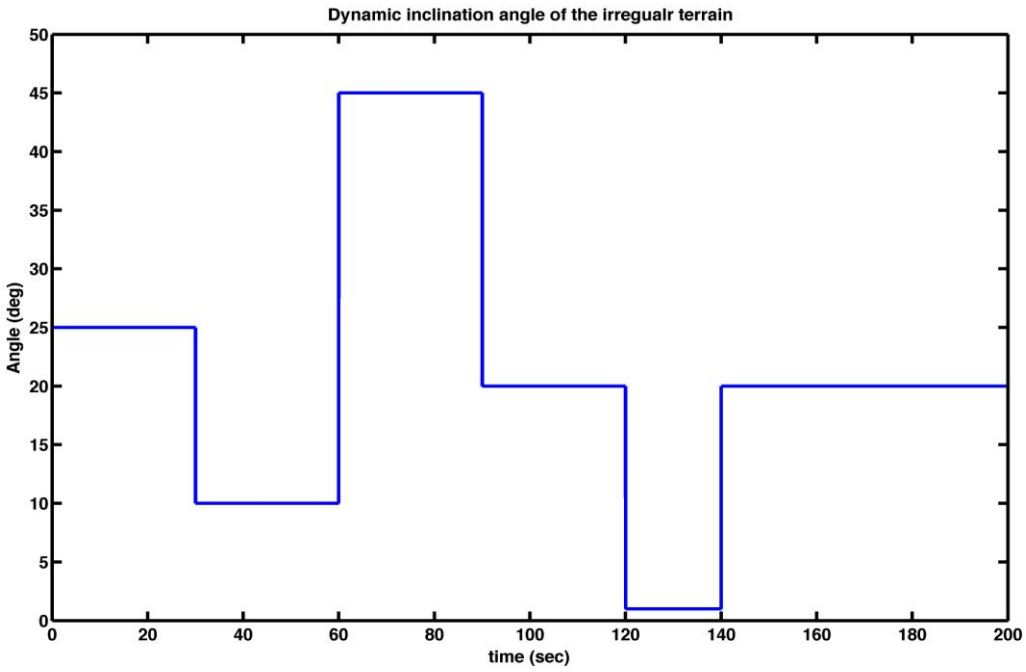

Figure 5.24: Dynamic inclination angle of the irregular terrain

Figure 5.25 represents responses of the vehicle components over the highly irregular terrain. It is clear that the vehicle was able to complete the commanded movement to a high degree of robustness and the control system managed to stabilise the vehicle during the simulation.

A small amount of oscillation was observed at the payload displacement response and the tilt angle; which is a result of the variable friction profiles of the terrain. However, these oscillations did not affect the stability of the system. Figure 5.26 shows the control efforts exerted to stabilise the vehicle over the terrain. A continuous control effort was exerted to stabilise the vehicle and adapt to the irregularity of the terrain. A larger amount of control effort was noticed during the simulation time between 60 – 120 seconds. This can be referred to the rapid change of the inclination angle between 0-45 degrees in addition to the random friction profile.

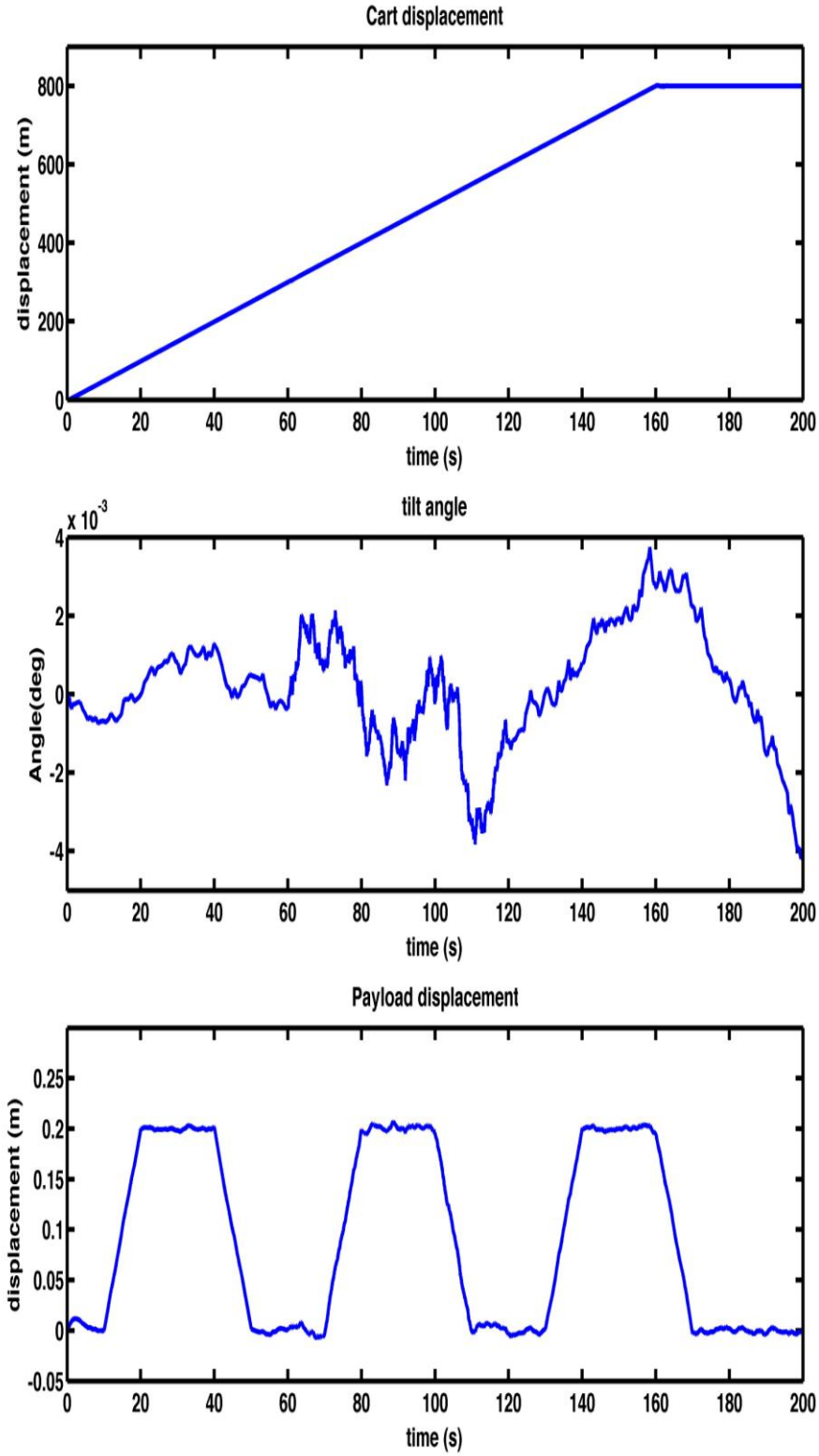

Figure 5.25: Vehicle response on a highly irregular terrain

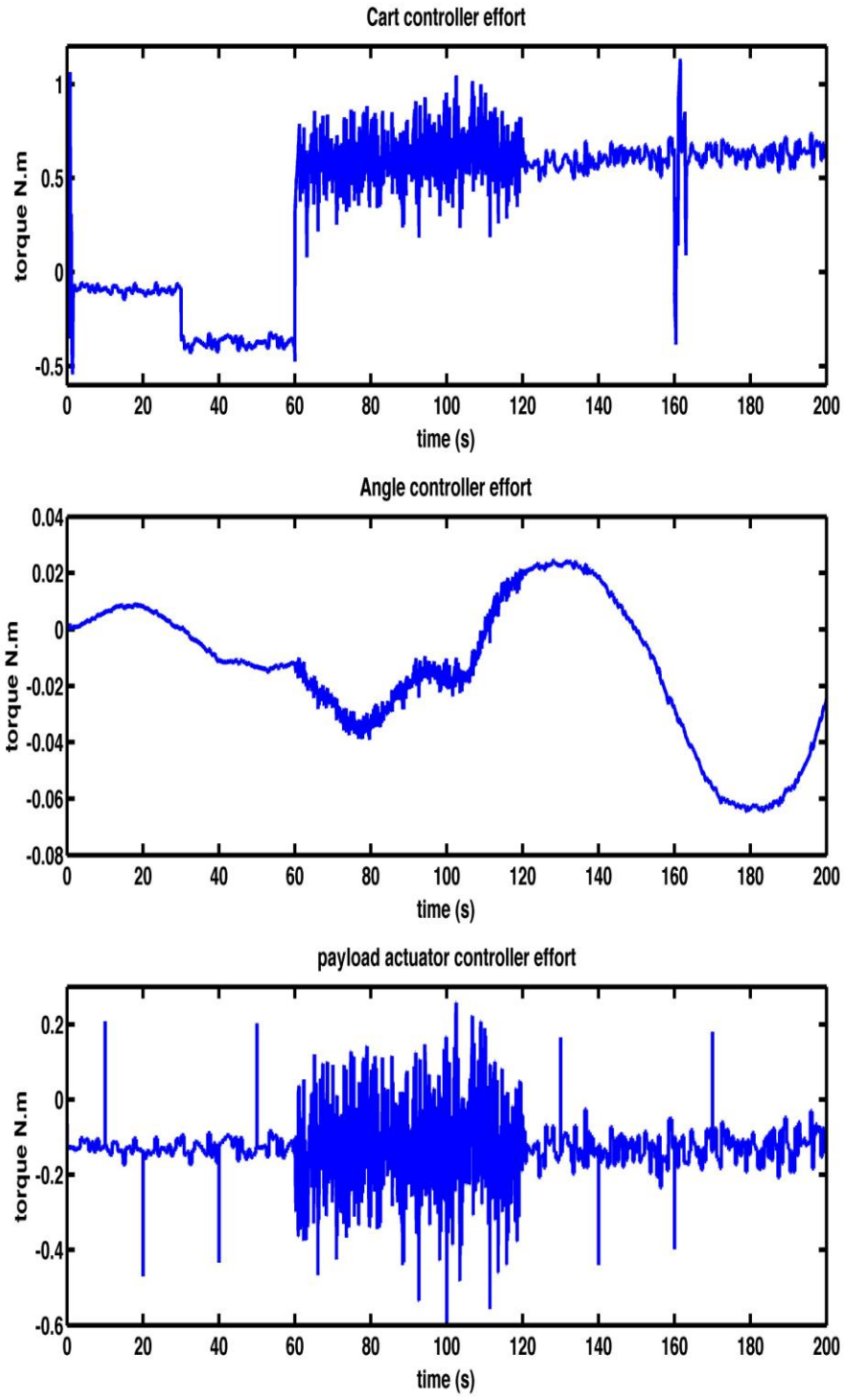

Figure 5.26: Control efforts of the vehicle components on a highly irregular terrain

5.6 Climbing up and down

To test the vehicle ability to climb on a hill way, the vehicle was commanded to move for a total distance of 8 meters to climb up and down a hill. The vehicle was first commanded to ascend up the hill with a surface slope of 40 degrees for 3 meters to reach the peak of the hill. Then, the vehicle was commanded to move on straight line for 2 meters. Finally, the vehicle descended from the hill with an inclination of 40 degrees down the hill, which is equivalent to 320 degrees clockwise on the unit circle, for 3 meters. Figure 5.27, illustrates the surface inclination angle values for the hill movement profile.

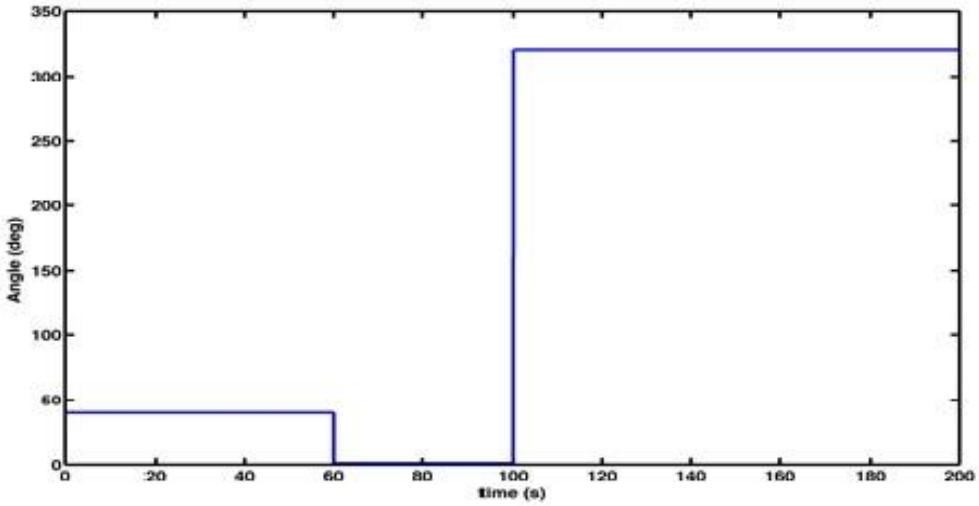

Figure 5.27: Hill movement scenario angle profile

The system was simulated according to the aforementioned movement scenario and the system response achieved is presented in Figure 5.28. It is noted that the vehicle was able to follow the predefined movement scenario with the dynamic angle profile without losing postural stability. Even though some overshoots appeared in the tilt angle response at instances of change of slope; they did not affect the overall system stability.

Figure 5.29 represents the system control efforts exerted to stabilise the vehicle during climbing up and down the hill. The cart controller exerted a constant effort of approximately 100 N.m while climbing the hill and moving on top of it. Almost equal amount of control effort was exerted to descend from the hill with but in the opposite direction to overcome the gravitational force. The tilt angle control effort exerted was almost constant except at instances of angle change where it reached a maximum of 25 N.m to keep the vehicle at the upright position.

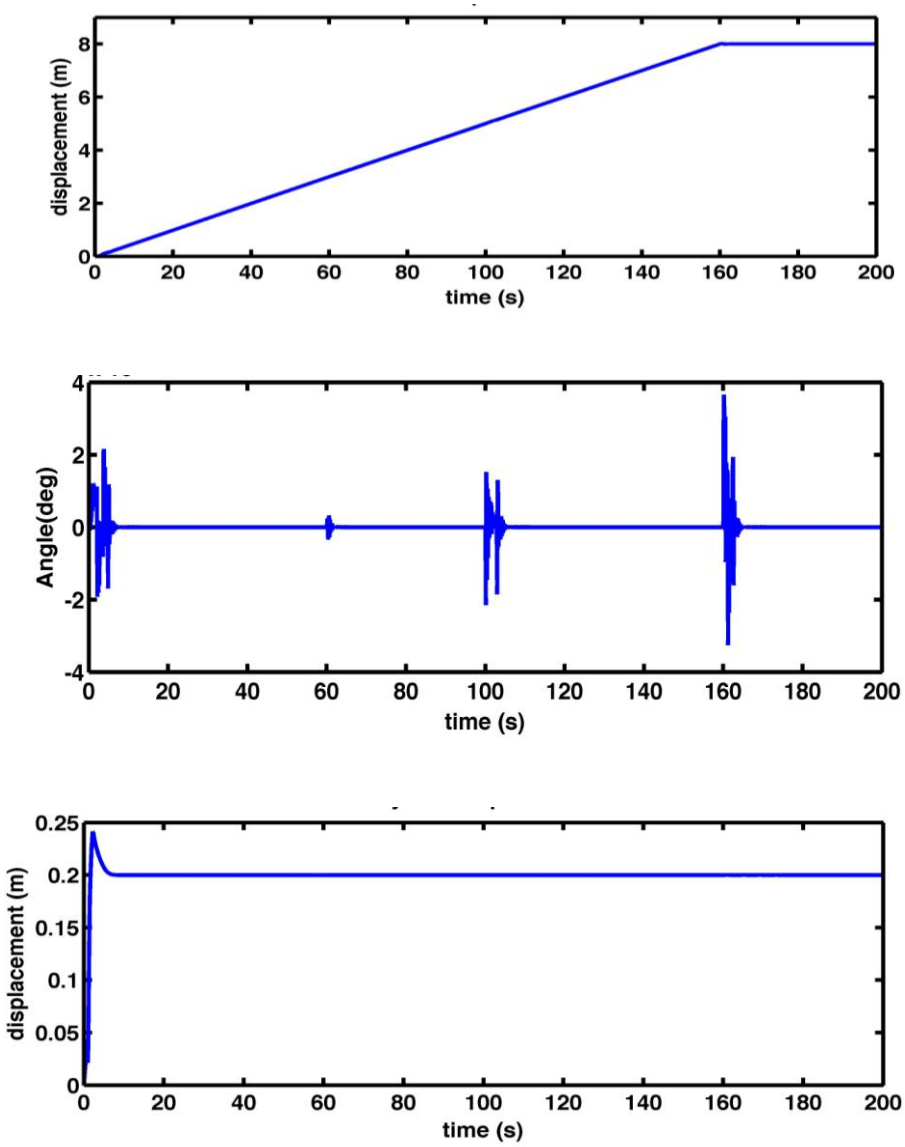

Figure 5.28: System response while moving up the hill

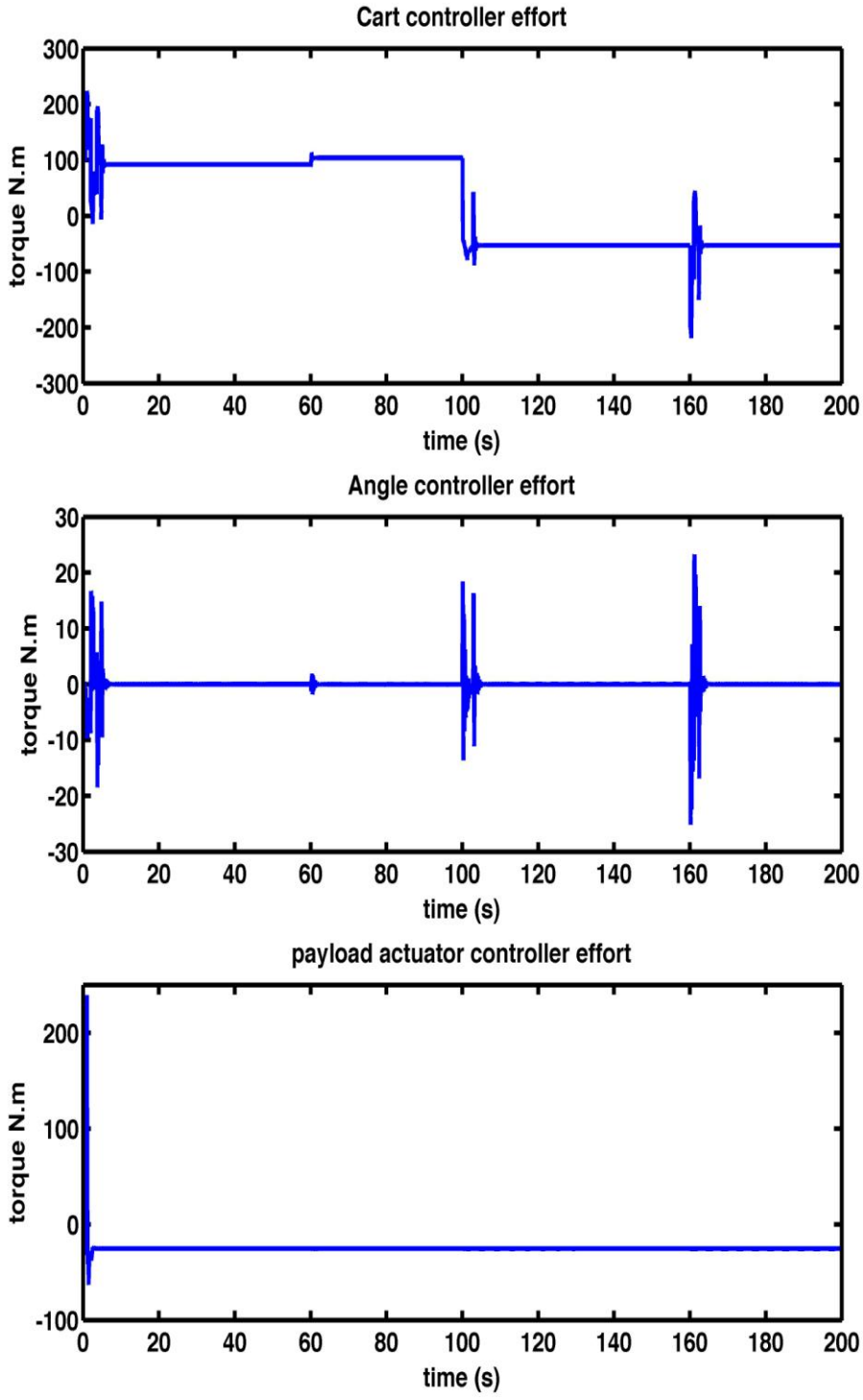

Figure 5.29: Control efforts of the vehicle controllers while moving up the hill

5.7 Summary

This chapter has presented the capability of the vehicle in driving on highly irregular terrains. Various simulation scenarios with different frictions and irregularities were carried out. The control system of the vehicle was able to cope with the variation of frictional elements of the surfaces as well as the inclinations and irregularities to a high degree of robustness. The vehicle was able to drive on irregular terrains showing a stable response and tracked the reference signal successfully. The successful response of the vehicle verifies the capability of the vehicle to serve as a basis for mobility solutions and encourages developing new applications.

Chapter 6

Real-time control of a two-wheeled robot

6.1 Introduction

Many modern inverted pendulums use gyroscopic sensors, expensive optical encoders and accelerometers with microprocessors or full-blown computers to implement their control algorithms. The most vital challenges which could be faced are in the balancing. Balancing depends on the control and the system design which depends on the weights, size and shape of the vehicle. The weight in the front and the back should be equal to keep the system in balance. Additionally, the control may as well keep the system stable while the vehicle is moving to stay away from any vibrations.

The aim of this chapter is to evaluate the control approaches on an experimental two wheeled robot with movable payload, in moving on balancing scenarios on flat and inclined surface.

6.2 The two-wheeled robot prototype

The test rig considered is shown in Figures 6.1, 6.2 and 6.3. This section describes the hardware and the software features of the robot and how they are interfaced with each other.

Figure 6.1: Real test rig, ACSE department, University of Sheffield

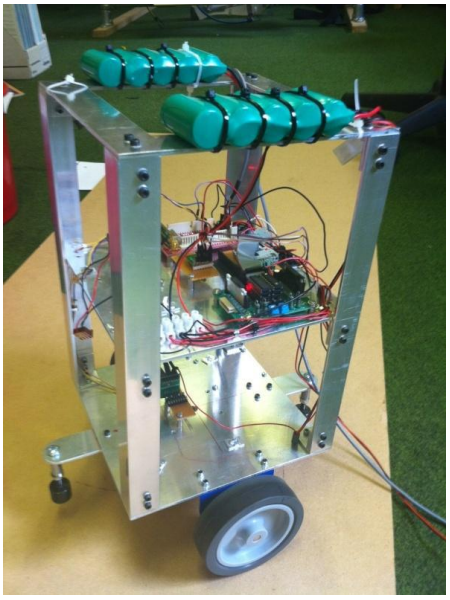

Figure 6.2: Robot chassis

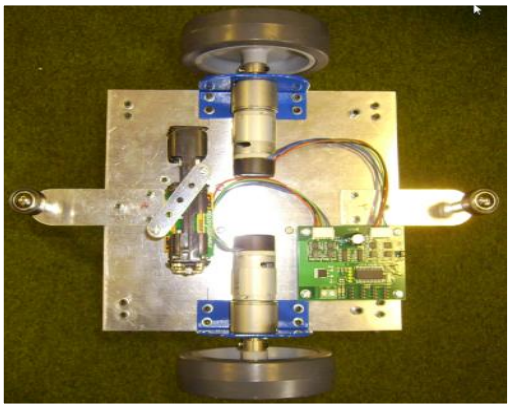

Figure 6.3: Bottom view of the test rig base

6.3 Hardware components

6.3.1 Chassis

The robot frame is built with aluminium. The batteries are located on the top level. On the bottom side of the first sheet are the wheels, the motor drive circuitry and DC motors. On the upper side of is the gyroscope sensor located. The second level houses microcontroller board, the linear actuator, and accelerometer. The base plate of the test rig is supported by means of two auxiliary rollers attached on both sides of the base plates.

6.3.2 DC motors

Two DC permanent magnet motors are used to drive the vehicle. The technical specifications of the motors are given in Table 6.1. Each motor is provided with a built-in shaft encoder with 360 counts/shaft revolution.

Table 6.1: Motor technical specifications

Specification	**Parameter**	**Units**
Voltage	12	*Vdc*
Torque	1.5	*Kg.cm*
Max. Speed	170	*rpm*
Max. Current	530	*mA*
No load speed	216	*rpm*
No load current	150	*mA*
Stall current	2.5	*A*
Rated power	4.22	*W*
Encoder	360	*counts*

6.3.3 Linear actuator

In order to provide the attached payload with the required sliding motion, a screw thread driver is used. The linear actuator is able to hold a weight of more than 1.3 kg while travelling through a maximum stroke of 48mm. The specifications are shown in Table 6.2.

Table 6.2: Screw thread driver technical specifications

Specification	**Parameter**	**Units**
Voltage	12	*Vdc*
Holding force	13.3	*N*
Max. Travel	48	*mm*
Step angle	7.5	deg *ree*
Step/rev	48	*mm*
Diameter – body	26.16	*mm*
Diameter – shaft	3.43	*mm*
Lead length	304.8	*mm*
Mounting hall spacing	34.9	*mm*

As can be noticed in Table 6.2, the shaft diameter of the screw thread will not be able to support the continuous motion of the attached payload. A transparent tube of 40 mm outside diameter is attached vertically to the intermediate aluminium board. The tube provides the payload, attached to the screw thread, with the necessary support and guide while moving up/down due to the actuation provided by the linear actuator.

6.3.4 Atmel TM ATMEGA32 Micro-Controller

ATMEGA32 is a high performance, low power AVR® 8-bit micro-controller manufactured by ATMELTM Corporation, Figure 6.4. The micro-controller has a CPU speed of 16 MHz (16 million instructions per second) and 32 Kbytes self-programmable flash memory. It has eight 10-bit Analog to Digital Converter (ADC) channels. Moreover it has four Pulse Width Modulation (PWM) channels, two 8-bit timers/counters and one 16-bit timer/counter.

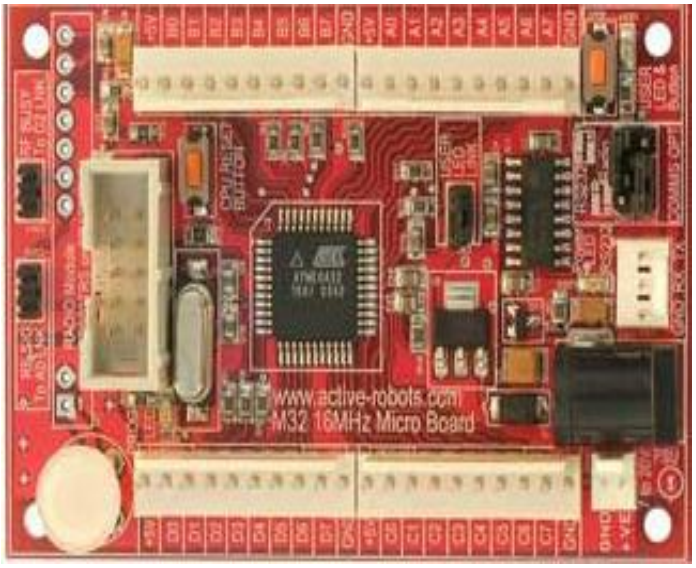

Figure 6.4 Microprocessor board

6.3.5 ANALOG 2-Axis Accelerometer ADXL203

The ADXL20***3*** is a small, low power, complete 2-axis accelerometer system with signal conditioned voltage outputs (Figure 6.5). It has 300 mV/g sensitivity for each axis; x-axis and y-axis. The output signals are analogue voltages that are proportional to acceleration. It can measure the static acceleration of gravity in tilt-sensing applications as well as dynamic acceleration from motion, shock

and vibration. The sensor is a poly-silicon surface-micro-machined structure built on top of a silicon wafer. This accelerometer is highly precise and temperature compensated which is an efficient option specifically for IMU (inertial measurement unit) and dead-reckoning applications.

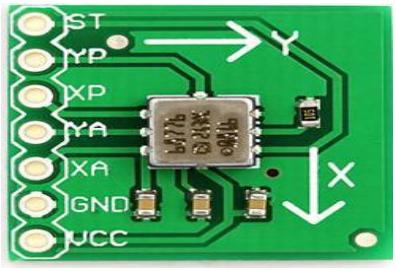

Figure 6.5: Accelerometer Sensor

6.3.6 Analogue Digital Gyroscope: MLX90609-N2

The MLX90609-N2 Angular Rate Sensor is a full gyroscopic system with high resolution and dynamic range (Figure 6.6). It shows two output signals, analog and digital (SPI) outputs which are proportional to the angular rate perpendicular to the device surface. This gyroscope typical has 26.67 mV/°/s sensitivity. The working principle is a z-axis rate-sensing device (yaw-rate sensing), positive output voltage for clockwise rotation around the axis normal to the device top, and negative for counter clockwise rotation.

Figure 6.6: Gyroscope Sensor

6.3.7 Motor Driver Board MD25-H Bridge Motor Driver

The MD25 is a robust I2C or serial dual motor drive designed for use with EMG30 motors (Figure 6.7). This driver has the capability of reading motor encoders and provides counts for determining distance traveled and direction. It drives two motors with independent or combined control, also motor current is readable. This device is very useful because, unlike stepper motors, the micro-controller does not use Pulse Width Modulation (PWM) for communicating with the motors, but instead uses commands for all the functions the MD25 has to offer.

Figure 6.7: H-Bridge Motor Drive

6.4 Software packages

6.4.1 WIN AVRTM

WIN AVRTM is a package of open source software development tools that enables the programmer to write in C, C++ or assembly codes for the ATMELTM AVR series micro-controllers. WIN AVRTM has a GNU C compiler (GCC) and debugging tools.

6.4.2 PONYPROG

This program is a serial device programmer application. PonyProg is an open source program that can be used to download the compiled codes (hex-files) to the micro-controller via the RS232 interface. It can be used in several types of micro-controller boards; programming of ATMELTM AVR micro-controllers.

6.5 Control strategy

This section describes the strategy and application of a controller for balancing the two-wheeled robot with a payload on flat and inclined surfaces. There are several control algorithms associated with two-wheeled platforms: PD controllers, feedback controllers, fuzzy logic control, and combined PID with feed-forward control. The importance of the algorithm is the speed and direction of the motors. The controller should read the values from the sensors and compare them with the reference value, where the main objective is to try to minimize the error between them at all times. If the error is positive, the robot should move in one direction; and if there is a negative error, the device should move in the opposite direction from the previous one. These movements are done at a speed that is proportional to the calculated error. The balancing behavior is achieved when the error is zero, or very close to zero, most of the time.

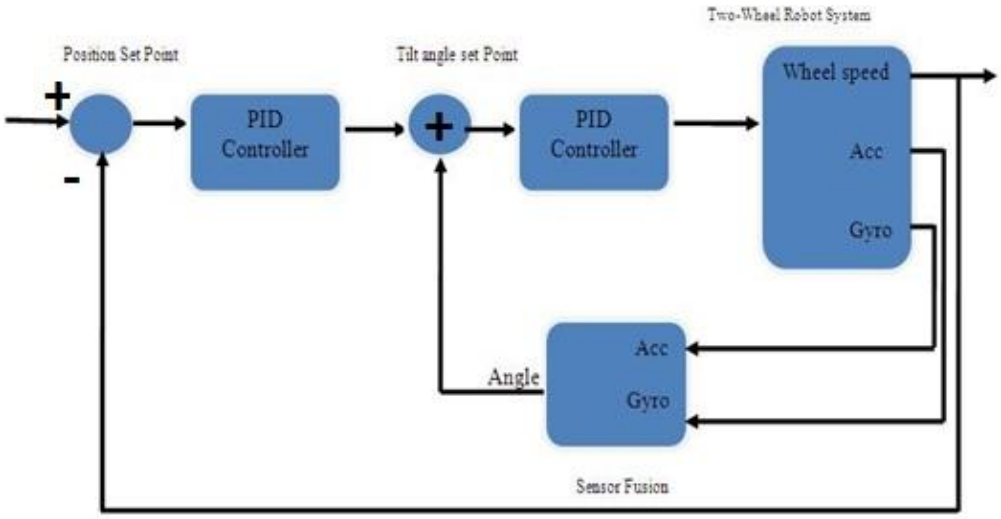

Figure 6.8: Closed loop control

The overall control structure of the system is shown in Figure 6.9. A PID controller was selected for implementation on the system. The PID controller code is summarized in three main parts; a proportional term, a derivative term and an integral term. Error measurement is based on the angle referring to the vertical balance position of the robot using an accelerometer and a gyroscope. For the integral term, it is important to create an anti-windup function so this term will not exceed a maximum value to cause an unstable behaviour.

6.5.1 Sensor fusion

This part gives information on gyroscope sensors and the accelerometer. The sensors fusion is based on Kalman filtering. The accelerometer is accurate for long time scales because the variations in the data are not drastic in a long period of time. However, the gyroscope which is accurate for short time scales because of the drift in time. In this algorithm (Figure 6.11), the tilt angle is given by both sensors. As the main problem of the gyroscope is the drift in time, it could be solved by using the output data from the accelerometer. In summary;

the accelerometer returns the correct angle in the long term. However, it is adversely affected by short term conditions.

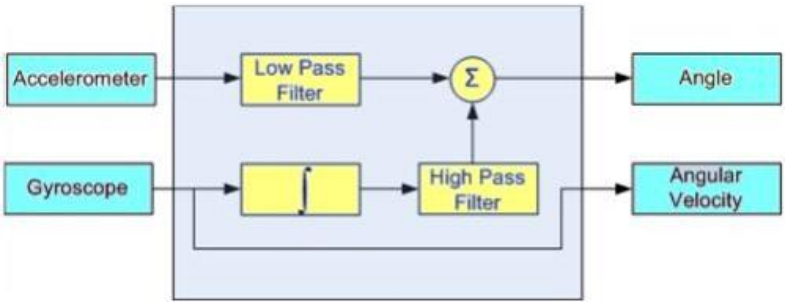

Figure 6.9: Diagram of filter for accelerometer and gyroscope

A simple solution is to implement a filter for the measurements of both sensors. A low-pass filter is used for the accelerometer output and a high-pass filter is used for the gyroscope output (Figure 6.10) combining these two filtered signals results in generating a reasonable angle estimate. The constants are the complimentary filter coefficients that are chosen.

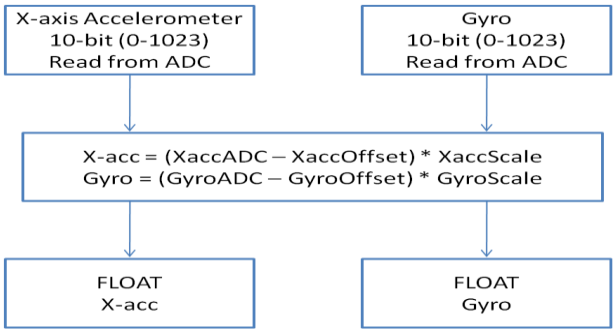

Figure 6.10: The accelerometer and gyroscope sensor fusion algorithm

The filter is described as:

$$Angle = (Coef_{1\,filter}) \times (Angle + Measure_{gyroscope} \times dt) + (Coef_{2\,filter}) \times X_{acc} \qquad (6.1)$$

$$\tau = \frac{a\ dt}{1 - a} \qquad (6.2)$$

where:

τ = constant, dt = sample period, a = Filter coefficient

Then, the tilt angle of the intermediate body can be calculated using the following equation:

$$y = a(y) + (1-a)(x) \tag{6.3}$$

where:

y = Tilt angle, a = Filter coefficient, x = Acceleration measured by the accelerometer

The filter coefficient can thus be obtained once the time constant and simple frequencies are chosen. In this case, to design the filter, the method of trial and error was chosen in order to check the sensors while the sampling period was used to obtain the filter coefficient. As the gyroscope has a bias (drift) of 5°/sec, a constant less than 2.5 seconds is needed to ensure that there is no deviation greater than few degrees in either direction in which the platform can move. If the time constant is greater than 2.5 seconds, only pass through the filter accelerations related to the gravity of the platform. However, for this particular time, the gyroscope measurements provide important errors as many deviations occur during that time. Moreover, with a small time constant, noise in the horizontal acceleration passes through the filter which will cause errors in the tilt angle. The following sets of parameters were used:

τ =0.45, dt =0.01, a =0.9

τ defines the limit at which the gyroscope and the accelerometer will work properly. If time interval is less than half a second (0.45s), the gyroscope integration becomes superior and the noise from the horizontal acceleration

filtered. For a longer period of time; more than half a second, the average measure of the accelerometer will have a greater weight from the gyroscope measurements which at this point may have the drift over time.

This method was used to solve the problems associated with the two sensors; the noise in the accelerations from the accelerometer, horizontal accelerations due to gravity effect and the deviation in time (drift) due to the gyroscope. Furthermore, the tilt angle will be quickly calculated and with no delays, improving stability of the platform. Finally, this method doesn't use excessive memory of the micro-controller.

Data acquisition consists of 10 bit analog/digit converter (ADC), which is used to sample both the accelerometer signal and the gyroscope at rate of 100 samples per second, whereas the speed data is taken from the encoder at a rate of 10 per second.

6.6 Experimental results

The experimental results of the two-wheeled platform are presented in this section to demonstrate the current behaviour of the robot. The results include the angle error with the accelerometer, the angle error with the gyroscope, and the angle error using both sensors on flat and inclined surfaces. The controller parameters were manually tuned using a heuristic approach.

6.6.1 Balancing and control of two wheeled robot on flat surface

A. Using accelerometer only

Figures 6.11 and 6.12 show the angles calculated from the output data of the accelerometer. A comparison is made between the results from the

accelerometer using the Average Window method. The data from the analog accelerometer is very noisy but accurate in long periods of time. Because of this an average window algorithm was chosen. This method obtains an average from the values depending on the "window size" that is selected. For example, if the "window size" is five (5), the first value will be without modification, the second one will be added to the first one and the result divided by two (2), the third value will be added to the previous two values and divided by three (3), the next values are going to use the same procedure until the fifth one, from that value (which, in this case, is the "window size") all the sum of the next ones will be divided by the maximum number that is always the "window size".

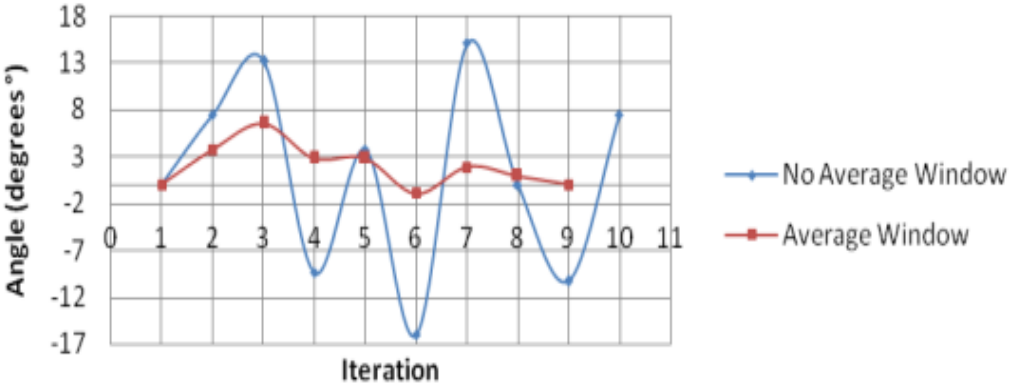

Figure 6.11: Tilt angle, window size 10

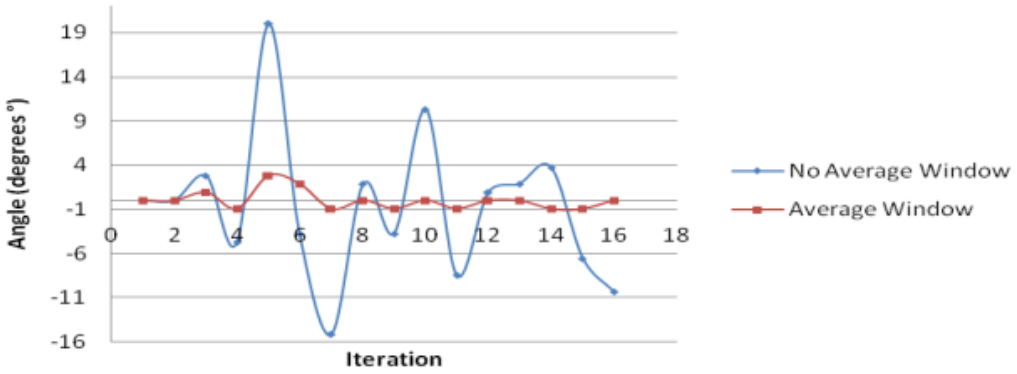

Figure 6.12: Tilt angle, window size 16

It can be concluded from the results in Figures 6.11 and 6.12 that the greater the size of the window the smoother platform behaviour without sudden changes to its acceleration. This leads to smoother results for the tilt angle and greater consistency in the values of the speed of the wheels and in the angular position of the intermediate body. When the sample frequency is changed to a higher value it will indicate a faster entry into the interrupt routine. Also, it is important to note that even though the changes are smooth with large values of window size, it produces a lag because this method spends time moving and obtaining the average of the values from the accelerometer. This could cause a lag in the feedback controller that can be solved by changing the sampling frequency.

B. Using gyroscope only

It is important to notice that in cases where the gyroscope has been used, different positions of the platform cannot be used to obtain results, only the balancing position. This is because when the robot is stationary, the gyroscope will show a constant value because the angular velocity is not changing. Due to this phenomenon, the shown graph in Figure 6.13 is only for the tilt angle when the robot is trying to balance. As shown in Figure 6.13, it can be concluded that the robot is close to achieve the balance position. On the other hand, after a few measurements, the angle starts increasing without control, leading to losing the balance condition after a period of time.

C. Using accelerometer and gyroscope

Figure 6.15 shows the tilt angle of the platform when it is trying to achieve a balance position. As explained before, because the gyroscope is one of the

sensors used, only the balancing position can be analysed. An acceptable behaviour of the two-wheeled platform has been obtained by using both sensors. As noted the angle was contained within a range of ±5°, which is considered an acceptable deviation from the target upright balance position. After analysing the results shown in Figures 6.11 – 6.14 ; using accelerometer only, gyroscope only and using both accelerometer and gyroscope sensors, it can be concluded that using both sensors has improved the results in terms of containing the tilt angle to a small value. Furthermore, the drift problem has disappeared due to using the accelerometer for calculating the inclination angle of the platform.

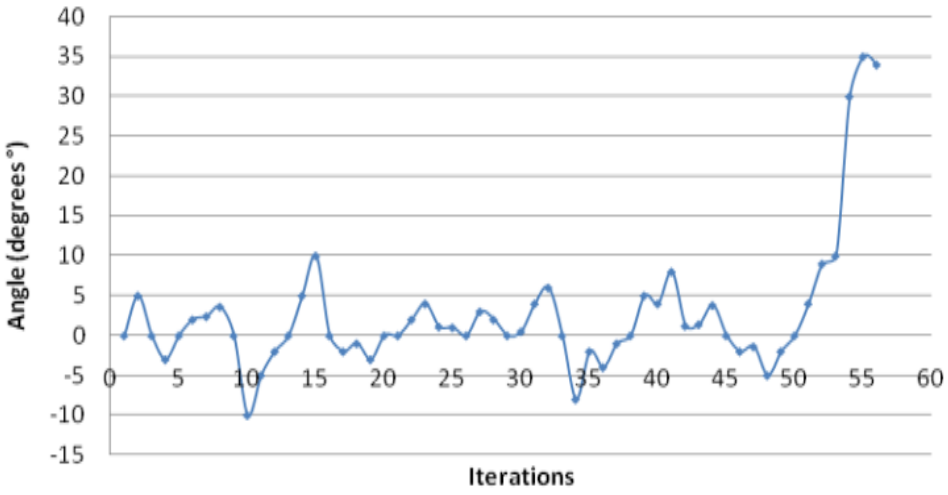

Figure 6.13: Tilt angle measurement using gyroscope only

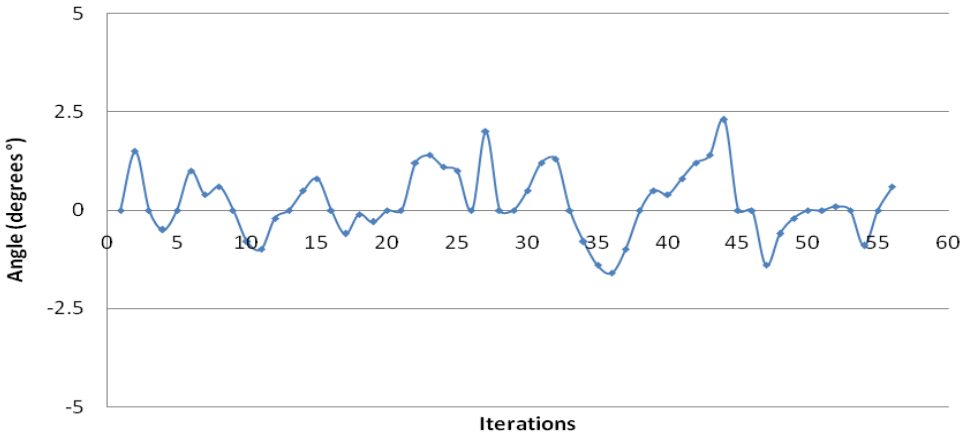

Figure 6.14: Tilt angle measurement using gyroscope and accelerometer

6.6.2 Balancing and control of two wheeled robot on inclined surface

The experiment involved testing the balancing of the robot on inclined plane assuming that the robot is initially balanced and positioned at the middle of the plane, as shown in Figure 6.15.

Figure 6.15: The setup of the experiment

The first test was conducted on a 5 degrees inclined surface. Figure 6.16 and Figure 6.17 show the real time performance of the robot in terms of the tilt angle and the normalized wheels speed. As noted the controller maintained the robot balance effectively keeping the tilt angle within ±1º.

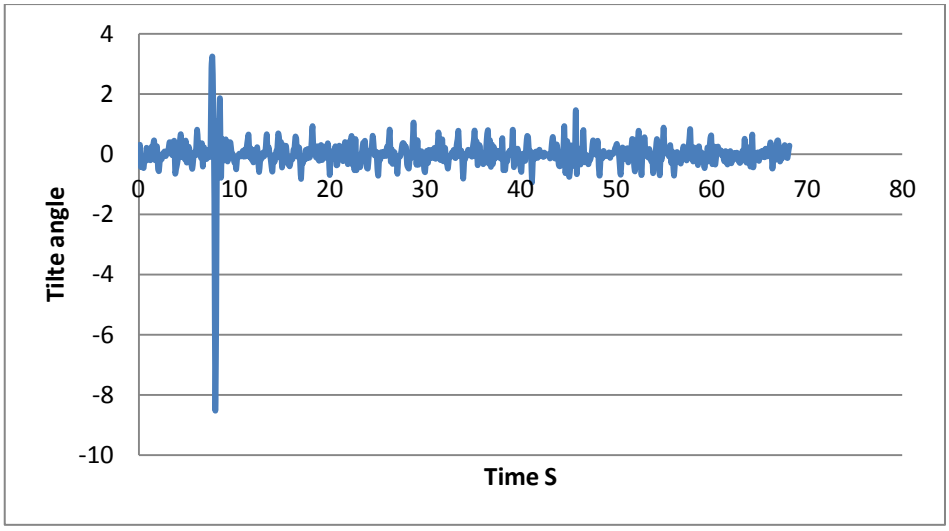

Figure 6.16: Tilt angle of the robot on 5 degree inclined surface

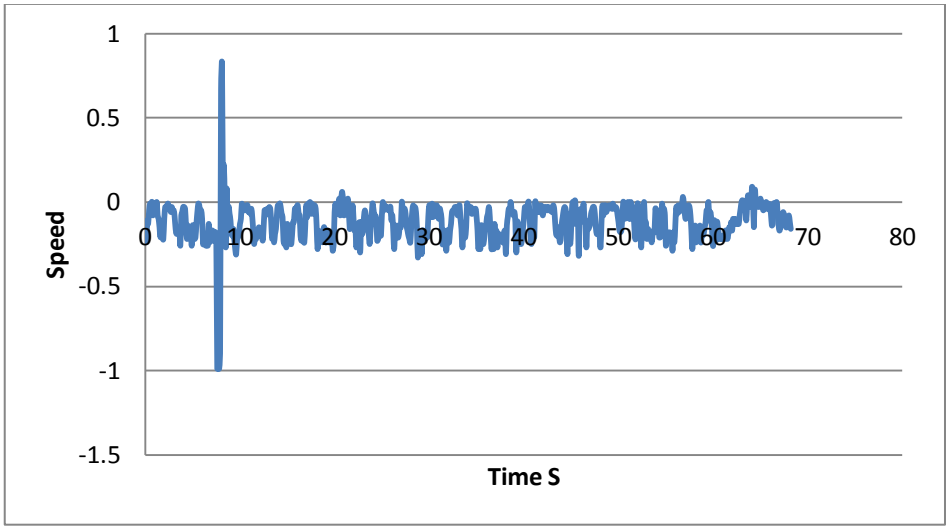

Figure 6.17: Normalized wheels speed of the robot on 5 degree inclined surface

Two more tests were conducted on surface inclination angles of 7.5 and 10 degrees. The controller successfully kept the robot balanced in the two experiments within acceptable range of the tilt angle. However it failed to maintain the position of the robot on the 10 degrees inclined surface and the robot started to drug backwards due to the increased force of horizontal

component of its weight. Figures, 6.18 , 6.19 and 6.20 illustrate the performance of the robot on 7.5º inclined surface in terms of the tilt angle, the normalized wheels speed and position, whereas, Figure 6. .21, 6.22 and 6.23 illustrates the performance of the robot on 10º inclined surface.

Analyzing the results of the normalized speed (the controller effort) for the three tests in Figures 6.17, 6.19, and 6.22, it is clearly noted that the mean of the data was bigger than zero, which represents the additional wheels torque that is required to counter act the drug force due to the weight of the robot.

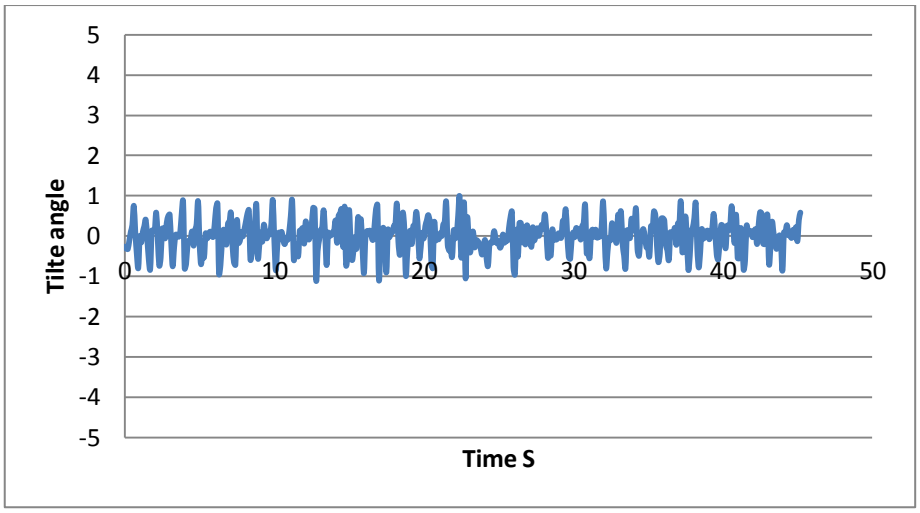

Figure 6.18: Tilt angle of the robot on 7.5 degree inclined surface

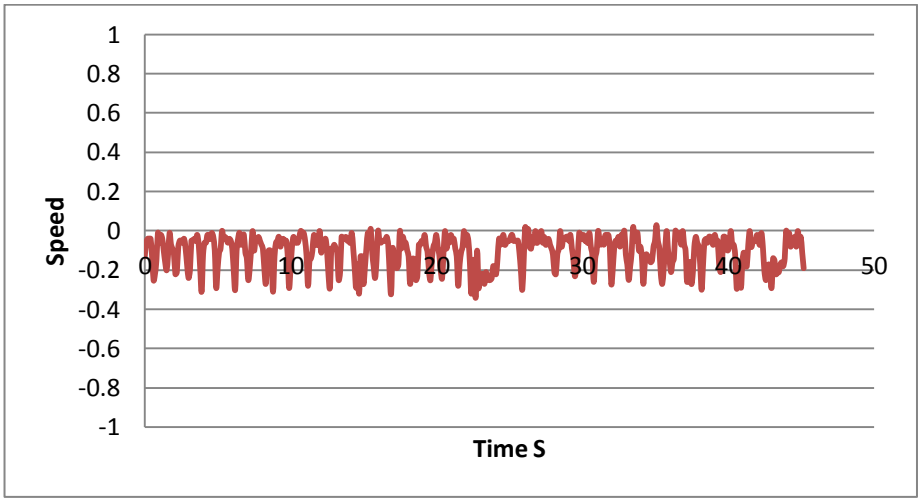

Figure 6.19: Normalized wheels speed of the robot on 7.5 degree inclined surface

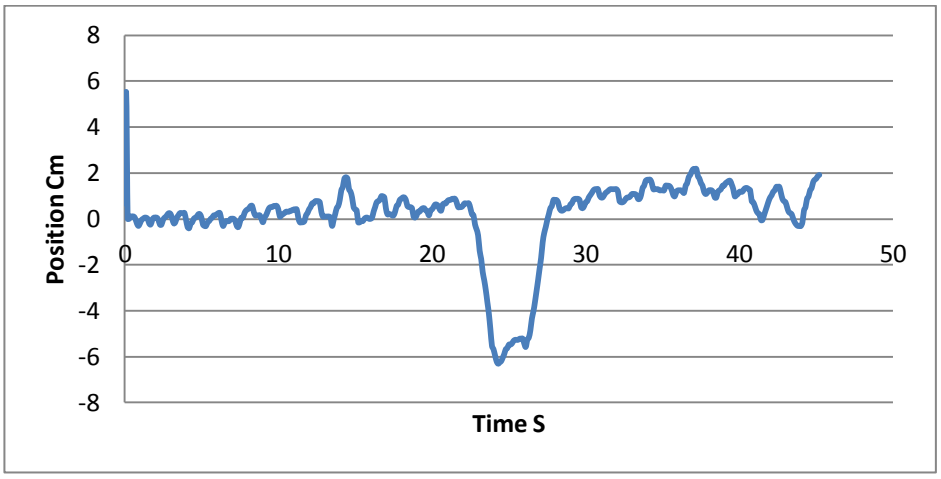

Figure 6.20: Robot's position of the robot on 7.5 degree inclined surface

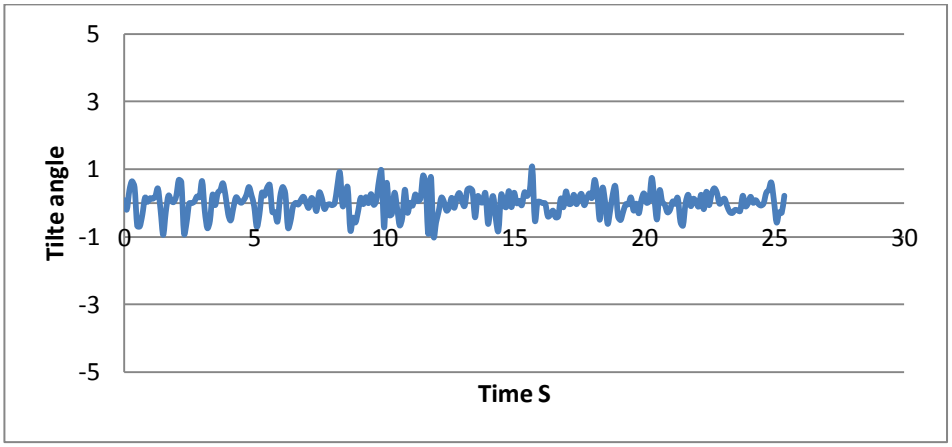

Figure 6.21: Tilt angle of the robot on 10 degree inclined surface

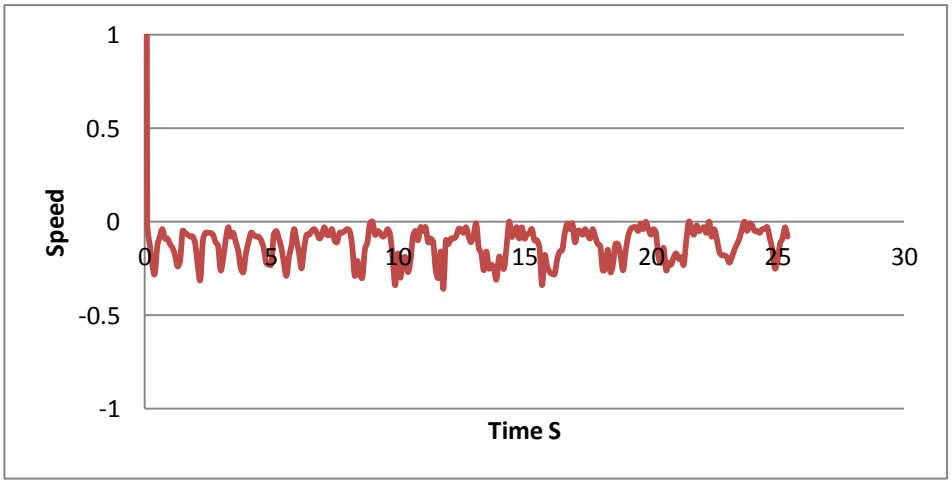

Figure 6.22: Normalized wheels speed of the robot on 10 degree inclined surface

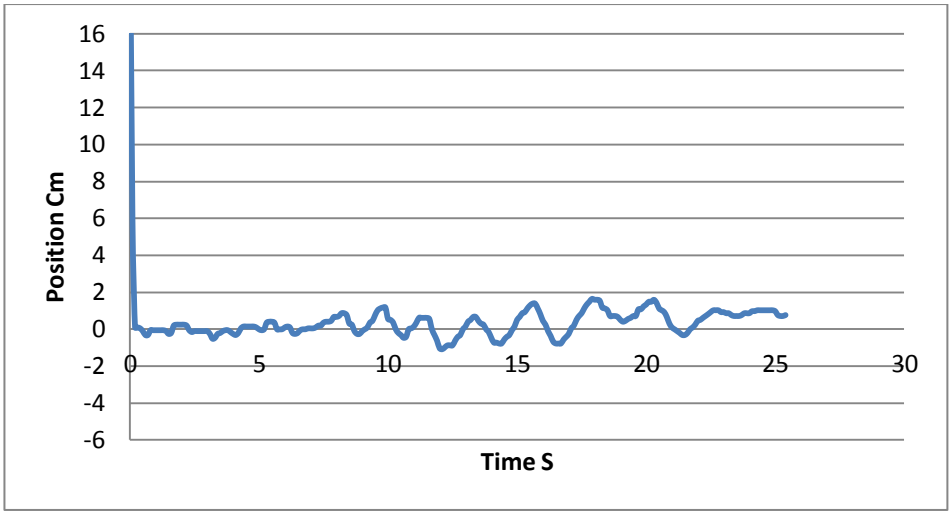

Figure 6.23: Robot's position of the robot on 10 degree inclined surface

6.7 Summary

The software and hardware aspects of the two-wheeled platform have been described and tests on practical implementation aspects have been carried out. The two sensors used in this prototype – the accelerometer and the gyroscope – complement each other. The accelerometer produces noisy data and the gyroscope drifts over time. Using a high-pass filter for the integrated data from the gyroscope and a low-pass filter for the accelerometer will give an accurate tilt angle. This angle has been used as an input to the feedback controller. It has been demonstrated that the selected control design the two-wheeled robot gives good results. The system has performed well on flat and inclined surfaces with the developed control approach.

Chapter 7
Conclusion and future work

7.1 Conclusion

The objective of this research was to model and develop suitable control approaches for a two-wheeled robotic vehicle based on a single IP with novel modifications that is able to drive on level and inclined surfaces and terrains of various frictional profiles. The research aimed to cover the aspects of modelling, control and validation of the model via different simulation scenarios that mimic the real life situations.

The developed model of the vehicle is a two wheeled robotic vehicle based on single IP design with a dynamic payload. The vehicle has the capability of driving on irregular terrains in the presence of external disturbances and inclinations and has been validated through simulations in this study. The vehicle design is of 3 degrees of freedom that would serve as a basis to develop mobility applications such as robotic wheelchairs and personal transporters.

The study has begun by modelling the vehicle with a static payload on inclined surfaces. A mathematical model of the vehicle has been derived utilizing Euler-Lagrange modelling approach using the kinetic and potential energy of the vehicle components. A mathematical model consisting of highly nonlinear and coupled differential equations has been presented. In the Matlab Simulink environment the model was built and verified via simulations. An initial control strategy consisting of PID controllers has been adopted to test the model controllability. The tests have proved successful in stabilising the system.

The model has also been simulated using MSC Visual Nastran package to gain more confidence about the validity of the model.

The model was then extended to include a dynamic payload to allow lifting the payload to a wanted height. The mathematical model was derived using Euler-Lagrange method and the system equations of motion were presented. A more robust control strategy based on fuzzy control was designed and adopted. The fuzzy control strategy adds more robustness to the vehicle control system to cope with various dynamics and uncertainties of the vehicle while moving on perturbed environments and inclinations. The system was simulated over various smooth inclined surfaces and the control strategy was proven to be efficient in stabilising the vehicle. Thus, the objective of the modelling and control has been achieved.

To achieve an optimal control performance that minimises the exerted energy as well as improve the overall response, QABFA optimisation algorithm has been adopted to optimise the control system of the vehicle. A constrained optimisation within the stability region of the vehicle has been designed to find the proper gains for each controller. The optimised controller has shown significant improvement in the system response and thus achieving an optimal control system for the developed vehicle.

Rigorous simulation scenarios have been carried out to analyse the vehicle behaviour in different operating conditions. The vehicle was tested to drive on smooth frictionless surfaces of different inclination angles and has shown a successful performance. The maximum inclination angle that the vehicle can operate was found and thus identifying the operating limits of the vehicle.

The robustness of the vehicle control system in rejecting external disturbances has been presented via simulating the vehicle in perturbed environments. External disturbances were applied on the vehicle of various amplitudes to study the impact on the vehicle stability and control performance. The vehicle has shown a stable response and has coped well with disturbances and thus meeting the aimed objective of developing a robust controller.

Level and inclined terrains of contrastive friction profiles were simulated to test the vehicle performance in challenging movement scenarios. To add more complexity to the simulation, dynamic and static payload movements were simulated. The vehicle has been tested on various terrains of simple and complex irregularities and complex operating conditions and has been proven to have a high degree of robustness in working in such environments. Thus, concluding the main objective of the research in developing a vehicle that is able to work on irregular and inclined terrains of various frictional profiles.

The developed control approach has been tested on a two-wheeled robot prototype. A PID control strategy was used as an initial step to control the prototype. Real time experiments over flat and inclined surfaces were carried out, for the first time, with good results achieved. It is difficult to compare the results with similar works in the literature as, to the author's best knowledge, this configuration has not been tested in real-time before.

The configuration of a novel structure two-wheeled robot with extendable payload has been presented in this research. The vehicle mathematical model has been derived and validated by simulations with FLC and PID control schemes. The developed vehicle is able to drive on irregular and inclined

terrains of different frictions and the presented results have validated these capabilities. Thus, concluding and fulfilling the objectives and goals of this research.

7.2 Recommended future work

With the promising results presented in this study, the vehicle capabilities can be extended and validated via a number of suggested future works.

- A steering system can be developed by separating the wheels motors and thus increasing the degrees of freedom of the design. A simple steering strategy such as differential steering would add more flexibility in manoeuvring over predefined paths with such capability, more steering scenarios could be completed to study the system reaction with the existence of ramps and obstacles, and in different environments with various frictions and grounds such as sloppy and muddy grounds.
- Studying the effect of changing the payload mass and study the system limitations.
- It would be beneficial to study the scalability of the vehicle in order to allow wider application designs for mobility solutions.
- Studying the effect of using anti-windup with PID controller.
- The development of the prototype and implementing FLC strategy and comparative assessment between theoretical and experimental results to validate the model.
- Studying the impact of adding a further DOF to the system to develop more mobility solutions such as sit-to-stand balancing wheelchairs, lower

extremity exoskeleton for the disabled and elder people and mobility assistive vehicles.

Appendix A

Mathematical model constants

$C_1 = 4l_l + {l_l}^2 + 4l_l l_u$

$C_2 = 4l_l + 2l_u$

$C_3 = 4{l_l}^2 + 4{l_u}^2 + 8l_l l_u$

$C_4 = 4l_l + 4l_u$

$C_5 = 2l_l + l_u$

$C_6 = 2l_l + 2l_u$

$C_7 = M_c + M_l + M_a + M_u + M_m$

$C_8 = \frac{1}{2}(M_u + M_m)$

$C_9 = \frac{1}{2}M_l{l_l}^2 + \frac{1}{2}J_l + \frac{1}{2}M_a{l_a}^2 + \frac{1}{2}J_a$

$C_{10} = M_l l_l + M_a l_a$

$C_{11} = M_c g + M_l g + M_a g + M_u g + M_m g$

$C_{12} = \frac{1}{2}M_u + \frac{1}{2}M_m + \frac{1}{2}M_u + \frac{1}{2}M_m$

$C_{13} = \frac{1}{2}C_2 M_u + \frac{1}{2}C_4 M_u + \frac{1}{2}M_u(C_2 - 2L_g) + \frac{1}{2}M_m(C_4 - 2L_g)$

$C_{14} = C_9 + \frac{1}{2}C_1 M_u + \frac{1}{2}C_3 M_m + \frac{1}{2}M_u{L_g}^2 - M_u L_g C_5 + \frac{1}{2}M_u C_1 + \frac{1}{2}M_m{L_g}^2 + \frac{1}{2}M_m C_3 - M_m C_6 L_g$

$C_{15} = C_{10} + M_u C_5 + M_m C_6$

$C_{16} = M_m + M_u$

$C_{17} = M_u C_5 + M_m C_6$

$C_{18} = C_{10} + C_{17}$

$L_u = C_5 + Q$

$L_m = C_6 + Q$

${L_u}^2 = Q^2 + C_2 Q + C_1$

${L_m}^2 = Q^2 + C_4 Q + C_3$

$J_u = M_u\{Q^2 + (C_2 - 2L_g)Q + {L_g}^2 - 2L_g C_5 + C_1\}$

$J_m = M_m\{Q^2 + (C_4 - 2L_g)Q + {L_g}^2 - 2L_g C_6 + C_3\}$

References

Abeygunawardhana, P, & Toshiyuki, Murakami. (2007). Stability improvement of two wheel mobile manipulator by real time gain control technique. Paper presented at the *International Conference o*n. *Industrial and Information Systems, 2007. ICIIS 2007.*

Aguilar-Ibañez, C., F. Gutierrez, et al. (2008). "*Controlled Lagrangian approach to the stabilization of the inverted pendulum system.*" *Revista mexicana de física 54(4): 329-335.*

Ahmad, S. (2010). Modelling and Fuzzy Control of Two-Wheeled Wheelchairs. doctoral dissertation. The University of Sheffield, Sheffield, United Kingdom

Ahmad, Salmiah, Aminnuddin, Muthanna, & Shukor, MA. (2012). *Modular hybrid control for double-link two-wheeled mobile robot*. *International Conference on Computer and Communication Engineering (ICCCE), 2012.*

Ahmad, Salmiah, Siddique, NH, & Tokhi, MO. (2012). Modular Fuzzy Logic Controller for Motion Control of Two-Wheeled Wheelchair.

Akesson, Johan, Blomdell, Anders, & Braun, Rolf. (2006). Design and control of YAIP—an inverted pendulum on two wheels robot. Paper presented at the *Computer Aided Control System Design, IEEE International Conference on Control Applications, 2006.*

Alam, MS, & Tokhi, MO. (2008). Hybrid fuzzy logic control with genetic optimisation for a single-link flexible manipulator. *Engineering Applications of Artificial Intelligence, 21(6), 858-873.*

Almeshal, A. M., Goher, K. M., & Tokhi, M. O. (2013). Dynamic modelling and stabilization of a new configuration of two-wheeled machines. *Robotics and Autonomous Systems, 61(5), 443-472. doi: 10.1016/j.robot.2013.01.006.*

Bogdanov, Alexander. (2004). Optimal control of a double inverted pendulum on a cart. *Oregon Health and Science University, Tech. Rep. CSE-04-006, OGI School of Science and Engineering, Beaverton, OR.*

Brown, William, Moseman, Eric, & Van Sickle, Corey. (2012). Balancing Robot.

Bugeja, Marvin. (2003). Non-linear swing-up and stabilizing control of an inverted pendulum system. Paper presented at *the EUROCON 2003. Computer as a Tool. The IEEE Region 8.*

Bush, Lawrence. (2001). Fuzzy logic controller for the inverted pendulum problem. *Computer Science Department, Rensselaer Polytechnic Institute, Troy, New York.*

Chakraborty, Nilanjan, & Ghosal, Ashitava. (2005). Dynamic modeling and simulation of a wheeled mobile robot for traversing uneven terrain without slip. *Journal of Mechanical Design, 127(5), 901-909.*

Chan, Ronald Ping Man, Stol, Karl A., & Halkyard, C. Roger. (2013). Review of modelling and control of two-wheeled robots. *Annual Reviews in Control, 37(1), 89-103. doi: http://dx.doi.org/10.1016/j.arcontrol.2013.03.004*

Cheng-jun, Ding, Ping, Duan, Ming-lu, Zhang, & Yan-fang, Zhang. (2009). Double inverted pendulum system control strategy based on fuzzy genetic algorithm. Paper presented at the *IEEE International Conference on Automation and Logistics, 2009. ICAL'09.*

Chung, Chung Choo, & Hauser, John. (1995). Nonlinear control of a swinging pendulum. *Automatica, 31(6), 851-862.*

Eltohamy, Khaled Gamal, & Kuo, Chen-Yuan. (1999). Nonlinear generalized equations of motion for multi-link inverted pendulum systems. *International journal of systems science, 30(5), 505-513.*

Fiacchini, M, Viguria, A, Cano, R, Prieto, A, Rubio, FR, Aracil, J, & Canudas-de-Wit, C. (2006). Design and experimentation of a personal pendulum vehicle. Paper presented at the Proc. *Seventh Portuguese Conf. Automatic Control.*

Furuta, Katsuhisa, Yamakita, Masaki, & Kobayashi, S. (1991). Swing up control of inverted pendulum. Paper presented at the *International Conference on* Industrial Electronics, Control and Instrumentation. *IECON'91, 1991.*

Goher, Khaled MK, & Tokhi, MO. (2008). Modelling, Simulation and Balance Control of a Two-Wheeled Robotic Machine with Static Variation in Load Position. Paper presented at the *Proceedings of the 22nd European Conference on Modelling and Simulation, Nicosia, Cyprus, June.*

Goher, KM, & Tokhi, MO. (2010). A New Configuration of Two-Wheeled Inverted Pendulum: A Lagrangian-Based Mathematical Approach. Cyber Journals: *Multidisciplinary Journals in Science and Technology, Journal of Selected Areas in Robotics and Control (JSRC), December Edition, 1(02), 1-5.*

Grasser, Felix, D'Arrigo, Aldo, Colombi, Silvio, & Rufer, Alfred C. (2002). JOE: a mobile, inverted pendulum. *IEEE Transactions on* Industrial Electronics, *49(1), 107-114.*

Ha, Hyunuk, Ryu, Sungmin, & Lee, Jangmyung. (2010). A robust control of mobile inverted pendulum using single accelerometer. Paper presented at the *The Fifteen International Symposium on Aritificial Life and Robbotics.*

Ha, Kyung-Jae, & Kim, Hak-Man. (1997). A genetic approach to the attitude control of an inverted pendulum system. Paper presented at the *Ninth IEEE International Conference on* Tools with Artificial Intelligence, 1997.

Hladek, Daniel. (2007). Multi-agent fuzzy control of the robotic soccer. SAMI 2007 Proceedings, 329-341.

Hu, Jia-Sheng, Tsai, Mi-Ching, Hu, Feng-Rung, & Hori, Yoichi. (2010). Robust control for coaxial two-wheeled electric vehicle. *Journal of Marine Science and Technology, 18(2), 172-180.*

Huang, Jian, Guan, Zhi-Hong, Matsuno, Takayuki, Fukuda, Toshio, & Sekiyama, Kosuke. (2010). Sliding-mode velocity control of mobile-wheeled inverted-pendulum systems. *IEEE Transactions on Robotics, 26(4), 750-758.*

Ibanez, Carlos Aguilar, & Frias, O Gutiérrez. (2008). Controlling the inverted pendulum by means of a nested saturation function. *Nonlinear Dynamics, 53(4), 273-280.*

Jadlovský, Slávka, & Sarnovský, Ján. (2013). Modelling of Classical and Rotary Inverted Pendulum Systems–A Generalized Approach. *Journal of Electrical Engineering, 64(1), 12-19.*

Jeong, Seonghee, & Takahashi, Takayuki. (2008). Wheeled inverted pendulum type assistant robot: design concept and mobile control. Intelligent Service Robotics, 1(4), 313-320.

Kausar, Zareena, Stol, Karl, & Patel, Nitish. (2010). Performance enhancement of a statically unstable two wheeled mobile robot traversing on an uneven surface. Paper presented *at the IEEE Conference on Robotics Automation and Mechatronics (RAM), 2010.*

Kausar, Zareena, Stol, Karl, & Patel, Nitish. (2012). The Effect of Terrain Inclination on Performance and the Stability Region of Two-Wheeled Mobile Robots. *Int J Adv Robotic Sy, 9(218).*

Kawamoto, S. (1996, 8-11 Sep 1996). Nonlinear control and rigorous stability analysis based on fuzzy system for inverted pendulum. Paper presented at *the Fifth IEEE International Conference on* Fuzzy Systems, 1996.

Kim, Yeonhoon, Kim, Soo Hyun, & Kwak, Yoon Keun. (2005). Dynamic analysis of a nonholonomic two-wheeled inverted pendulum robot. *Journal of Intelligent and Robotic Systems, 44(1), 25-46.*

kouda, Noriaki, Matsui, Nobuyuki, Nishimura, Haruhiko, & Peper, Ferdinand. (2005). An Examination of Qubit Neural Network in Controlling an Inverted Pendulum. *Neural Processing Letters, 22(3), 277-290. doi: 10.1007/s11063-005-8337-2*

Kwon, Youngkuk, Son, Joonbae, Lee, Jaeoh, Han, Jongho, & Lee, Jangmyung. (2011). Optimal posture control of two wheeled inverted pendulum robot on a slanted surface.

Lee, Howon, Lee, Junseok, & Lee, Jangmyung. (2009). Hill climbing algorithm of an inverted pendulum. Paper presented at the *IEEE International Symposium on* Computational Intelligence in Robotics and Automation (CIRA*), 2009.*

Li, Jingtao, Xueshan, Gao, Huang, Qiang, & Matsumoto, Osamu. (2008). Controller design of a two-wheeled inverted pendulum mobile robot. Paper presented *at the IEEE International Conference on Mechatronics and Automation, 2008. ICMA 2008.*

Lin, Zongli, Pachter, Meir, & Banda, Siva. (1998). Toward improvement of tracking performance nonlinear feedback for linear systems. *International Journal of Control, 70(1), 1-11*.

Lingyan, Hu, Guoping, Liu, Xiaoping, Liu, & Hua, Zhang. (2009). The computer simulation and real-time stabilization control for the inverted pendulum system based on LQR. Paper presented at *the Fifth International Conference on Natural Computation, 2009.*

Mahfouf M. (2004), Fuzzy logic modelling and control – ACS6112, theoretical and practical aspects of fuzzy systems, Department of Automatic Control and Systems Engineering, the University of Sheffield, MSc Control Systems Course Notes.

Mamdani, Ebrahim H, & Assilian, Sedrak. (1975). An experiment in linguistic synthesis with a fuzzy logic controller. *International Journal of Man-Machine Studies, 7(1), 1-13.*

Maravall, Darío, Zhou, Changjiu, & Alonso, Javier. (2005). Hybrid fuzzy control of the inverted pendulum via vertical forces. *International Journal of Intelligent systems, 20(2), 195-211.*

Miyagawa, T., & Ishida, Y. (1995). Neural network-based model reference control for inverted pendulum. Paper presented at the *IEEE International Conference on Neural Networks*, Nov/Dec 1995.

Mladenov, Valeri. (2011). Application of neural networks for control of inverted pendulum. WSEAS *Transactions on Circuits and Systems, 10(2), 49-58.*

Muskinja, Nenad, & Tovornik, Boris. (2006). Swinging up and stabilization of a real inverted pendulum. *IEEE Transactions on Industrial Electronics, 53(2), 631-639.*

Nasrallah, Danielle Sami, Michalska, Hannah, & Angeles, Jorge. (2007). Controllability and posture control of a wheeled pendulum moving on an inclined plane. *IEEE Transactions on Robotics, 23(3), 564-577.*

Nawawi, SW, Ahmad, MN, & Osman, JHS. (2008). Real-time control of a two-wheeled inverted pendulum mobile robot. World Academy of Science, Engineering and Technology, 39, 214-220.

Ogata, K. (2002), Modern control engineering, Prentice-Hall, Inc., USA

Park, Mun-Soo, & Chwa, Dongkyoung. (2009). Swing-up and stabilization control of inverted-pendulum systems via coupled sliding-mode control method. *IEEE Transactions on Industrial Electronics, 56(9), 3541-3555.*

Pathak, Kaustubh, Franch, Jaume, & Agrawal, Sunil K. (2005). Velocity and position control of a wheeled inverted pendulum by partial feedback linearization. *IEEE Transactions on Robotics, 21(3), 505-513.*

Prasad, Lal Bahadur, Tyagi, Barjeev, & Gupta, Hari Om. (2012). Modelling and Simulation for Optimal Control of Nonlinear Inverted Pendulum Dynamical System Using PID Controller and LQR. Paper presented at *the Sixth Modelling Symposium (AMS), 2012, Asia.*

PID Control Website http://www.expertune.com/tutor.html (date of last update: 2004)

Ratiroch-Anant, Phornsuk, Anabuki, Masatoshi, & Hirata, Hiroshi. (2004). Self-tuning control for rotational inverted pendulum by eigenvalue approach. Paper presented at the *IEEE Region 10 Conference TENCON 2004,*.

Ren, Tsai-Jiun, Chen, Tien-Chi, & Chen, Chun-Jung. (2008). Motion control for a two-wheeled vehicle using a self-tuning PID controller. Control Engineering Practice, 16(3), 365-375.

Roshdy, Amr A, zheng Lin, Yu, Mokbel, Hany F, & Wang, Tongyu. (2012). Stabilization of Real Inverted Pendulum Using Pole Separation Factor.

Salerno, Alessio, & Angeles, Jorge. (2005). Modeling and controllability of two-wheeled quasiholonomic robots. Dept. Mech. Eng., Centre Intell. Mach., McGill Univ., Montreal, QC, Canada, Tech. Rep. TR-CIM, 5.

Sun, Liang, & Gan, Jiafei. (2010). Researching of two-wheeled self-balancing robot base on LQR combined with PID. Paper presented at *the 2nd International Workshop on Intelligent Systems and Applications (ISA), 2010.*

Sun, Ya Lei, & Er, Meng Joo. (2004). Hybrid fuzzy control of robotics systems. *IEEE Transactions on Fuzzy Systems, 12(6), 755-765.*

Takahashi, Y., & Tsubouchi, O. (2005). Modern control approach for robotic wheelchair with inverse pendulum control. The 5th International Conference on Intelligent Systems Design and Applications ISDA 2005, pp. 364–369.

Tsai, Ching-Chih, Huang, Hsu-Chih, & Lin, Shui-Chun. (2010). Adaptive neural network control of a self-balancing two-wheeled scooter. *IEEE Transactions on Industrial Electronics, 57(4), 1420-1428.*

Wang, & Jia-Jun. (2012). Stabilization and tracking control of inverted pendulum with sliding-mode control. *ISA Transactions. 51(6), 763-770.*

Wang, Dongyun, & Fan, Fuling. (2009). Parameters tuning of fuzzy controller for rotated pendulum based on improved particle swarm optimization. Paper presented at *the International Conference on Computational Intelligence and Software Engineering (CiSE 2009).*

Wang, Jia-Jun. (2011). Simulation studies of inverted pendulum based on PID controllers. Simulation Modelling Practice and Theory, 19(1), 440-449.

Wang, Zhen-Yu, Dai, Ya-Ping, Li, Yong-Wei, & Yao, Yuan. (2010). Application of adaptive critic design on angle bracket inverted pendulum control. Paper presented at *the International Conference on Machine Learning and Cybernetics (ICMLC 2010).*

Xu, Yangsheng, & Sun, Loi Wah. (2000). Stabilization of a gyroscopically stabilized robot on an inclined plane. Paper presented at the *IEEE International Conference on Robotics and Automation* (*ICR 2000).*

Yamada, A., Yamakawa, S., & Fujimoto, H. (2004). Switching control for inverted pendulum system based on energy modification. Paper presented *at the Annual Conference SICE 2004.*

Zadeh, Lotfi A. (1973). Outline of a new approach to the analysis of complex systems and decision processes. *IEEE Transactions on Systems, Man and Cybernetics, (1), 28-44.*